2023

Functional Residues of CjpatA

Robert Lamont
lamo3690@mylaurier.ca

Characterization of Functional Residues of *Cj*PatA

by

Robert Campbell Lamont

Chemistry/Biochemistry, Wilfrid Laurier University, 2023

THESIS

Submitted to the Department of Chemistry and Biochemistry

in partial fulfilment of the requirements for

Master of Science in Chemistry

Wilfrid Laurier University

Abstract

Antibiotic resistance in pathogenic bacteria continues to challenge clinicians and threaten the lives of infected individuals. For this reason, new classes of antibiotics or new targets for antibiotic therapy are needed to circumvent this global health crisis. In Gram-negative bacteria, the enzymes peptidoglycan *O*-acetyltransferase A and B (PatA and PatB), are responsible for adding acetyl groups to the C-6 hydroxyl group of *N*-acetyl muramic acid (MurNAc) in peptidoglycan (PG). These acetyl groups are responsible for inhibiting the activity of lysozyme from host organisms that hydrolyze the β1-4 glycosidic linkage between MurNAc and *N*-acetylglucosamine (GlcNAc). The acetyl groups also regulate the rate of autolysis by precluding the activity of lytic transglycosylases, that contribute to this process. PatB from several sources has been experimentally characterized, but PatA still lacks the same amount of characterization due to difficulties with its expression and purification. Here, initial attempts to express and purify *Proteus mirabilis* and *Campylobacter jejuni* PatA are presented. Efforts to characterize functional residues of *Cj*PatA were made by utilizing *in situ* assays developed to compare the resistance to lysozyme and the rates of autolysis in nutrient-deprived environments of *C. jejuni* strains with *patA* mutations. Point mutations to *CjpatA* were engineered for the site-specific replacements of S122, R164, H275, R283, and H315 to test the significance of these proposed catalytic residues. A preliminary application of this autolysis assay, suggested S122, H275, R283, and H315 do act as functional residues because their populations did not decrease as much as their progenitor strain, an *oap* operon knockout with a *patA* and *patB* complementation. O-acetylation data from the respective strains could not be generated to verify these findings.

Acknowledgements

I would like to thank my advisor, Dr. Anthony Clarke, for providing me with the opportunity to expand my skill set and grow as a person by taking me on as a Master of Chemistry/Biochemistry student. I was provided with an excellent environment in which to grow and thrive personally and professionally. Dr. Clarke has been extremely patient and understanding of the difficulties that encompass scientific research as a new graduate student, which has been a truly humbling, frustrating, but ultimately cathartic and exciting time. I would also like to thank the institution of Wilfrid Laurier University and all its wonderful faculty that have helped to make my time as a graduate teaching assistant and student a great experience.

My fellow lab members provided so much insight and help during my time as a master's student. Without their guidance, optimism, patience, and kindness, I would have had a much harder time adjusting to becoming an independent graduate student, and also to the hardships of the Covid-19 pandemic which provided an extra challenge to overcome when it came to the completion of my studies. I would like to thank my family for their continued support. Without the help of my partner, Maddy Armstrong, and my parents, Bill and Linda Lamont, I would not have had the opportunity to complete my education without their financial and moral support.

Table of Contents

List of Figures

List of Tables

List of Appendices

List of Important Abbreviations

1,6-anh	1,6-anhydro
4MU-Ac	4-Methylumbelliferyl-acetate
Ac-CoA	Acetyl-Coenzyme A
Ape	Acetyl peptidoglycan esterase
AT3	Acetyltransferase 3
BCIP	5-Bromo-4-chloro-3-indolyl phosphate
bPBP	B-Class penicillin-binding protein
BSA	Bovine serum albumin
DAP	Diaminopimelate
EDTA	Ethylenediaminetetraacetic acid
GlcNAc	*N*-acetylglucosamine
IMAC	Immobilized metal affinity chromatography
IPTG	Isopropyl β-D-1-thiogalactopyranoside
LPS	Lipopolysaccharide
LT	Lytic transglycosylases
LB	Luria-Burtani
MBOAT	Membrane-bound *O*-acetyltransferase
MurNAc	*N*-Acetylmuramic acid
MSRA	Methicillin-resistant *Staphylococcus aureus*
MH	Muller-Hinton
NBT	Nitro blue tetrazolium
NTA	Nitrilotriacetic acid
OafA	O-Antigen acetyltransferase-fused A
OafB	O-Antigen acetyltransferase-fused B
OAP	*O*-Acetylpeptidoglycan

OatA	*O*-Acetyltransferase A
PBP	Penicillin-binding protein
PBS	Phosphate buffered saline
PCR	Polymerase chain reaction
PatA	Peptidoglycan *O*-acetyltransferase A
PatB	Peptidoglycan *O*-acetyltransferase B
PG	Peptidoglycan
PgdA	PG *N*-deacetylase
pNP-Ac	*p*-Nitrophenyl acetate
SB	Super Broth
SDM	Site-directed mutagenesis
SDS-PAGE	Sodium dodecyl sulfate-polyacrylamide gel electrophoresis
TBS	Tris-Buffered Saline
TBST	Tween-20 Tris-buffered saline
TB	Terrific Broth
UDP	Uridine diphosphate
UndP	Undecaprenyl phosphate
WTA	Wall teichoic acid
WT	Wild-type

Introduction

1.1 Antibacterial resistance

Overuse of common antibiotics has led to the development of antibiotic resistance among previously treatable pathogens. The mechanisms that lead to the rise of antibiotic resistance include sharing of antibiotic resistance genes through horizontal gene transfer, secondary mutations that preserve the usefulness of antibiotic resistance genes when faced with newer modified antibiotics [1–3]. Another instance of the generation of new resistance mechanisms are the multi-drug efflux pumps that have been found in many non-antibiotic producing bacteria [1–3]. These pumps may have originated from efflux pumps used, for example, for cell signaling [1–3]. Over time, bacteria that were previously easily treated by multi-target antibiotics, such as the β-lactams, have continued to grow more resistant prompting the search for new antibiotics [1–3].

Methicillin-resistant *Staphylococcus aureus* (MSRA) has garnered great concern in the recent past and it is one of the most common causes of nosocomial infections. Methicillin resistance in *S. aureus* surged after the introduction of the penicillin to the clinic. This selected for *S. aureus* that had acquired the gene, *mecA,* from a mobile genetic element which encodes a penicillin-binding protein (PBP) that is not inhibited by penicillins [4,5]. MRSA would typically be treated with vancomycin, but since the early 2000s, cases of vancomycin resistance in *S. aureus* increased, prompting the need for new antibiotics[6,7]. The same is true for the Gram-negative bacterial pathogen, *Neisseria gonorrhoeae,* where it was found that resistance to the common antibiotics used for its treatment (azithromycin, fluoroquinolones, and the cephalosporin, cefixime) had been acquired [7].

1.2 Peptidoglycan structure and significance

Peptidoglycan (PG) plays a very significant role in the survival of bacteria. PG serves to resist the osmotic "turgor" pressure that results from the high solute concentration of the cell's cytoplasm[8]. PG is a polymer that comprises the cell wall of almost all prokaryotic cells. It is made of repeating units of *N*-acetylglucosamine (GlcNAc) and *N*-acetylmuramic acid (MurNAc) that are linked together via β-1,4 linkages [9]. In all Gram-negative, and some Gram-positive bacteria, the glycan strands terminate with 1,6-anhydroMurNAc residues, while in other Gram-positive bacteria, PG strands end with reducing GlcNAc or MurNAc residues[10]. This variation in the resultant PG of Gram-positive and Gram-negative bacteria is a consequence of the autolytic enzymes used in cell wall biosynthesis and recycling of both Gram-positive or Gram-negative bacteria (discussed below). These repeating units of GlcNAc and MurNAc form strands that are linked together through interacting stem peptides that extend from MurNAc residues. The variance of these stem peptides leads to over 50 different variations of the complete of PG sacculus [11].

Stem peptides are bound to the C-3 D-lactyl group of MurNAc residues and they are made up of D- and L- amino acid isomers [10]. The general structure of stem peptides initially synthesized in Gram-negative bacteria is L-Ala-γ-D-Glu-*meso*-diaminopimelate (DAP)-D-Ala-D-Ala [10]. When comparing Gram-negative and Gram-positive bacteria, some of the amino acids are more variable than others. For example, the third position is the most variable and is shown to contain a lysine instead of m-DAP in most Gram-positive bacteria, whereas D-alanine in the fourth position is the least variable and it is commonly found there in bacteria [10]. The second position is usually filled by D-glutamate in Gram-negative bacteria but D-isoglutamine in Gram-positive. The

first and fifth positions are relatively consistent with few exceptions [10]. Generally, stem peptides crosslink with each other through the side chain amino group of position three to the backbone carboxyl group of the position four residue of another stem peptide from a separate chain [10]. Gram-positive bacteria follow the same cross-linkage pattern except that they tend to include a "peptide bridge" instead of linking directly, as exemplified by *S. aureus* and *Streptococcus pneumoniae* [11] (Figure 1.1).

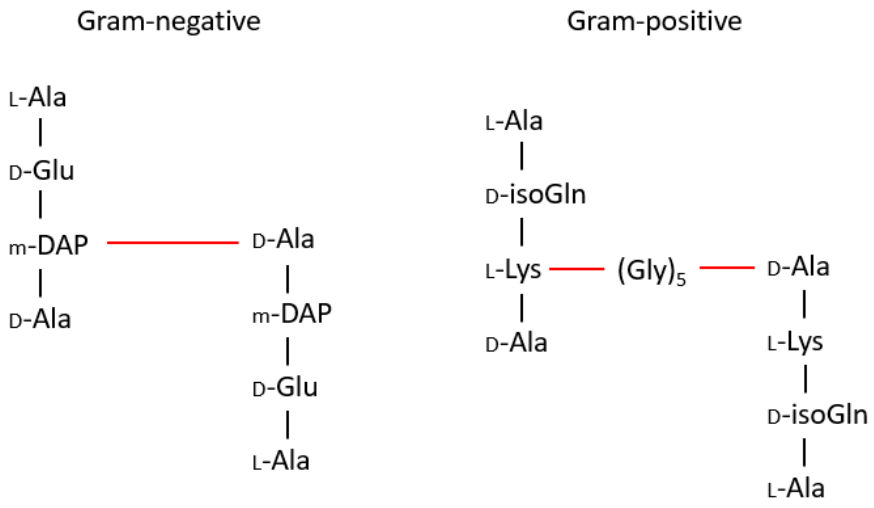

Figure 1.1. **General differences between Gram-negative and Gram-positive stem peptide crosslinking.** In Gram-negative bacteria, the crosslinking will most often occur between the third position (usually m-DAP) on one stem peptide, and the fourth position of the other which is D-alanine. This is similar to Gram-positive bacteria except that there is usually a peptide bridge that exists between the third and fourth cross-linking positions. Also, the third position will most often be L-lysine instead of m-DAP, and the second position D-isoGln instead of D-Glu. The fifth D-Ala residue on stem peptides is cleaved by carboxypeptidases before stem peptide crosslinking.

Gram-negative bacteria have two membranes that sandwich the PG layer and define the periplasm (Figure 1.2), which is a protein-dense intermediary region between the cytoplasm and the outside environment [12]. The inner membrane is made of phospholipids, and while the outer

membrane is similar, the outer leaflet of the outer membrane is primarily composed of lipopolysaccharides (LPS) instead of phospholipids [12]. Given their anionic character, divalent cations, such as Mg^{2+} and Ca^{2+}, serve to stabilize the LPS layer. Consequently, synthetic and natural chelators, such as ethylenediaminetetraacetic acid (EDTA)[13] and lactoferrin[14], respectively, as well as tri-sodium phosphate, serve to permeabilize the outer membrane of Gram-negative bacteria, including that of *Campylobacter jejuni*, *Escherichia coli*, and *Pseudomonas fluorescens*. High concentrations of membrane permeabilizing agents such as 5 mM EDTA cause the death of over 99.95% of bacteria subjected to this treatment, but lower concentrations can instead cause more subtle permeabilization of the outer membrane that keeps the membrane intact and prevents overall lysis as observed when using 2 mM tri-sodium phosphate [15]. To provide additional stabilization, the outer membrane of Gram-negative bacteria is attached to the PG sacculus by a lipoprotein called Braun's lipoprotein [11]. This protein uses the amino group of its C-terminal lysine residue to covalently bind to the backbone carboxyl group of DAP in the stem peptides [9].

In contrast to Gram-negative bacteria, Gram-positive bacteria have a phospholipid bilayer-based cytoplasmic membrane followed by the PG sacculus. The PG sacculus in Gram-negative bacteria is only a few layers thick, whereas in Gram-positive bacteria it has been measured to be between 30-100 nm [12]. Wall teichoic acids (WTA) are only found in Gram-positive bacteria. These WTAs bind covalently through a phosphodiester linkage to the C-2 hydroxyl group of MurNAc residues and serve to reinforce the PG sacculus [12]. Lipoteichoic acids also increase the structural stability of the PG sacculus, but they are bound to the cytoplasmic membrane and stabilize portions of the sacculus that are closest to the cytoplasmic membrane [16] (Figure 1.2).

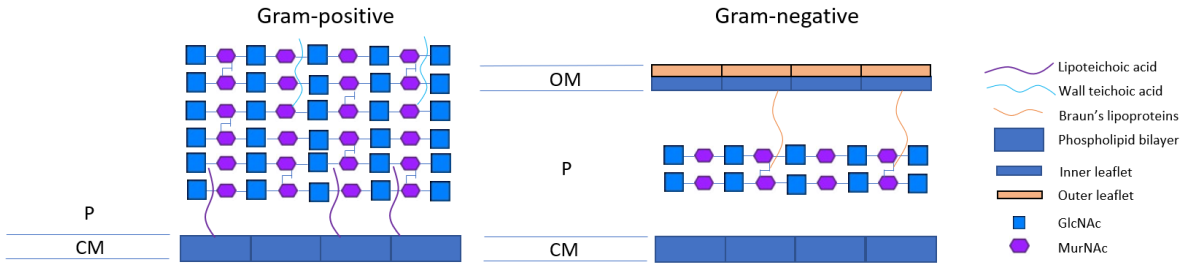

***Figure 1.2*. General structure of Gram-positive and negative cell envelopes.** Gram-positive cells have a thick layer of PG that is reinforced through the addition of wall and lipoteichoic acids. There is only one membrane that lies underneath the PG layer. In Gram-negative bacteria, the PG layer is very thin and is positioned between two different membranes. Braun's lipoprotein is used in gram-negative bacteria to anchor the outer membrane to the PG layer. The outer leaflet differs from the inner leaflet of the outer membrane by its composition where the outer membrane is composed mostly of glycolipids instead of phospholipids. CM, cytoplasmic membrane; OM, outer membrane; P, periplasm.

1.3 PG biosynthesis

The biosynthesis of PG is a complex process. It requires a precursor unit to PG (lipid II) to be produced in the cytoplasm and then translocated across the cytoplasmic membrane where it is added to the growing nascent PG polymer. The generation of lipid II starts with the production of uridine diphosphate (UDP)-GlcNAc from fructose-6-phosphate via the enzymes, GlmS, GlmM, and GlmU in four enzymatic steps, where GlmU catalyzes the last two steps [17] (Figure 1.3). At the same time, the enzymes, MurA and B work together to generate UDP-MurNAc from UDP-GlcNAc[11,17]. The stem peptide is then formed through the actions of MurC, D, E, and F, which sequentially ligate the first three amino acid residues to the C-3 lactyl group of UDP-MurNAc which creates UDP-MurNAc-3p. A D-Ala-D-Ala peptide is synthesized separately and then added to UDP-MurNAc-3P to generate UDP-MurNAc-5P [11,18]. Through the action of MraY, UDP is replaced with undecaprenyl phosphate (UndP) creating UndP-MurNAc-5p or lipid I [11,18]. Lipid II is

finally generated when the GlcNAc residue from UDP-GlcNAc is added by the glycosyltransferase, MurG to UndP-MurNAc-5p forming UndP-MurNAc-5p-GlcNAc [11,18].

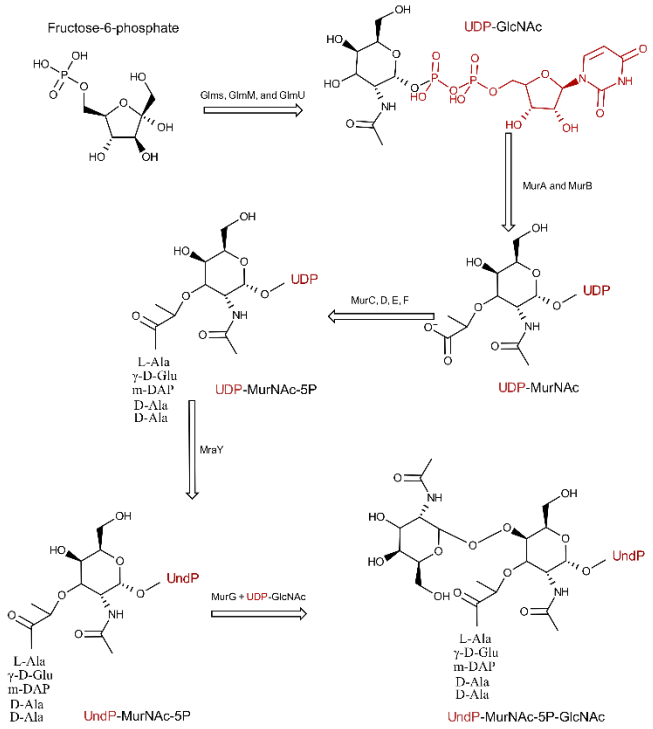

Figure 1.3. **General summary of Lipid II biosynthesis**. This figure was adapted from reference 17.

Until recently, two different enzymes were proposed to translocate lipid II across the inner membrane to its periplasmic face, FtsW and MurJ. Controversy over the involvement of these two enzymes continued for several years until MurJ was finally identified as the "flippase" [19], while FtsW was shown to function as a transglycosylase when complexed with its associated B-class penicillin-binding protein (bPBP; PBPs with only transpeptidase activity) to polymerize PG [19]. In the later stages of PG synthesis, PBPs are used by bacterial cells to both catalyze glycan strand polymerization and cross-linking the stem peptides through transglycosylation and transpeptidation reactions, respectively [20]. Other PBPs function as peptidases to remove terminal D-alanine residues from the stem peptide (DD-carboxypeptidation) and thereby serve to control

the extent of crosslinking [20]. PBPs are used for both cell division and elongation and function in the divisome and elongasome complexes, respectively. These complexes are comprised of the proteins MreB and FtsZ, which also have autolysins included that can lyse PG and make room for the insertion of new flagella, secretion proteins, and pili [11].

1.4 PG degradation

PG is degraded for a few reasons. Bacterial cells, even more so in Gram-negative than Gram-positive, recycle their PG while undergoing cellular division [21]. Although it is currently unknown why cell wall recycling occurs so often, it is hypothesised that an existing PG strand serves as a template for the formation of new PG before the former is removed and its constituents recycled [21]. Also, the cell wall fragments that are released during PG hydrolysis may be used to communicate within bacterial colonies, but they also alert the host immune system to the bacterial presence [22]. In Gram-negative bacteria, these fragments are released as anhydro-muropeptides and in Gram-positives they are released as simple muropeptides [11]. One reason for this difference is that anhydro muropeptides are moved from the periplasm to the cytoplasm through the AmpG permease transmembrane protein in Gram-negative bacteria, and there has been no recorded orthologue of this enzyme in Gram-positive bacteria [22]. This could mean that there would be less use for developing these anhydromuropeptides for cell wall recycling in Gram-positive bacteria [22].

Autolysins are important proteins in the process of cell wall recycling. They ensure that there is space to insert new surface proteins. One class of autolysin is the lytic transglycosylases (LTs), which despite their mechanism of action are nonetheless members of the glycoside hydrolase

family of enzymes [23–27] (http://www.cazy.org/)[28]. LTs cleave the β-1,4 linkage that binds MurNAc to GlcNAc [22] with the formation of I,6-anhydroMurNAc termini [19] (Figure 1.4). LTs can recycle PG

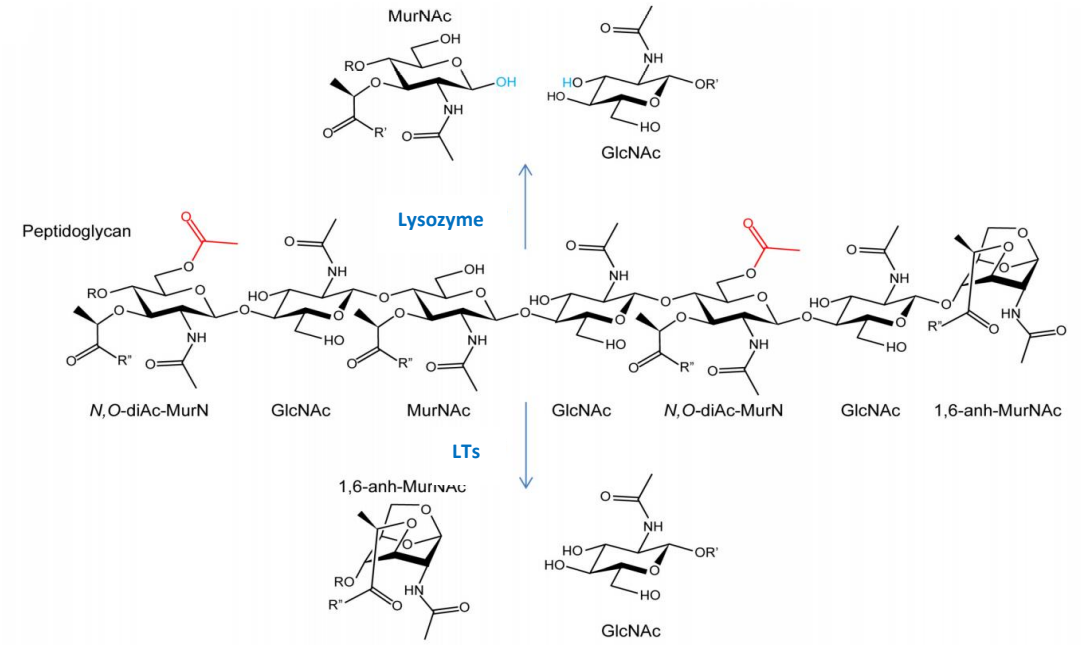

Figure 1.4. **PG lytic reactions catalyzed by lytic transglycosylases (LTs) and lysozyme.** The non-hydrolytic mechanism of LTs generates the 1,6-anh-MurNAc residues that are most often seen in Gram-negative bacteria. The hydrolytic mechanism of lysozyme hydrolyzes the β-1,4-glycosidic linkage and produces MurNAc and GlcNAc. The O-acetylation of the C-6 hydroxyl group of MurNAc, shown in red, protects against the activity of these enzymes.

by promoting glycosidic cleavage using their critical Glu or Asp catalytic residue as a general-acid proton donor which can donate a proton to the oxygen that comprises the β-1,4-glycosidic link between GlcNAc and MurNAc [21]. The component proton of the C-6 hydroxyl group of MurNAc is then abstracted by the now basic catalytic Glu or Asp which reprimes the active site of the LT and permits the intramolecular nucleophilic attack leading to the formation of the 1,6-anh-MurNAc (Figure 1.5) [21]. Bacteria, such as *N. gonorrhoeae*, produce many different LTs, in this case, five, that work in concert with different PBPs for the purpose of cell wall recycling [22]. Overexpression or deletion of the encoding genes causes cell death and so gene expression is tightly controlled [22].

The immune response in host organisms can be triggered by the bacterial anhydromuropeptides that are released by the actions of LTs. This can lead to the recruitment of lysozymes by the host organisms to destroy the pathogen. Defensins and lactoferrin are also used to help lysozyme move through the outer membrane of Gram-negative bacteria and access PG [11]**.** Lysozyme is similar to LTs, where they cleave β-1,4 linkages of PG, but lysozyme uses a hydrolytic mechanism that creates MurNAc residues instead of 1,6-anhMurNAc [29]. The most commonly proposed hydrolytic mechanism of hen egg white lysozyme (HEWL) begins with the

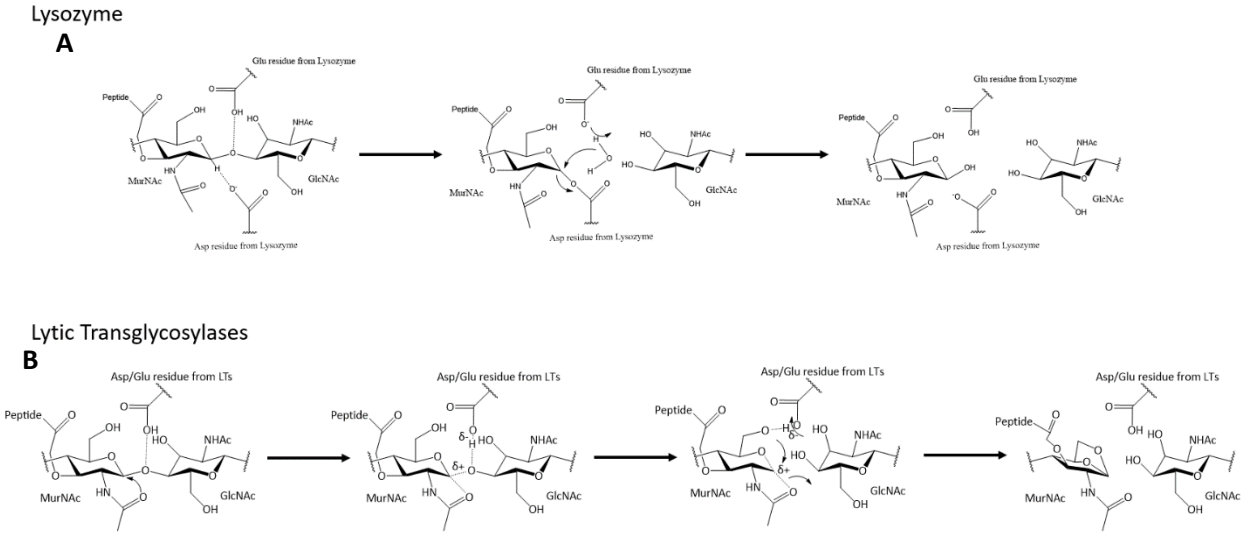

***Figure 1.5*. General mechanism of lysozyme and LTs.** The mechanism of lysozyme (A) was adapted from reference 14. A catalytic Glu residue in lysozyme will donate a proton to the glycosidic ester while the catalytic Asp residue stabilizes a transition state by binding to the C-1 of MurNAc. A proton from a water molecule is abstracted by the catalytic Glu residue to replenish it to its active state. The associated hydroxide now forms by proton abstraction by Glu and replenishes the catalytic Asp residue. A hydroxyl group is left behind on the C-1 position of MurNAc (A) The mechanism of LTs (B) was adapted from reference 22. The catalytic Glu or Asp residue donates a proton to the glycosidic ester bond between MurNAc and GlcNAc to facilitate the first transition state. The negatively charged oxygen then binds to the C-6 hydroxyl group which facilitates the second transition state. The proton from the C-6 hydroxyl group is abstracted by the catalytic Glu/Asp, which causes the now negatively charged oxygen bound to C-6 to bind to the positively charged C-1 carbon and form the 1,6-anhMurNAc product.

donation of a proton by catalytic a Glu35 residue to the oxygen of the glycosidic linkage between MurNAc and GlcNAc. This facilitates nucleophilic attack by Asp52 resulting in bond cleavage and formation of a covalent intermediate. Deprotonated Glu35 then acts as a base to abstract a

proton from water, and the resulting hydroxide attacks the covalent linkage of the MurNAc-Asp52 intermediate releasing the hydrolytic product [14] (Figure 1.5).

Low concentrations of lysozyme can usually be used to lyse Gram-positive bacteria due to their exposed PG sacculus. Gram-negative bacteria avoid immediate lysis by lysozyme due to the shielding of their PG sacculus by their outer membrane [14]. This natural defense mechanism of Gram-negative bacteria can be circumvented by permeabilizing the outer membrane with different chemicals, natural or synthetic, as mentioned previously in section 1.2.

1.5 PG modifications

PG can host a wide range of modifications that increase cellular viability by generating resistance to host immune functions and regulating the anabolism and catabolism of PG. The addition or subtraction of acetyl moieties to PG has been a topic of study for a very long time. For example, the N-deacetylation of GlcNAc residues has been observed in Gram-positive pathogens, such as *S. pneumoniae* [30], *Bacillus cereus* [31], and *Bacillus anthracis* [32]. Incubating fragments of PG with acetic anhydride, which N-acetylates GlcNAc residues, has been shown to increase lysozyme susceptibility in tested PG fragments [31–33]. The de-N-acetylation of GlcNAc residues has since been observed in other pathogenic organisms, such as *Enterococcus faecalis* [34] and *Streptococcus suis* [35], among others.

O-Acetylation of the C-6 hydroxyl group of MurNAc residues (Figure 1.4) was first observed in *Streptococcus faecalis* [36] and *Micrococcus luteus* [37], and it is a notable modification because it has been shown to help pathogens increase their resistance to lysozyme. Later, it was observed directly that O-acetylated PG is resistant to lysozyme [8,38]. The *O*-acetyl modification inhibits lysozyme binding by sterically hindering the productive binding of PG at the lysozyme active site

[39]. PG O-acetylation is now known to occur in many Gram-positive and Gram-negative bacteria [19]. Interestingly, when observing the amount of O-acetylation in different staphylococcus species, O-acetylated PG was found to be specific to pathogenic staphylococci [40], providing insight into how important this modification is for pathogenicity. This modification also regulates the recycling of cell walls and has been shown to be present on approximately 20-70% of MurNAc residues in pathogenic bacteria [8,41].

The pathway for PG O-acetylation was investigated initially through pulse-chase experiments following PG metabolites with *Proteus mirabilis* [42] and *S. aureus* [43] where new non-acetylated PG subunits were observed to be incorporated into the already *O*-acetylated polymer and then were acetylated themselves. Initially, it was hypothesized that the source of the acetate for O-acetylation came from the *N*-2 position of GlcNAc or MurNAc which would be transferred by an unknown acetyltransferase to the C-6 position of MurNAc [8,41]. However, more recent evidence does not support this mechanism, and it is now proposed that acetyl groups are translocated from a cytoplasmic source across the cytoplasmic membrane for addition to MurNAc residues within the cell wall (discussed more in section 1.6).

1.6 PG O-acetylating enzymes

Peptidoglycan *O*-acetyltransferase A (PatA) and PatB in Gram-negative bacteria and *O*-acetyltransferase A (OatA) in Gram-positive bacteria are responsible for O-acetylating PG (Figure 1.6) [11]. OatA was first identified in *S. aureus* [44], and it was named so based on its ability to acetylate disaccharide peptides. OatA is a bi-modular integral membrane protein with an N-terminal membrane-spanning domain that is recognized as a member of the acetyltransferase 3

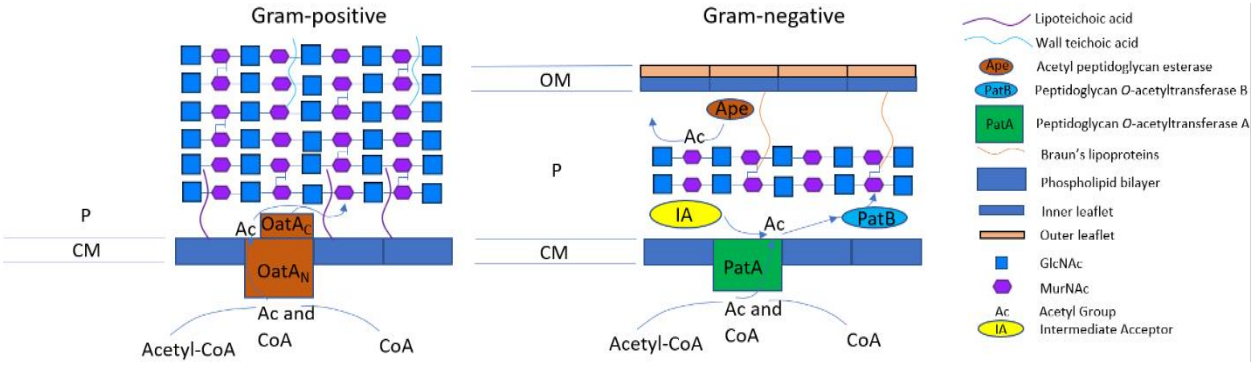

***Figure 1.6*. The pathways for PG O-acetylation involving the *O*-acetyl transferases PatA, PatB, OatA, and acetyl peptidoglycan esterase (Ape).** In Gram-positive bacteria, the N-terminal domain of OatA is postulated to take acetyl groups from acetyl donors and translocate them across the cytoplasmic membrane to the C-terminal domain for addition to PG. In Gram-negative bacteria, two distinct enzymes, PatA and PatB, catalyze these functions, respectively. Whether the acetyl group is passed directly between the two, or a periplasmic carrier is involved is not known. Ape functions in Gram-negative bacteria to remove acetyl groups for cell wall recycling.

(AT3) protein family and a C-terminal extracellular domain that belongs to the SGNH/GDSL protein family[11,45]. The structure of the C-terminal domain of OatA ($OatA_C$) from *S. aureus* (*Sa*$OatA_C$)[46] and *S. pneumoniae* (*Sp*$OatA_C$)[46] was solved and the artificial substrates 4-methylumbelliferyl-acetate (4MU-Ac) and *p*-nitrophenyl acetate (pNP-Ac) were used to characterize the kinetics of $OatA_C$[46–48]. $OatA_C$ exhibits a preference for chitooligosaccharide acceptor substrates containing four or more subunits, and when the acceptor substrate, muroglycan-5p (GlcNAc-MurNAc-*L*-Ala-D-Glu-*L*-Lys-D-Ala-D-Ala), is incubated with *Sa*$OatA_C$ and *Sp*$OatA_C$, preference for the O-acetylation of muroglycans with pentapeptide stems and tetrapeptide stems is observed, respectively [47]. Furthermore, it was determined that $OatA_C$ uses its Ser-His-Asp catalytic triad, which is common to SGNH family proteins, to transfer acetyl groups to the C-6 hydroxyl group of MurNAc residues [46–48]. Additional enzyme kinetic studies using *Sp*$OatA_C$ found that a ping-pong bi-bi catalytic mechanism was used in the O-acetylation of PG [48]. Essentially, $OatA_C$ proceeds to transfer acetyl groups that it receives from the AT3 domain to the C-6 hydroxyl group of MurNAc [48]. Other proteins that are a part of the AT3 family have been proposed to move acetyl groups across the plasma membrane as well. Instances of this function

have been observed in a few cases such as the gene product of *nodX* in *Rhizobium leguminosarum biovar viciae*, which also belongs to the AT3 family and is involved in producing nodulation factors that can bypass the nodulation resistance of Afghanistan peas [50]. This is achieved by NodX O-acetylating the C-6 hydroxyl group of nodulation factors that are primarily composed of 4 or 5 GlcNAc residues [51]. Another instance of AT3 activity includes the O-acetylation of the O-antigen in *Salmonella enterica* by the bi-modular integral membrane proteins, O-antigen acetyltransferase-fused A and B (OafA and B)[52]. OafA and B have been proposed to translocate an acetyl group across the plasma membrane using the AT3 domain over to the fused SNGH/GDSL hydrolase domain [52]. Recently, full-length OatA was shown to transfer acetyl groups from acetyl-CoA to pentaacetyl-chitopentaose (G5) *in vitro*, while the N-terminal AT3 or C-terminal SGNH domains could not do so individually [49]. This evidence suggested that acetyl-CoA could be utilized as a source of acetyl groups for the O-acetylation of PG in Gram-positive pathogens and that the AT3 domain of OatA was needed for this purpose.

PatA and PatB were identified within *N. gonorrhoeae* strain FA1090 as being responsible for PG O-acetylation in Gram-negative bacteria [53,54]. In particular, PatA was designated as part of the membrane-bound *O*-acetyltransferase (MBOAT) protein family [54], and PatB as an SGNH/GDSL hydrolase [55] similar to $OatA_C$ [55]. The genes encoding PatA and PatB exist within a group of three genes that was named the *O*-acetylpeptidoglycan (OAP) gene cluster [54] because these genes were shown to be involved in the O-acetylation of PG [54]. The genes within the OAP cluster were named *pacA* and *pacB* by Dillard and Hackett (2005) while leaving the third gene unnamed. At the same time, these genes were also named peptidoglycan *O*-acetyltransferase (*pat*), *O*-acetylpeptidoglycan esterase 1 (*ape1*), and *ape2* by Weadge and coworkers (2005). PatA was

found to be homologous to the MBOAT protein, AlgI in *Pseudomonas aeruginosa* [54]. AlgI is responsible for O-acetylating alginate, an additional cell wall polymer found in this bacteria [56]. There was speculation that O-acetylation of PG was carried out involving a two-protein mechanism similar to the O-acetylation of alginate in *P. aeruginosa* [53,54], when Ape2 was discovered to function as an *O*-acetyltransferase; it was renamed PatB. PatB activity *in vivo* was found to be dependent on an integral membrane protein, which was assumed to be PatA, that could translocate acetyl groups across the cytoplasmic membrane into the periplasm [57]. Later, PatA and PatB were conclusively shown to work in conjunction within *N. meningitidis*, while the esterase Ape1 was shown to be nonessential to growth *in vitro* [58]. PatA was also shown to be important in conferring resistance to lysozyme in *Helicobacter pylori* and demonstrated that without PatA and an *N*-deacetylase protein, PG *N*-deacetylase (PgdA), PG from *H. pylori* would be five times more susceptible to PG degradation by the action of lysozyme [59]. A combination of knockout mutations of *patA, patB, and ape1* in *N. meningitides* confirmed that the combination of PatA, PatB, and Ape1 were required for proper O-acetylation of PG [58].

Progress has been made in characterizing the function of PatB from *N. gonorrhoeae* (*Ng*PatB) through enzyme kinetic analyses. Using the chromogenic artificial substrate, *p*NP-Ac, and monitoring the release of the product, *p*-nitrophenol, the first Michaelis-Menten kinetics for the enzyme were recorded [60]. The assay accounted for spontaneous hydrolysis of *p*NP-Ac by incubating it alone and with chitotriose sugar substrates, which demonstrated no increase in spontaneous hydrolysis [60]. When *Ng*PatB was incubated with *p*NP-Ac and chitotriose as the acceptor substrate, the production of *p*-nitrophenol increased. The first recorded enzyme kinetic values for the transacetylation of acetyl groups from *p*NP-Ac to chitotriose via *Ng*PatB were

determined to be K_{cat} of 0.74 s^{-1}, K_M of 2.63 mM, and a K_{cat}/K_M of 280 $M^{-1}s^{-1}$ [60]. Further insights into the substrate specificity of *Ng*PatB were gained when multiple acetyl donors for *Ng*PatB were tested against oligomers composed of alternating MurNAc and GlcNAc residues (muroglycans) with varying degrees of stem peptide polymerization [61]. *Ng*PatB preferred to O-acetylate muroglycans with attached tetrapeptide stems, while was only weakly active on muroglycans with attached tripeptide stems [61]. *Ng*PatB also showed preference for chitooligosaccharides that contained five or six subunits as opposed to four subunits or less [61]. PatB possesses the Ser-His-Asp catalytic triad that is common in SGNH/GDSL hydrolases, and it was proposed to operate using a ping-pong bi-bi catalytic mechanism [62], similar to $OatA_C$.

The search for potential inhibitors of *Ng*PatB and *Sa*$OatA_C$ started with success when benzothiazolyl-pyrazolo-pyridine was shown to reduce the growth of *N*. *gonorrhoeae* by 90%, although the concentration that was used was almost at its solubility limit [63]. The coumarin-based inhibitors, esculin, esculetin, and scopoletin were also shown to have inhibitory effects on both *Ng*PatB and *Sa*$OatA_C$ *in vitro* [63]. Esculin and scopoletin could not inhibit the growth of *S. aureus* and *N. gonorrhoea* colonies, but there was success with esculetin, which reduced the growth of *N. gonorrhoea* and *S. aureus* colonies by 25% and 10%, respectively [63]. However, esculetin also reduced the growth of *E. coli* colonies, which hinted at additional unrecognized targets that this inhibitor may affect [63]. To proceed with a thorough analysis of new antibiotic targets, more information will be needed on the N-terminal domain of OatA and PatA. This will allow for more comprehensive searches for potential inhibitors of the O-acetylation system.

1.7.1 Thesis statement

Not much is known about the structure and function of PatA, including information that would be useful for proving the principle that this integral membrane protein is a viable antibiotic target. Even the source of acetyl groups and how it is translocated across the membrane remains unknown. Furthermore, without any evidence of direct association between PatA and PatB, it could also be possible that there is an intermediary carrier molecule that would accept the acetyl group and make it available to PatB. Previous work in the Clarke laboratory involved structural predictions of PatA from *N*. *gonorrhoeae* (*Ng*PatA) using Phyre2 one-to-one threading [64,65]. According to the prediction based on the MBOAT protein DltB from *S. thermophilus* (PDB 6BUH) as the template, *Ng*PatA would have a conserved catalytic core that forms a funnel-shaped tunnel [65]. The overall structure as predicted by the topology prediction program, CCTOP, showed 11 transmembrane domains with the N-terminus situated in the cytoplasm and the C-terminus in the periplasm. The overall predicted structure of *Ng*PatA was quite different from the CCTOP prediction where the Phyre structure did not model the last 87 residues of *Ng*PatA that are supposed to form two transmembrane helices [65]. Being apparently unique to PatB, it was hypothesised that the C-terminus could be involved in associating PatA with PatB or to an intermediary acceptor molecule [65]. However, the topology predictions can be inaccurate, and a significant amount of weight should not be put on their accuracy. Indeed, the topology prediction of the N-terminal region of OatA produced an inaccurate 2D representation when compared to the PhoA-LacZα fusion map [66]. With DltB, the topology map generated by the program, TOPCONS [67], predicted five fewer helices than experimentally observed in the crystal X-ray structure (Figure 1.7).

Work was initiated to clone and express *patA* from both *P. mirabilis* and *C. jejuni,* as this was the original goal of the project. As time progressed and more expression conditions were exhausted, effort was redirected to characterize functional residues of *CjpatA,* specifically using an *in-situ* assay while work progressed on developing strategies to properly express and produce PatA homologues in a unified effort by other members of the lab. A bioinformatics approach was adopted to identify potential substrate-binding and catalytic residues in PatA for their subsequent replacement by site-directed mutagenesis (SDM) of the *patA* gene. Success with this approach would provide preliminary evidence in support of a postulated mechanism of action.

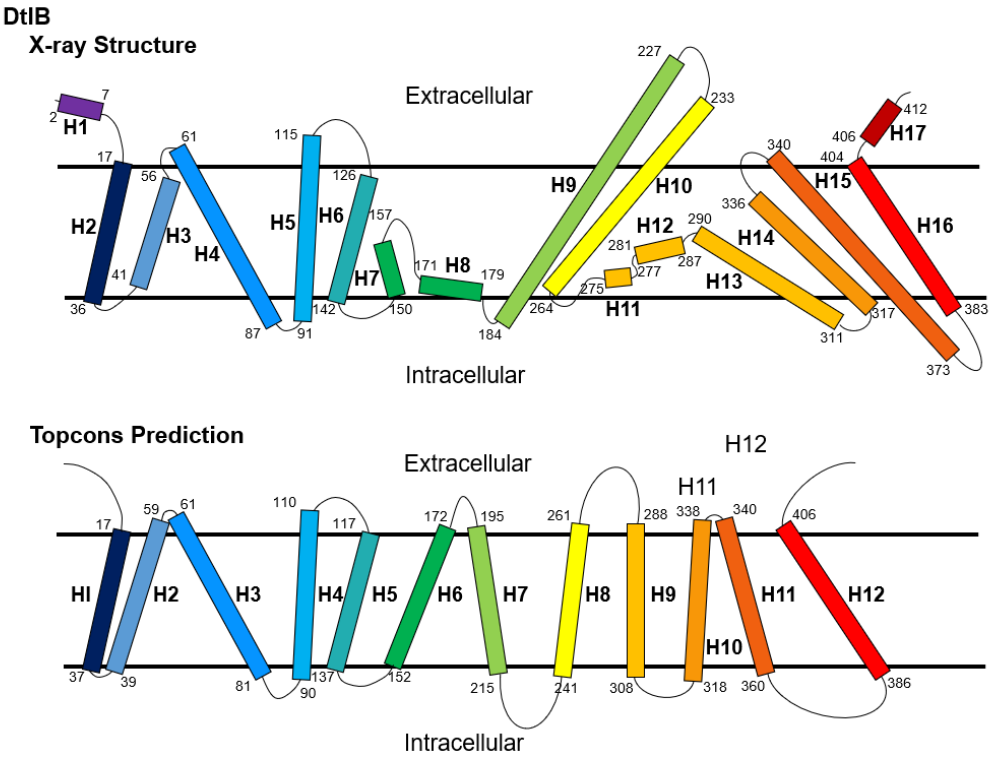

***Figure 1.7*. Comparison of the prediction of DltB by the Topcons topology prediction program [49] with the topology map of the crystal structure.** The prediction is more organized but fewer helices were predicted in total than what is shown by the crystal structure. The prediction also did not correctly predict the occurrence of the two extracellular helices, or that some of the helices are not present on both sides of the plasma membrane.

1.7.2 Hypothesis

Based on the limited data available to date on the structure and function of PatA homologues, and its paralog in Gram-positive bacteria OatA, I hypothesize that the invariant residues in *Cj*PatA, which are positioned appropriately in hypothetical models of PatA structures will serve as critical residues in the catalytic mechanism of *Cj*PatA. These findings could then be extrapolated to all other PatA homologues. A decrease in the O-acetylation of the C-6 hydroxyl group of MurNAc and an increase in *C. jejuni* 81-176's lysozyme and LT sensitivity will directly correlate with the replacement of these residues.

1.7.3 Objectives

To determine what residues of *Cj*PatA are of great importance for the catalytic mechanism, I proposed to identify possible catalytic residues of *Cj*PatA and test the significance of the residues through *in situ* assays. To this end, I proposed to:

1. Identify functional residues using bioinformatic processes
2. Use site-directed mutagenesis to replace proposed functional residues of *Cj*PatA
3. Test the *C. jejuni* mutants using two *in situ* assays that depend on lysozyme resistance and resistance to cell wall recycling that is mediated by LTs
4. Test directly the percent O-acetylation of MurNAc residues in the *C. jejuni* 81-176 mutants.

Methods

2.1 Bacterial strains and growth conditions

The bacterial strains used in this work are listed in Table 2.1. *E. coli* was grown in Luria-Burtani (LB; Difco, Detroit, MI) media with shaking or on LB agar at 37 ^{O}C or 15 ^{O}C. Growth of *C. jejuni* strains was conducted differently as they are microaerophilic and are susceptible to lysis at temperatures below 37 ^{O}C [68]. Thus, *C. jejuni* strains were grown on Muller-Hinton (MH; Difco, Detroit, MI) agar plates incubated within airtight containers with a lit candle to create a microaerophilic environment. A wet paper towel was folded into a corner of the jar to help generate a humid environment for optimal cell growth. MH broth cultures of *C. jejuni* strains were incubated in 15 mL conical tubes (FroggaBio, Concord, ON), 10 mL test tubes, or 1 mL cuvettes without lids while in the airtight containers at 37 ^{O}C with light agitation. Larger volumes of *C. jejuni* and volumes requiring constant monitoring of growth were grown in MH broth supplemented with 0.0022% (*w/v*) sodium bicarbonate. The resulting increased percentage of carbon dioxide in the contained atmosphere allowed for the effective growth of *C. jejuni* strains. *E. coli* and *C. jejuni* strains with resistance to specific antibiotics were grown on plates or in broth that were supplemented with the following antibiotics, alone or in combination as required: Ampicillin (50 μg/ml), Kanamycin (50 μg/ml), Trimethoprim (10 μg/ml; *C. jejuni* strains only), Vancomycin (5 μg/ml; *C. jejuni* strains only), and Chloramphenicol (16-25 μg/ml).

Table 2.1: Bacterial strains

Bacterial Strain	Description/Genotype	Reference
E. coli C43 (DE3)	Used in attempts to express *PmpatA* and *CjpatA*. F – ompT hsdSB (r_B- m_B-) gal dcm (DE3)	[69] Sigma Aldrich
E. coli DH5α	Used in cloning procedures and in the replication and harvesting of plasmids. F– ϕ80lacZΔ M15 Δ (*lacZYA-argF*) *U169 recA1 endA1 hsdR17* (rK– mK+) *phoA supE44* λ- *thi–1 gyrA96 relA1*	ThermoFisher Scientific
E. coli BL21 (DE3)	Used in attempts to express *PmpatA* and *CjpatA*. F– *omp*T *hsdS*$_B$ (r_B^-, m_B^-) *gal dcm* (DE3)	Thermofisher Scientific
E. coli BL21 (pLysS)(DE3)	F$^-$*omp*T *hsd*SB (r_B^-, m_B^-) *gal dcm rne*131 (DE3) pLysS (Cam^R)	ThermoFisher Scientific
C. jejuni 81-176	Human pathogenic variant of *C. jejuni*.	[70]
C. jejuni 81-176 Δ*patA*	*patA* knockout variant of *C. jejuni* 81-176 with *patA* replacement with *kan*^{r}.	[70]
C. jejuni 81-176 Δ*patA*$_C$	*C. jejuni* 81-176 *patA* knockout variant with *cat* and *patA* recombined back into one of three different rRNA intergenic sites.	[70]
C. jejuni 81-176 Δ*oap*	*oap* operon knockout variant of *C. jejuni* 81-176 with the *oap* operon replaced with *kan*^{r}.	[70]
C. jejuni 81-176 Δ*oap*$_{C\ (CjpatA\ +\ B)}$	*C. jejuni* 81-176 *oap* operon knockout variant with *cat*, *patA*, and *patB* recombined back into one of three different rRNA intergenic sites.	This study
S122A	Variant of *C. jejuni* 81-176 Δ*oap*$_{C\ (CjpatA\ +\ B)}$ encoding (S122A)PatA.	This study
R164A	Variant of *C. jejuni* 81-176 Δ*oap*$_{C\ (CjpatA\ +\ B)}$ encoding (R164A)PatA.	This study
H275A	Variant of *C. jejuni* 81-176 Δ*oap*$_{C\ (CjpatA\ +\ B)}$ encoding (H275A)PatA.	This study
R283A	Variant of *C. jejuni* 81-176 Δ*oap*$_{C\ (CjpatA\ +\ B)}$ encoding (R283A)PatA.	This study
H315A	Variant of *C. jejuni* 81-176 Δ*oap*$_{C\ (CjpatA\ +\ B)}$ encoding (H315A)PatA.	This study

2.2 Cloning methods:

2.2.1 Polymerase chain reactions and site-directed mutagenesis

The plasmids used in this study are listed in Table 2.2. Primers listed in Table 2.3 were prepared by Integrated DNA Technologies (San Diego, CA; idtdna.com). Chromosomal or plasmid DNA was extracted from the various species of bacteria listed in Table 2.1 using a DNeasy Blood & Tissue Kit (Qiagen Inc. Canada, Montreal, PQ) or a GeneJET PCR purification Kit (Thermo Fisher Scientific, Mississauga, ON). All polymerase PCR and SDM attempts were carried out using the primers listed in Table 2.2 combined with KAPA HIFI Polymerase, KAPA HIFI Buffer, and DNTPs supplied (Kapa Biosystems Inc., Wilmington, MA). After attempts with SDM, template DNA was digested using 1 µL of *DpnI* restriction digest enzyme for 1 h at 37 ^{O}C. Reactions with *DpnI* were combined with 5 µL of 5X CutSmart Buffer and DNase free PCR appropriate MQ water (Millipore Canada Ltd., Toronto, ON) to a final volume of 50 µL. After completion of PCR or SDM, products of the reaction were cleaned up using GeneJET PCR purification Kit (Thermo Fisher Scientific, Mississauga, ON). In the case of new plasmids generated by SDM, GeneJET Miniprep Kit (Thermo Fisher Scientific, Mississauga, ON) spin columns were used to better capture the new plasmids. Products of PCR and SDM were analyzed by agarose gel electrophoresis using 1% (*w*/*v*) agarose gels (See section 2.3)

2.2.2 Restriction digestion and ligation

Restriction enzyme digests were performed using enzymes corresponding to the appropriate primers listed in Table 2.2. Restriction enzymes were incubated with 1000 ng of DNA and 5 µL of 5X CutSmart Buffer. The reaction volumes were adjusted to a final volume of 50 µL

using DNase-free MQ water (Millipore Canada Ltd., Toronto, ON). The final reactions were incubated at 37 ^{O}C for 1 h, and then the enzymes were heat inactivated at the specific temperatures and time requirements listed on the manufacturer's website for each enzyme (New England Biolabs (NEB), Whitby, ON). Vectors that were digested with restriction enzymes were subsequently treated with Antarctic phosphatase (NEB, Whitby, ON) by adding 1 µL of the enzyme and 5 µL of the 5X Antarctic phosphatase buffer and incubated for 1 h at 37 ^{O}C. Ligation reactions were performed using T4 DNA ligase and T4 DNA ligase buffer (NEB, Whitby, ON). A 3:1 molar ratio was used in the ligation reactions for insert and vector, respectively. These reactions were then incubated at ambient temperature for 1 h or overnight, and they were then heat-inactivated at 65 ^{O}C for 20 min. For both restriction digests and ligation products, samples were analyzed by agarose gel electrophoresis for confirmation of reaction completion.

2.3 Agarose gel electrophoresis

Agarose gel electrophoresis was used to verify the completion of PCR, SDM, restriction digests, and ligation reactions using 1% (*w*/*v*) gels. Results of the agarose gel electrophoresis were visualized by mixing 5 µL of sample with 1 µL of Sample Dye (Nippon Genetics, Düren, Germany). One lane in the gel was reserved for 1KB DNA Ladder (FroggaBio, Concord, ON) which would also be mixed in the same proportions with the sample dye as a sample to be tested. The sample dye contains a small proportion of MIDORI^{GREEN} Direct stain which allows visualization on a gel doc.

2.4 Transformation of *E. coli*

Various *E. coli* strains were used to propagate newly ligated plasmids or were used in early expression trials of *PmpatA* and *CjpatA*. All transformations of the various *E. coli* strains were

performed using 50 µL of chemically competent aliquots of cells for use in a heat shock transformation. The transformation process started with adding 1 – 5 µL of plasmid DNA to the cells and incubating them on ice for 30 min. Cells were then incubated at 45 ^{O}C for 1 min followed by incubation back on ice for 5 min. After the second incubation on ice, 600 µL of pre-warmed LB broth was added to the cells and the mixture was placed on a nutator for consistent agitation and incubated at 37 ^{O}C for 1 h. The mixture was centrifuged at 4000 x *g* for 2 min and 600 µL of the resulting supernatant was removed by pipette. The cell pellet was resuspended in the remaining 50 µL of solution and plated and LB agar plates with appropriate antibiotics.

2.5 Expression of *PmpatA* and *CjpatA* in *E. coli* strains

E. coli strains (Table 2.1) harbouring one of the *patA* homologue expression plasmids, PACAA1, PACBL1, or PACVP3 (Table 2.3) were induced with appropriate inducer molecule (1 mM Isopropyl β-D-1-thiogalactopyranoside (IPTG) in the case of PACVP3 and PACBL1, or L-arabinose for PACBL1) when cell suspensions were in the exponential phase of growth. In the case of *E. coli* strains harbouring PACVP3 and PACBL1, induction of cells with 1 mM IPTG occurred at various OD_{600} values within the exponential phase of growth in combination with different growth and induction temperatures of 15 ^{O}C, 22 ^{O}C, and 37 ^{O}C. Cell lysate samples were harvested at specific time points after induction as well. Cells were typically grown in high-nutrient broth such as Terrific Broth or Super Broth (Appendix B).

2.6 Protein purification of *Pm*PatA and *Cj*PatA

To purify any recombinant PatA, *E. coli* strains expressing *patA* and grown in high-nutrient broth were collected by centrifugation at 11 000 x *g* for 15 min at 4 ^{O}C and subsequently resuspended in pH 7.0 lysis buffer (Appendix B). After mixing the solution with the cell pellet for approximately 1 h at 4 ^{O}C on a nutator, the cell suspension was sonicated using 50% amplitude for 10-second pulses followed by 20-second pauses. The cell lysate was subjected to centrifugation at 18 500 x *g* to pellet cells that did not lyse and large cellular debris. The supernatant was incubated with cOmplete His-Tag purification resin and wash buffer (Appendix B) for 1 h at 4 ^{O}C with agitation. This allowed any His_6-tagged PatA to become bound to the beads. The beads were packed into a column and approximately 20 mL of the wash buffer was passed through the column four times. After washing the column, any bound PatA was eluted using 3 mL of elution buffer (Appendix B). Elution fractions were subjected to sodium dodecyl sulfate-polyacrylamide gel electrophoresis (SDS-PAGE) with Western Blot analysis to detect any overproduced PatA.

2.7 SDS-PAGE and Western blot

SDS-PAGE was performed to separate proteins in cell lysates and pure cellular fractions to detect any overproduced PatA. First, to test cell lysate, samples of whole cells were incubated with a variable amount of X5 SDS sample buffer and boiled at 100 ^{O}C for 20 min. Enough X5 SDS sample buffer was added to reduce the texture of the resulting cell lysate from a globular to a more fluid nature. Samples were applied to 12% polyacrylamide gels during SDS-PAGE and run for approximately 1 h if only one gel was being used in the same container. If two gels were

needed, then a 2 h run time was used. The Plus Protein All Blue Prestained Protein ladder (Bio-Rad, Mississauga, ON) was used to assess apparent molecular weights. After completion of electrophoresis, the contents of the gel were transferred to a nitrocellulose membrane for western blot analysis. The membrane was submerged in a small amount of Ponceau S stain (NEB; Whitby, ON) where only enough of the stain was added so that the surface of the membrane was covered, allowing this staining of any transferred protein to be visualized briefly. The Ponceau S stain was washed away with water and then the blot was rinsed in Tris-buffered saline (TBS) solution until all the stain was washed away. The blot was then submerged in a blocking solution that was commonly 3% bovine serum albumin (BSA) (Wisent Bioproductions, St-Bruno, QC) for 1 h at ambient temperature or overnight at 4 ^{O}C. The blot was then washed in tween-20 TBS (TTBS) twice for 5 min each and incubated with primary mouse anti-His6 antibody, washed again in TBST, then incubated in anti-mouse goat antibody that was conjugated to alkaline phosphatase (Bio-Rad, Mississauga, ON). Blots were then visualized using 5-bromo-4-chloro-3-indolyl phosphate (BCIP)/nitro blue tetrazolium (NBT).

2.8 Growth curves of *E. coli* strains

E. coli strains (Table 2.1) were grown overnight from a single colony or a freezer glycerol stock at 37 ^{O}C with shaking at 200 rotations per min to ensure proper aeration and mixing of the culture over time in LB broth. Cell suspensions were incubated with appropriate antibiotics to select strains harbouring plasmids intended for study. Aliquots of overnight suspension were resuspended in fresh LB to a starting OD_{600} value of approximately 0.05. Cell suspensions were grown at 37 ^{O}C with shaking in the 200 µL wells of a 96-well micro-plate. Measurements of OD_{600} were taken every 10 min using a Synergy H1 microplate reader (BioTek, Santa Clara, CA). Breath-

Easy gas permeable sealing membrane (Diversified Biotech, Boston, MA) was used to seal the wells of the microplate.

2.9.1 Natural transformation of *C. jejuni*

Variants of *C. jejuni* 81-176 were created by naturally transforming the shuttle vector, pRRC [71], or the subsequent derivatives (Table 2.3) into *C. jejuni* 81-176 cells as it is a naturally-competent strain. Before any plasmid was incubated with the cells, they were methylated at *EcoRI* cut sites using *EcoRI* methyltransferase (NEB, Whitby, ON) to allow the natural uptake of the DNA by *C. jejuni* [72]. The pRRC vector had been used previously [70] to introduce complement *oap* operon genes back into the *C. jejuni* chromosome. *C. jejuni* mutants with *patA*, *patB*, and *ape1* knockouts were previously supplied to the Clarke lab for this purpose. The complementation of *oap* operon genes would also allow for selection of these complemented mutants using chloramphenicol [70] (Figure 2.1). Once specific residues were chosen for mutation, the constructs generated through site-directed mutagenesis were reintroduced back into the chromosome using homologous recombination as performed previously [70]. These residues were tested for their importance in the catalytic mechanism *Cj*PatA by a series of *in situ* assays.

To begin naturally transforming *C. jejuni* 81-176 with pRRC and derivatives as described above, an aliquot of cells was grown to approximately 0.5 $OD_{600,}$ and then 1mL of the sample was washed in phosphate-buffered saline (PBS) twice. Cells were subjected to centrifugation at approximately 10 000 x *g* during the wash process, and then they were resuspended in 200 µL of

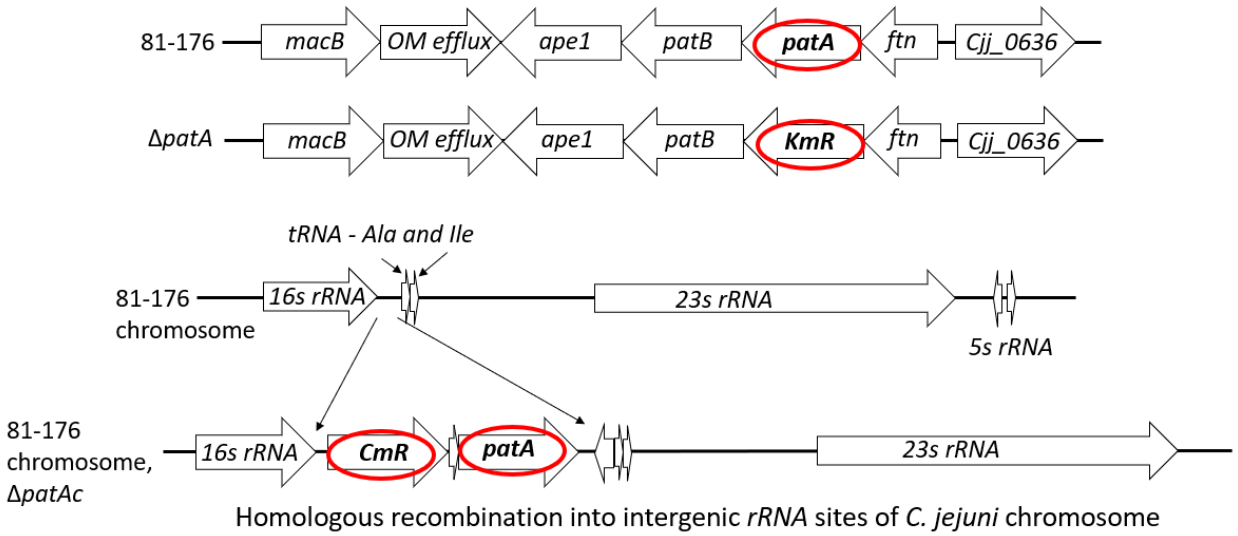

***Figure 2.1*. Illustration of the generation of complement mutants of *C. jejuni* 81-176.** Knockout mutants were supplied by Professor Gaynor (UBC). A Kanamycin resistance cassette was used to knockout a gene of interest in the *oap* operon, in this case *CjpatA*. The gene would be cloned into the pRRC vector which contains complementary regions to rRNA intergenic sites in the chromosome. The upstream chloramphenicol resistance cassette and downstream *CjpatA* are then combined back into the chromosome with homologous recombination. This image was adapted from Ha et al. (2016).

PBS. This cell suspension was spotted three times in 20 µL volumes onto MH agar plates containing 5µg/ml vancomycin and 10 µg/ml trimethoprim. Subsequently, 5-10 µL of approximately 20 ng/µL methylated plasmid was aspirated into each cell suspension spot. The MH agar plates were incubated in air-tight jars with a candle to ensure a microaerophilic environment and left to grow at 37 ^{O}C for 2-5 days or until colonies appeared. Colonies were picked and spread on new MH agar plates with appropriate antibiotics. In all cases, these MH agar plates contained 5µg/ml vancomycin 10 µg/ml trimethoprim, 50 µg/ml kanamycin, and 20 µg/ml chloramphenicol.

2.10 Lysozyme sensitivity and autolysis assay of *C. jejuni* and mutants

Attempts were made to develop an appropriate functional assay to investigate the possible role of specific amino acid residues in *Cj*PatA activity. For a phenotypic assay involving

continuing cell growth, varying concentrations of lysozyme ranging from very low to very high (0.3 – 65 mg/ml) were incubated with *C. jejuni* cells and associated variants. Different incubation times, temperatures, and media were tested to create an identifiable difference in survivability between wild-type (WT), knockout *CjpatA* (Δ*patA*), and complemented *CjpatA* (Δ*patA*c) strains. Later, these assays were attempted with knockout *Cjape1* (Δ*ape1*), knockout *oap* (Δ*oap*), and complemented *CjpatA* and *CjpatB* ($\Delta oap_{C\,(CjpatA+B)}$) strains to create a more identifiable difference in survivability due to the expected larger difference in PG O-acetylation levels. Generally, MH broth was used for these lysozyme assays.

Also, an *in situ* autolysis assay was developed based for use on *N. gonorrhoeae.* [73]. This assay was adapted for *C. jejuni* 81-176 mutants as per the following: cells were obtained by centrifugation at 6,000 x *g,* washed, and resuspended in 0.05M HEPES buffer (Fisher Scientific, Ottawa, ON) prior to the addition of EDTA (4mM or 10mM; Fisher Scientific, Ottawa, ON) to induce autolysis of cells. This autolysis was monitored recording OD_{600} measurements over a period of 2 h, with time points taken every 20 min.

2.10.1 Turbidity assay

Attempts were made to monitor the autolysis of cells turbidometrically. Cells grown to different stages were harvested by centrifugation at forces between 4000 to 6000 x *g* and then resuspended in various media (MH broth, 0.05M Hepes buffer, MQ water, or PBS). Additional compounds, such as membrane permeabilizers (EDTA and lactoferrin **(**Sigma-Aldrich, Darmstadt, Germany)) in the absence or presence of lysozyme were added to the resuspension media, and

measurements of OD_{600} were recorded immediately at steady intervals until increases or decreases in OD_{600} readings diminished in magnitude significantly.

2.10.2 Spot assay

Cultures of *C. jejuni* were grown overnight and the OD_{600} values of 1 mL samples were adjusted to a specific OD_{600} value using fresh MH broth with appropriate antibiotics. These adjusted samples were incubated in conical tubes or 10 mL test tubes for up to 6 h in the absence and presence of various lysozyme concentrations. In some cases, the cultures were supplemented with concentrations of lactoferrin up to 3 mg/ml. All cultures were incubated with agitation at 37 ^{O}C in a low-oxygen environment. After the incubation period, the samples were serially diluted by tenths until a dilution of x 10 000 000 was reached. Volumes of 5 µL from the serial dilutions were spotted onto MH agar plates and then incubated for 2 days at 37 ^{O}C in a microaerophilic environment. The confluence of the growth in each spot for each dilution was compared between samples to see which *C. jejuni* variant was most and least affected by the experimental conditions. Differences in cell survivability could then be attributed to the functionality of the PatA variants.

2.10.3 Plate assay: *C. jejuni* 81-176 strains

Microtitre plate assays were used when consistent OD_{600} measurements were required to analyze growth patterns, resistance to autolysis, and resistance to lysozyme. These assays were conducted using a Synergy H1 microplate reader (BioTek). Like the turbidity assay (Section 2.9.1), samples of *C. jejuni* were grown overnight in MH broth and then the resulting concentration of cells was adjusted to an OD_{600} value of 0.05. Cells were typically resuspended in

MH broth supplemented with appropriate antibiotics, 0.0022% (*w/v*) sodium bicarbonate, and the absence and presence of lysozyme and EDTA if the sample was an experimental sample rather than a control sample. Cells were typically resuspended in 0.05 M HEPES in the case of an autolysis assay and were incubated with EDTA concentrations of 4 mM to 10 mM if it was an experimental sample. All samples were added to the 96-well plate at final volumes of 200 µL. To limit exposure to typical atmospheric air composition, Breath-Easy gas permeable sealing membrane was used once again to seal the wells during incubation and measurement periods.

2.11 Analysis of percent O-acetylation of PG

PG was collected from *C. jejuni* 81-176 strains based on the isolation protocols described by Brott and Clarke[74]. In brief, *C. jejuni* 81-176 strains were grown in 1 L cultures to an OD_{600} below 0.6 to collect cells in exponential phase, which would take approximately 18 hours. Cells were examined for the presence of coccoid cells which would indicate their entry into stationary phase. Cell pellets were washed in 10mM sodium phosphate buffer and then resuspended in 25mM sodium phosphate buffer pH 6.0. This solution was then added to an equivalent volume of 25mM sodium phosphate buffer pH 6.0 containing 8% SDS and then boiled for 2-3 h in round bottom flasks. Cells were washed in sodium phosphate buffer and subjected to ultracentrifugation at 145000 x g for 20 min at 22 ^{O}C to collect PG from samples. This process was repeated until traces of SDS could not be detected using the Stains-All assay[73]. PG samples were incubated overnight at 37 ^{O}C as directed with the addition of 100 µg/ml α-amylase, 10 µg/ml DNase, 50 µg/ml RNase, and 100 µg/ml pronase. This was subsequently boiled in 2% (*w*/*v*) SDS sodium phosphate buffer, collected via ultracentrifugation, and washed in 25mM sodium

phosphate buffer pH 6.0 until traces of SDS were not detected. Samples were lyophilized for storage until required.

Control samples (WT, Δ*patA*$_C$, Δ*oap*, Δ*ape1*, Δ*oap*$_C$) and mutant samples (S122A, R164A, H275A, R283A, H315A) of PG were suspended in 10 µL and 30 µL of 10 mM sodium phosphate buffer for 3 h, respectively, to serve as negative controls for the acetate analysis. Control samples and mutant samples were then suspended in 10 µL and 30 µL of 150mM NaOH for 3 h at 37 ^{O}C, respectively, to release acetate from the suspended PG. Samples were centrifuged at 20 000 x g for 15 min to pellet PG, and the acetate content in the supernatant was subsequently quantified using an Acetic acid quantification kit (Megazyme; Bray, Ireland). PG samples used for the acetate analysis were acid hydrolyzed in 6M HCL at 100 ^{O}C overnight in microcentrifuge tubes *in vacuo*. Muramic acid content in the samples was quantified using High-Performance Anion-Exchange Chromatography with Pulsed Amperometric Detection (HPAEC-PAD). The nanomoles (nmoles) of muramic acid in 10 µL of the acid-hydrolyzed sample were then related to the nmoles of acetate released from the PG samples to determine the percent O-acetylation of the samples.

Table 2.2: Primers used for cloning and site-directed mutagenesis

Primer Name/Melting Temperature (°C) /GC Content %	**Primer Sequence**	**Primer Use**	**Resulting Plasmid**
*Pm*PatA pBAD18-cm FWD *NheI*	5' TGA TGC TAG CAG GAG GTC TAT ATA ATG AAT TTT TTT TCA TTC GAG TTT C 3'	Forward primer used to clone *PmpatA* out of the genomic DNA of *P. mirabilis* with cut site *NheI*.	PACBL1
*Pm*PatA pBAD18-cm REV *HindIII*	5' CAC TAA GCT TTC AAT GGT GGT GGT GAT GGT GAA AGC TGG CAT AAA TAA ATC C 3'	Forward primer used to clone *PmpatA* out of the genomic DNA of *P. mirabilis* with cut site *NheI*.	PACBL1
*Cj*PatA S122A FWD/ 61.0 °C/ 26.7%	5' GAT TTA GTA TTA CCA ATA GGA ATT AGT TTT TAT ACC TTT ACT TCT ATC ACT TAT CTT GTG 3'	Forward primer used to replace Ser122 with Ala in *CjpatA*	PACBL4
*Cj*PatA S122A REV/ 60.6 °C/ 31.3%	5' CAC AAG ATA AGT GAT AGA AAA GGT ATA AAA AGC AAT TCC TAT TGG 3'	Reverse primer used to replace Ser122 with Alain *CjpatA*	PACBL4

*Cj*PatA R164A FWD/ 64.6 °C/ 39.6%	5’ CAC TAC TTT CAG GGC CTA TTA TGG CAA GTT CTT TTT TCT TTG AAC AGG 3’	Forward primer used to replace Arg164 with Ala in *CjpatA*	PACBL5
*Cj*PatA R164A REV/ 64.6 °C/ 39.6%	5’ CCT GTT CAA AGA AAA AAG AAC TTG CCA TAA TAG GCC CTG AAA GTA GTG 3’	Reverse primer used to replace Arg164 with Ala in *CjpatA*	PACBL5
*Cj*PatA H275A FWD/ 64.3 °C/ 36.5%	5’ CCT AAA AGA TTT TTG GGC TAG ATG GGC TAT CAG TCT TTC AAC CTT TAT AAG A 3’	Forward primer used to replace His275 with Ala in *CjpatA*	PACBL6
*Cj*PatA H275A REV/ 64.3 °C/ 36.5%	5’ TCT TAT AAA GGT TGA AAG ACT GAT AGC CCA TCT AGC CCA AAA ATC TTT TAG G 3’	Reverse primer used to replace His275 with Ala in *CjpatA*	PACBL6
*Cj*PatA R283A FWD/ 62.3 °C/ 32.8%	5’ CTA GAT GGC ATA TCA GTC TTT CAA CCT TTA TAG CAG ATT ATA TCT ATA TAC CTT TAG G 3’	Forward primer used to replace Arg283 with Ala in *CjpatA*	PACBL7
*Cj*PatA R283A REV/ 62.3 °C/ 32.8%	5’ CCT AAA GGT ATA TAG ATA TAA TCT GCT ATA AAG GTT GAA AGA CTG ATA TGC CAT CTA G 3’	Reverse primer used to replace Arg283 with Ala in *CjpatA*	PACBL7
*Cj*PatA H315A FWD/ 65.3 °C/ 38.0%	5’ GCT TTT ATA CTT TCA GGT ATG TGG GCT GGC AAT ACA CTT GCT TTT ATT GT 3’	Forward primer used to replace His315 with Ala in *CjpatA*	PACBL8
*Cj*PatA H315A REV/ 65.3 °C/ 38%	5’ ACA ATA AAA GCA AGT GTA TTG CCA GCC CAC ATA CCT GAA AGT ATA AAA GC 3’	Reverse primer used to replace His315 with Ala in *CjpatA*	PACBL8
Cat-2/ 47.3 °C/ 27.3%	5’ GTT TTT TGG ATG AAT TAC AAG A 3’	Forward primer that binds to the 3’ end of the *cat* gene.	None
Ak233/ 55.1 °C/ 40.0%	5’ GCA AGA GTT TTG CTT ATG TTA GCA C 3’	Reverse primer for the first *rRNA* intergenic site. To be used in tandem with a suitable reverse primer.	None
Ak234/ 57.6 °C/ 50%	5’ GAA ATG GGC AGA GTG TAT TCT CCG 3’	Reverse primer for the second *rRNA* intergenic site. To be used in tandem with a suitable reverse primer.	None
Ak235/ 52.2 °C/ 42.9%	5’ GTG CGG ATA ATG TTG TTT CTG 3’	Reverse primer for the third *rRNA* intergenic site. To be used in tandem with a suitable reverse primer.	None
CjPatB Complement FWD NheI/ 67.4 °C/ 43.5%	5’ GCG GCG GCT AGC CTT TTG GGG TTC TTT TTA TGA TCT ATC CTT TA 3’	Primer used to generate a *patB* PCR product with an N-terminal *NheI* cut site.	None
CjPatB Complement REV MfeI/ 67.4 °C/ 43.5%	5’ GCG GCG CAA TTG TGA GTA TGG AAT CTA TTG TGT CAT TTG TAT TTA 3’	Primer used to generate a *patB* or *patA* + *patB* PCR product with a C-terminal M*feI* cut site on PatB.	PACBL8
CjPatA comp FWD NheI/ 66.6 °C/ 45.5%	5’ GCG GCG GCT AGC GGT ATG TAA GCG AAC AAC ACG AA 3’	Primer used to generate a *patA* or *patA* + *patB* PCR product with an N-terminal *NheI* cut site on PatA.	PACBL2 and PACBL8
CjPatA comp rev MfeI/ 64.0 °C/ 37.8%	5’ GCG GCG CAA TTG ACC AAG CCA AGC ACT ATA ATC AAA ATA A 3’	Primer used to generate a *patA* PCR product with a C-terminal *MfeI* cut site.	PACBL2

Table 2.3: Plasmids generated and/or used in this study

Plasmid/Vector Name	Description	Source/Reference
pET-21(a)	A vector containing an IPTG inducible T7 promoter where the addition of IPTG relieves repression of the *lac* operator by the *lac* repressor.	Novagen
pBAD-18cm	A vector containing an L-arabinose inducible P_{BAD} promoter where the addition or absence of L-arabinose promotes or represses transcription, respectively.	[75]
PACAB10	A pET-21(b) vector that contains full-length *N. gonorrhoaea patA* (1-478) fused to a C-terminal His_{10}-tag.	A. Brott
PACVP3	A pET-21(a) vector that contains full-length *P. mirabilis patA* (1-486) fused to a C-terminal His_6-tag.	V. Petrucelli
pRRC	A derivative vector of pGEM-T easy which includes a fragment of rRNA gene cluster (PRR) cloned into the vector in combination with a Cam^r cassette cloned into the PRR region.	[71]
PACAA1	pET-21(a) containing full-length *C. jejuni* 81-176 *patA* (1-459) with a C-terminal His_6-tag.	A. Anderson
PACBL1	pBAD-18cm containing full-length *P. mirabilis patA* (1-486) with a C-terminal His_6-tag.	This study
PACBL2	pRRC vector containing full-length *C. jejuni patA*	This study
PACBL3	pRRC vector containing full-length *C. jejuni patA* and *patB.*	This study
PACBL4	pRRC vector containing full-length *C. jejuni patA* with an S122A mutation and full-length *C. jejuni patB*.	This study
PACBL5	pRRC vector containing full-length *C. jejuni patA* with an R164A mutation and full-length *C. jejuni patB*.	This study
PACBL6	pRRC vector containing full-length *C. jejuni patA* with an H275A mutation and full-length *C. jejuni patB*.	This study
PACBL7	pRRC vector containing full-length *C. jejuni patA* with an R283A mutation and full-length *C. jejuni patB*.	This study
PACBL8	pRRC vector containing full-length *C. jejuni patA* with an H315A mutation and full-length *C. jejuni patB*.	This study

Results

3.1 Expression attempts of *patA* homologues

Preliminary attempts at expressing *patA* were met with some apparent success by a previous master's student, Victoria Petrucelli [65]. Initial data collected from western blots suggested that expression of *patA* resulted in a 37 kilodalton (kDa) band size, while the predicted

size of the protein is 55 kDa. Previous work involving the isolation and purification of the Gram-positive orthologue, OatA, showed that the protein appears lesser in mass by SDS-PAGE compared to its theoretical size. Given this, the same phenomenon was considered for PatA appearing to be smaller by SDS-PAGE than its expected 55 kDa mass. The first attempt in the current study to replicate *PmpatA* expression using the plasmid PACVP3 (Table 2.3) resulted in no detectable expression. Analysis by SDS-PAGE of protein production (Figure 3.1) showed no distinct banding pattern relating to overexpression of *PmpatA* in the 37 kDa or 55 kDa region. Western blot analysis of this PAGE separation confirmed the lack of any His-tagged *Pm*PatA production (data not shown). For this reason, alternate expression conditions were considered to attempt to mitigate the suspected toxic effects of expressing *patA*.

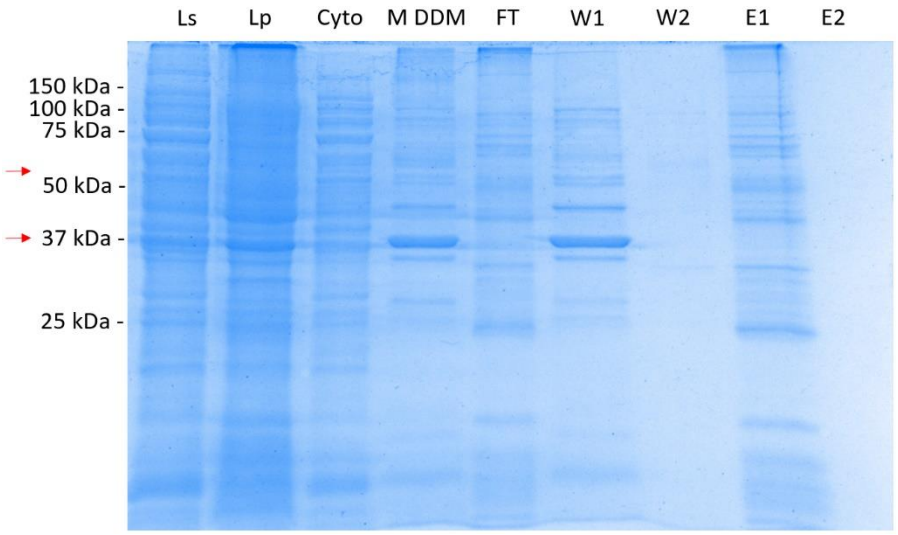

***Figure* 3.1. SDS-PAGE analysis of collected cell fractions after induction of *E. coli* C43 harbouring the PACVP3 plasmid.** Fractions were loaded onto the gel alongside Protein Plus Dual Prestained Protein Ladder: cell lysate supernatant (Ls), cell lysate pellet (Lp), cytoplasmic fraction (Cyto), membrane fraction in DDM (M DDM), flowthrough (FT), wash 1 (W1), wash 2 (W2), elution fraction 1 (E1), and elution fraction 2 (E2).

Different expression conditions were tested by examining cell lysates of induced cells by SDS-PAGE with western blot analysis. Ten mL cultures grown in either LB, Terrific Broth or Super

Broth to an OD_{600} of 0.6 were divided further for incubation at either 16 ^{O}C or 37 ^{O}C after induction. The OD_{600} of the cultures was monitored following induction for 4 h or 18 h whereby 1 mL aliquots were removed, and the cell lysate used for Western Blot (Figure 3.2A and B). Unfortunately, the combinations of the various conditions did not lead to the detection of any protein bands at either the 37 kDa or 55 kDa regions via SDS-PAGE analysis. Next, cells were induced with 1 mM IPTG at an OD_{600} value of ~1.200 and incubated at 16 ^{O} C for 18 h in both LB medium and SB medium (Figure 3.2C). Although a banding pattern indicative of a possible cleavage product of *Pm*PatA appeared here is this trial with both samples, this could not be

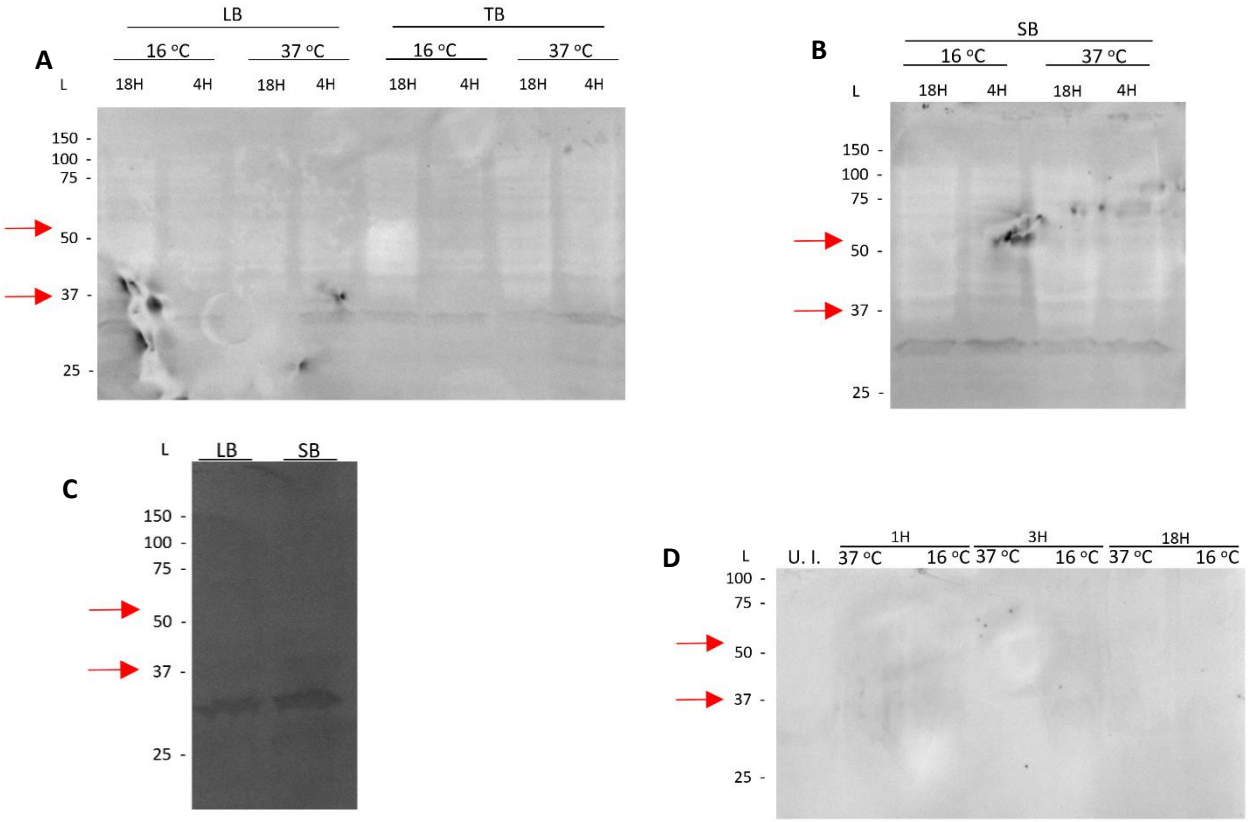

***Figure 3.2*. Western blot analyses of expression trials of *PmpatA* (PACVP3) by *E. coli* C43.** Cells were grown for 18 h or 4 h and incubated at 16 ^{O}C or 37 ^{O}C after induction with IPTG. Media used for the growth and induction process were Luria-Bertani Broth (LB) or Terrific Broth (TB) in (A), and Super Broth (SB) shown in (B). Western blot analysis was conducted on cell lysate from *E. coli* C43 samples containing PACVP3 after induction at ~1.2 OD_{600} and grown for 18 h at 16 ^{O}C (C). Cell lysate samples of *E. coli* C43 containing PACVP3 were also collected at time points of 1, 3, and 18 h after induction (D). Cells were incubated at 37 ^{O}C or 16 ^{O}C after induction with IPTG. A sample of cell lysate from *E. coli* C43 harbouring PACVP3 that was never induced with IPTG served as a uninduced control (U. I.). MW markers are shown on the left of each panel.

replicated (Figure 3.2D). In this replication experiment, OD_{600} readings were collected at 1, 3, and 18 h after induction at OD_{600} of ~1.4 with incubation temperatures of 37 ^{O}C as well as 15 ^{O}C. Cell lysate collected from uninduced *E. coli* C43 containing the PACVP3 plasmid served as the negative control. With both incubation temperatures, there was still no distinct banding pattern observed. Due to the possibility of sample loading error during the third repeat trial, the conditions were replicated again but showed no distinct banding pattern unique to *Pm*PatA protein production (data not shown).

With a lack of reproducibility of *PmpatA* expression under various conditions, work was performed to determine if the vector that was used to express *PmpatA* was the detrimental factor limiting expression, or perhaps if another homologue of *patA* would express better. New controls were used whereby the empty plasmid, pET-21b (Table 2.3), was transformed into *E. coli C43*. This served as a negative control to show that any identical banding patterns could be attributed to the *E. coli* strains or the vectors themselves in some way. Consistent with the previous protocol, samples were induced with 1 mM IPTG after the desired OD_{600} value of cultures of approximately 0.4-0.6 was attained. The recorded growth curves of samples of *E. coli* C43 harbouring the plasmid, PACVP3 (Figure 3.3C-E) displayed no differences or disruptions in growth relative to the empty pET-21b sample (Figure 3.3B) when cells were induced with IPTG, suggesting that there was little to no expression of *PmpatA*. Further proof for downregulated or non-existent expression of *PmpatA* was provided by the comparison of the growth curves of *NgpatA* expression in *E. coli* C43 using the plasmid PACAB10 (Table 2.2). The growth of these cells was disrupted by induction with 1 mM IPTG, suggesting that this homologue of *patA* could at least be initially expressed even though there had been no evidence of *Ng*PatA production by

SDS-PAGE with western blot analysis based on the work of Ashely Brott, a previous PhD student (Figure 3.3A and F). The samples were left to grow overnight and harvested the next morning. The cell lysate from each sample was then prepared for analysis by western blot which showed that there was no clear and distinct banding pattern present between the empty pET-21b control, *NgpatA* control, and the experimental samples (Figure 3.3F). With *PmpatA* expression trials, there were no growth defects evident in the growth curves after induction of gene expression, and although many bands occurred due to prolonged incubation and overexposure to NBT/BCIP, there was no distinct banding pattern observed between the subsequent uninduced and induced Western Blots . These observations suggested that rather than *Pm*PatA production stalling cellular growth resulting in degradation of recombinant protein as seen with *Ng*PatA, it was more likely that expression of *PmpatA* was not occurring at all.

To assess if a lack of detection of *Pm*PatA in cell lysates was a result of very low concentrations of the protein, attempts were made again to collect individual cell fractions for their concentration. *E. coli* C43 harbouring the PACVP3 plasmid was grown to an OD_{600} value of 1.2 in TB media before induction with 1 mM IPTG. Cell lysate from cells induced with IPTG and uninduced cells were harvested and subjected to IMAC Ni^{2+} column chromatography. The cell lysate was passed through the column and washed four times with wash buffer before two elution fractions were collected following the application of 3 mL of elution buffer through the column. The final elution fraction of the induced expression sample, corresponding to protein

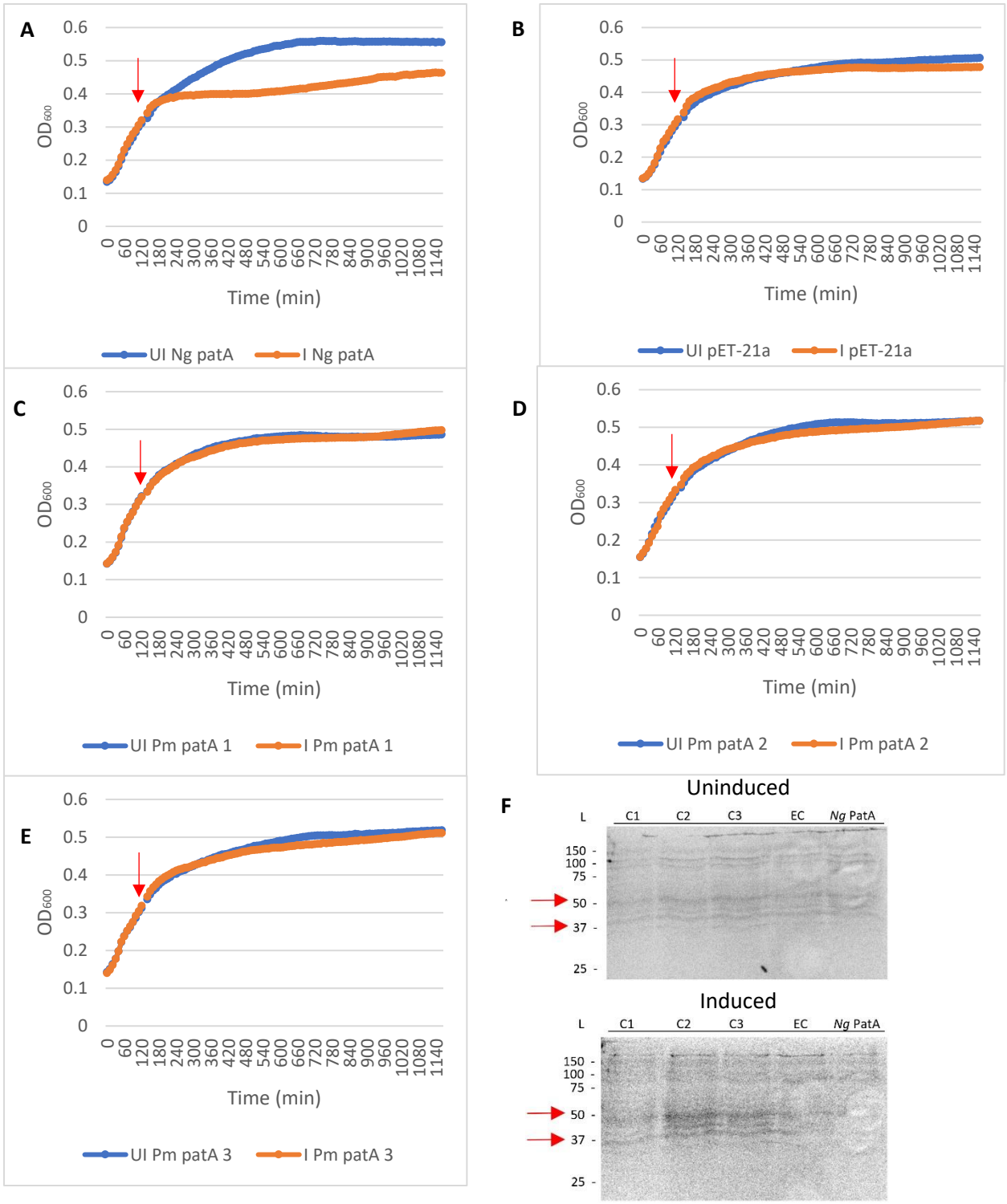

Figure 3.3. **Analyses of *N. gonorrhoeae* and *P. mirabilis patA* expression in *E. coli* C43.** Growth curves of induced (I) and Uninduced (UI) *E. coli* C43 harbouring empty pET-21b (A), PACAB10 (B), or PACVP3 (C-E). Cell cultures were induced with 1 mM IPTG approximately 3.5 h after growth from a starting OD_{600} value of 0.05 and grown overnight. (F) Western blot analysis of the cell lysates harvested from cells with induced and uninduced expression. Lanes on the blots from left to right; Colony 1 (C1), Colony 2 (C2), Colony 3 (C3), Empty pET-21b control (EC), and cells harbouring PABAC10 which contains *NgpatA* (*Ng*PatA). Colonies 1-3 correspond to cell lysate from growth curves in C-E. Red arrows indicate the time of induction.

eluted from the column with imidazole, showed a faint band representing a His-tagged protein of approximately 37 kDa (Figure 3.4A), while the uninduced sample showed no bands (Figure 3.4B). Additionally, the expression of *CjpatA* was also analyzed by incorporating cell lysate from induced *E. coli* C43 harbouring PACAA1 (Table 2.3), which also resulted in the detection of a darker band of approximately 37 kDa. This early expression trial for *CjpatA* was attempted because *CjpatB* had been shown to express in greater quantities than other *patB* homologous (A. Anderson, personal communication). For this reason, it was postulated that the *patA* homologue from *C. jejuni* might also express in greater quantities and/or possibly cause less toxicity to host cells from recombinant protein generation than other *patA* homologues. Since the band that represented recombinant protein from possible expression of *CjpatA* was much darker, it was assumed that expression of *CjpatA* as opposed to *PmpatA* could have been a viable alternative when attempting to generate recombinant PatA. Further attempts to express *PmpatA* from pET-21a resulted in protein products of similar size to hypothetical *Pm*PatA but were observed on western blots of cell lysates obtained from *E. coli* C43 with uninduced expression (Figure 3.4C and D). To test if leaky expression from the pET-21a vector was causing the fainter band, an empty pET-21a vector served as a negative control in the next trial. However, a similar banding pattern was obtained with lysates from induced cells harboring empty pET-21a compared to those transformed with PACVP3 (harboring *PmpatA*; Figure 3.4E), albeit with a much fainter band. This suggested that what was being observed was not recombinant protein from *PmpatA* expression. To ensure that the sample from the cell lysate with induced expression of *PmpatA* did not spill over into the elution fraction lane of the empty pET-21a cell lysate, both samples were loaded onto an SDS-PAGE many lanes apart and then analyzed again (Figure 3.4F). The band

was still observed in the negative control confirming that the other band detected in the elution fraction of the cell lysate with induced expression of *PmpatA* was not *Pm*PatA. However, the identity of the eluted protein was never confirmed by mass spectrometry analysis.

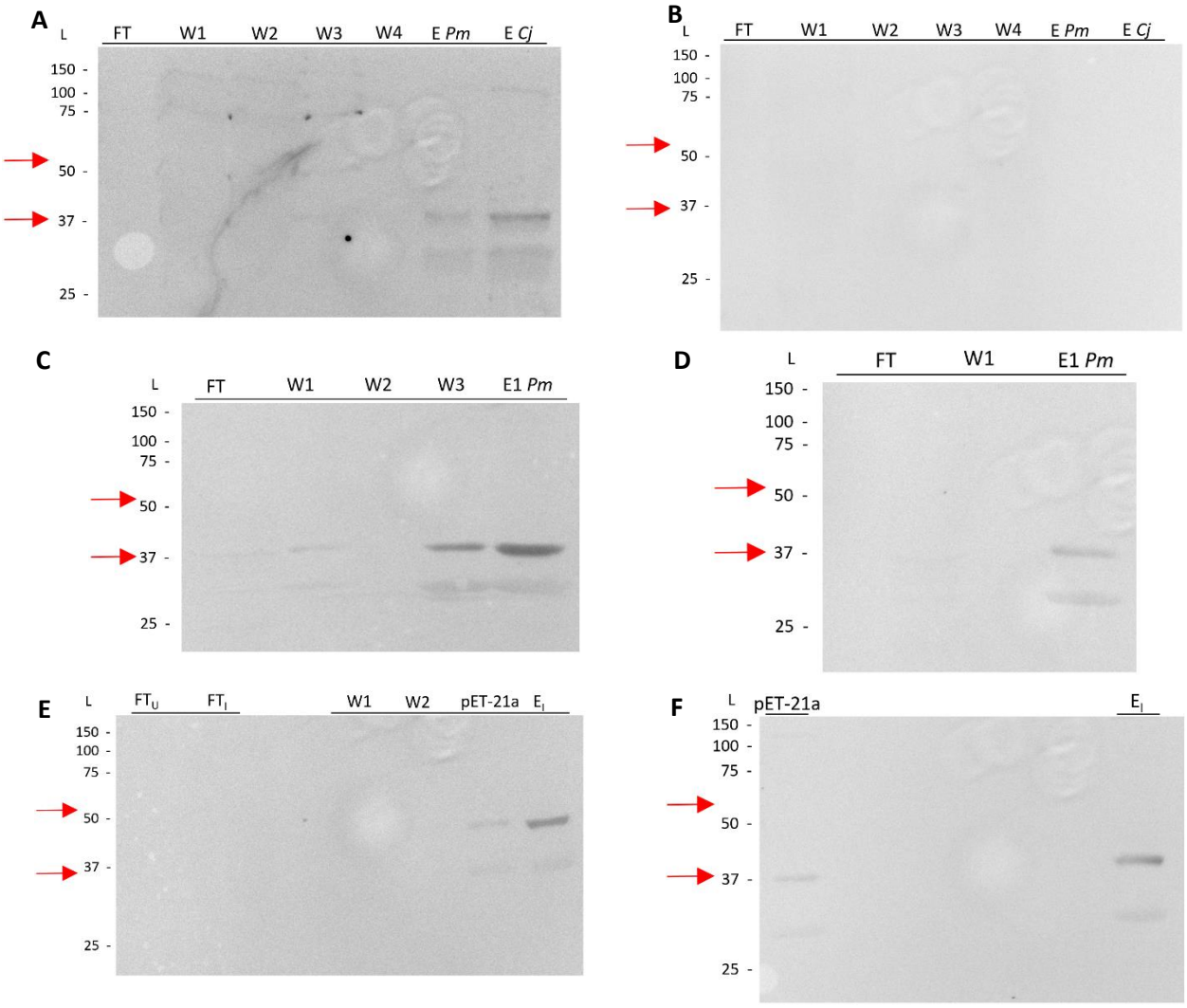

***Figure 3.4*. Western blot analysis of *Pm*PatA purification fractions.** Cell lysate from *E. coli* C43 harbouring PACVP3 and *E.coli* C43 harbouring PACAA1 (E *Cj)* with induced expression (A) and uninduced expression (B) were compared. Attempts to replicate figures A and B are shown as figures C and D where cell lysate from *E. coli* C43 cells harbouring PACVP3 that were induced with 1mM IPTG were analyzed for *Pm*PatA (C; induced, D; uninduced). A third replication trial using empty pET-21b serving as a negative control and cell lysate from *E. coli* C43 cells harbouring PACVP3 that were induced with 1mM IPTG as an experimental sample were compared (E). Elution samples from the trial shown in (E) were loaded back onto a gel, multiple lanes apart to test for any experimental sample leaking into the negative control lane (F). Western blot lane titles correspond to different fractions of cell lysate, whereby flowthrough ((FT) or ($FT_{U/I}$) for flowthrough of uninduced or induced fractions), wash (W), elution ((E), (E *Pm/Cj*) for the specific homologue analyzed, or ($E_{U/I}$) for elution of uninduced or induced fractions) were used to describe the lanes during the analysis.

To assess if recombinant protein was not being produced due to the suppression or ejection of transformed plasmids, *PmpatA* was ligated into a pBAD18-cm vector (PACBL1). This vector provides tighter control of expression and hence minimizes, if not precludes, leaky expression, thereby preventing cells from prematurely suppressing *PmpatA* gene expression before deliberate induction commenced. In tandem with this experiment, the construct PACAA1 (*CjpatA*), was used for comparison purposes as early western blotting results appeared to indicate that there might have been small amounts of PatA protein production as opposed to when overexpression of *PmpatA* occurred. Growth curves were generated (Figure 3.5A) of *E. coli* C43 cells transformed with PACBL1 and PACAA1 but unfortunately, the growth curves for cells transformed with PACBL1 indicated no growth defect, which can be indicative of overexpression of recombinant protein. Overexpression of *CjpatA* (PACAA1) appeared to occur, as it exhibited the same growth defect associated with overexpression of *NgpatA* (PACAB10). However, western blot analysis of the cell lysate of these samples of *E. coli* C43 overexpressing *CjpatA* showed no distinct banding pattern that would suggest that *Cj*PatA was present in the sample (Figure 3.5B).

Difficulties with expression of *Pm* and *CjpatA* meant that no information about their protein products could be obtained and that new strategies to elucidate form, function, and enzyme activity would need to be developed. This resulted in a plan to test the functional residues of *Cj*PatA using an *in-situ* assay that was able to relate the percent O-acetylation of MurNAc residues in the cell walls of *C. jejuni* 81-176 to its survivability in hazardous environments. The extent of how much *C. jejuni* 81-176 could survive in environments that would either stress cells to the point of inducing autolysis or their ability to resist the mechanism of lysozyme would then depend on the activity of *CjpatA*.

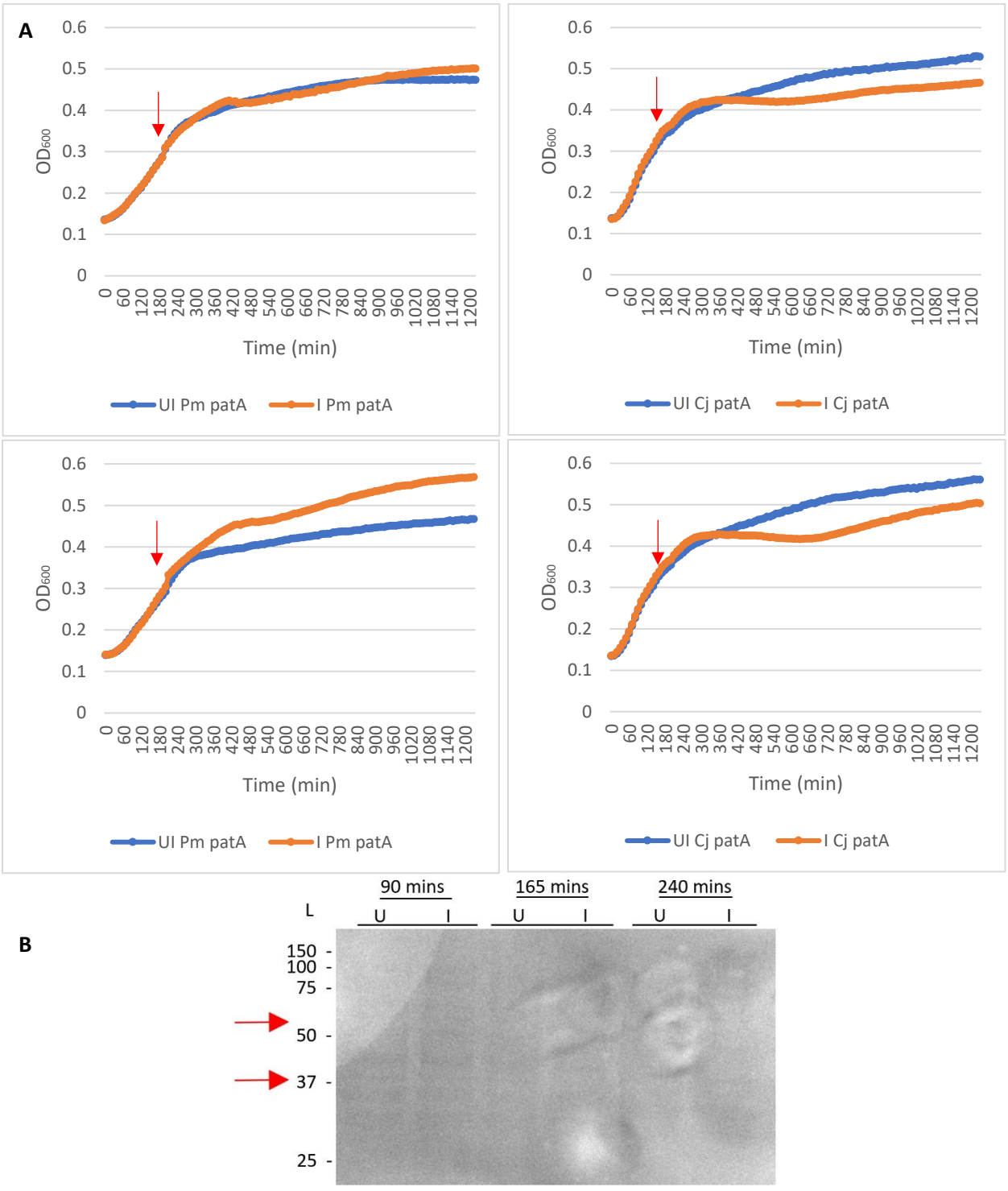

***Figure 3.5*. Analysis of *PmpatA* and *CjpatA* expression.** Induced (I) and uninduced (UI) (A) growth curves of *E. coli* C43 harbouring either (left) PACBL3 (*PmpatA*: pBAD18-cm) and (right) PACAA1 (*CjpatA*: pET-21a) compared in terms of growth, with and without induction of *patA* expression. Arrows indicate the time of expression. (B) SDS PAGE with western blot analysis of *E. coli* C43 cell lysates harbouring PACAA11. Cells were harvested at 90, 165, and 240 min without (U) and with (I) induction of *CjpatA* expression. Arrows indicate the theoretical sizes of *Pm*PatA (55 kDa) or the possible cleavage product of *Pm*PatA (37 kDa).

3.2 Functional residues of *Cj*PatA

The first step in testing functional residues of *Cj*PatA was to use a bioinformatic approach to identify possible functional residue targets that could be replaced with the objective of disrupting catalytic activity. A multiple sequence alignment of all known and hypothetical Pat*A* homologues was generated to identify invariant and highly-conserved residues recognizing these are often essential for function. These residues were compared to their equivalents found in other MBOAT proteins with characterized structures. These MBOAT family members included D-alanyl transfer protein DltB[76], Hedgehog acyltransferase (HHAT)[77], and diacylglycerol O-acyltransferase 1 (DGAT1)[78,79] which allowed for some inference into the possible importance of some of some the functional residues of *Cj*PatA. The residues of interest among PatA homologues were Ser122, Arg164, His275, Arg283, and His315. While these residues were not completely conserved in other MBOAT proteins, the equivalent residue of His315 in MBOAT proteins has been demonstrated to be essential for catalysis[75-78]. The other conserved His residue among Pat*A* homolouges, His275, had also been shown to be catalytically important in both DltB[76] and HHAT[77] as residues His289 and Asp339, respectively. The equivalently-located residue of His275 in DGAT1, Asn378 was shown to be important, but not essential, for catalytic function; only 20% residual activity remained when it was replaced [79]. The Ser122, Arg164, and Arg283 residues, while not known to directly serve roles in the catalytic mechanisms of the few charcterized MBOAT proteins known currently, were chosen based on their conservation and orientation with respect to possible catalytic function and possible binding potential to acetyl-CoA, discussed more below.

A predicted structure of *Cj*PatA was created by using Phyre2 one-to-one threading[64] to overlay the sequence of *CjpatA* onto the known structure of *S. thermophilus* DltB (PDB 6BUH) [76].

This structure was used to further help identify potential residues important for catalytic purposes and which residues may serve instead to maintain the structural integrity of *Cj*PatA. To disqualify conserved residues from experimentation, the identified residues were visualized in the simulated structure (Figure 3.5). Based on this analysis, Ser122, His275, and His315 were postulated to play a role in catalytic activity due to their orientation which points inwards into the active site funnel. The invariant residues Arg283 and Arg164 were recognized to possibly serve to bind to the negatively charged phosphate groups of the adenosine diphosphate head group of putative substrate acetyl-CoA. The Arg283 residue has one substitution in the observed PatA homologous sequences where a lysine residue serves in its place within *H*. *pylori*. However, because the substitution was to a lysine residue in this organism which contains a side chain amino group, it is possible that the lysine residue would suffice in the same role as an arginine residue. The Arg164 has one substitution to methionine in *Providencia alcalifaciens* which may not serve as great a role as a lysine or arginine and might signal that this residue is not as important as the Arg283 residue in the context of binding to the polar head group of acetyl-CoA. With the the orientation and conservation of these residues considered within this *in silico* strucutre, and with the consideration that the *in silico* strucuture may not be an accurate representation of the enzyme overall, these were determined to be the most important catalytic residues of *Cj*PatA and thus targeted for further investigation.

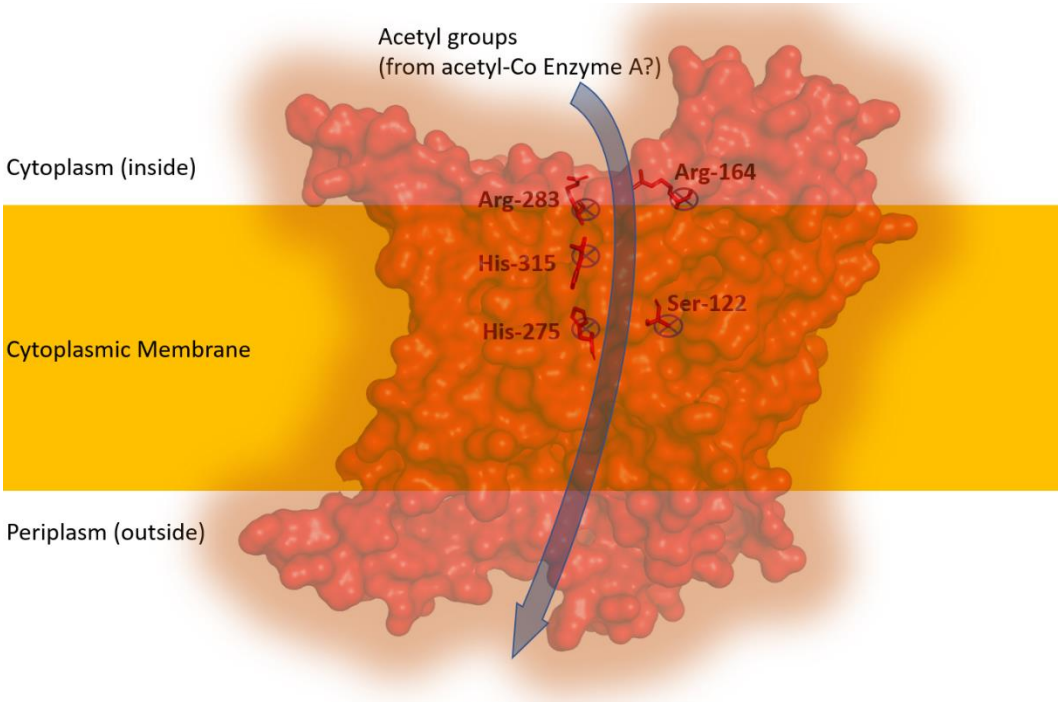

***Figure 3.6*. Predicted structure of *Cj*PatA generated from Phyre2 one-to-one threading with DltB as a template.** The residues H315, H275, R283, R164, and S122 were chosen for site-directed mutagenesis to alanine residues based on conservation within PatA homologues, orientation within the simulated *Cj*PatA structure and possible catalytic function with reference to other characterized MBOAT enzymes and with context to binding of acetyl-CoA. The confidence in the model over 361 residues was 79% modelled at >90% confidence.

3.3.1 Lysozyme sensitivity: Spot assay

An attempt to develop a lysozyme sensitivity assay was made to provide the opportunity to assess knockout strains of *C. jejuni* 81-176 lacking one or more genes of the *oap* cluster, and transformants harboring engineered mutant forms of *patA.* Glycerol stocks of *C. jejuni* 81-176 consisting of the wildtype (WT) strain, knockout *patA* (Δ*patA*) variant of 81-176, and the Δ*patA* variant with *patA* complemented back into one of three different intergenic rRNA sites within the chromosome (Δ*patA*$_C$) were revived and prepared for testing for sensitivity to lysozyme. Presumably, with a *patA* deletion and replacement with a kanamycin resistance cassette[70,80], this *C. jejuni* 81-176 mutant was more susceptible to the hydrolytic activity of lysozyme due to its reduction in PG O-acetylation; 12.5 ± 0.71% for the WT strain, down to 2.45 ± 0.14% for the

Δ*patA* mutant[70]. Based on this information, an attempt was made to demonstrate a repeatable and distinguishable difference between the susceptibility of lysozyme between WT and Δ*patA*.

Many variations of the lysozyme sensitivity assay were attempted. These included using different individual media, such as PBS, pure MilliQ H_2O, 50% LB, and 50% diluted PBS supplemented with 1 g/L glucose, and finally a mix of different media containing MH broth, LB broth, and MilliQ H_2O supplemented with 5.5 mM NaCl. Various incubation times with differing concentrations of lysozyme and lactoferrin or EDTA (the latter two added as potential permeabilizers of the outer membrane) combined with different starting concentrations of cells were also utilized to optimize the assay. The results of these initial trials were hard to interpret due to the many variables contributing to the variance of the results, and much of the variance might be attributed to improper handling of the fastidious organism that is *C. jejuni* 81-176.

Eventually, attempts were also made to titrate lysozyme alone to detect any differences in lysozyme sensitivity between the WT and Δ*patA* (Figure 3.7A). Samples of WT and Δ*patA* were grown overnight in MH broth and then adjusted to a starting OD_{600} value of approximately 0.500 in tubes containing 50% MH broth and 50% 5.5 NaCl solution with or without final concentrations of 30 – 50 mg/ml lysozyme. The concentrations of lysozyme used here were similar to the concentrations used against knockout *patA* and *pgdA* strains of *H. pylori* [59]. After 4 h of incubation with 50 mg/ml lysozyme, there appeared to be a significant difference in cell survival between WT and Δ*patA*. A 10-fold difference in survival was found between WT and Δ*patA* (compare survival of 10^5–10^6 to 10^4–10^5 cells, respectively) (Figure 3.7B). An initial trial was made to use these conditions on the *patA*-complemented strain Δ*patA*$_C$, but surprisingly this resulted in a cell

population much closer in size to Δ*patA* from the first trial when incubated for 4 h with 50mg/ml lysozyme (Figure 3.7C).

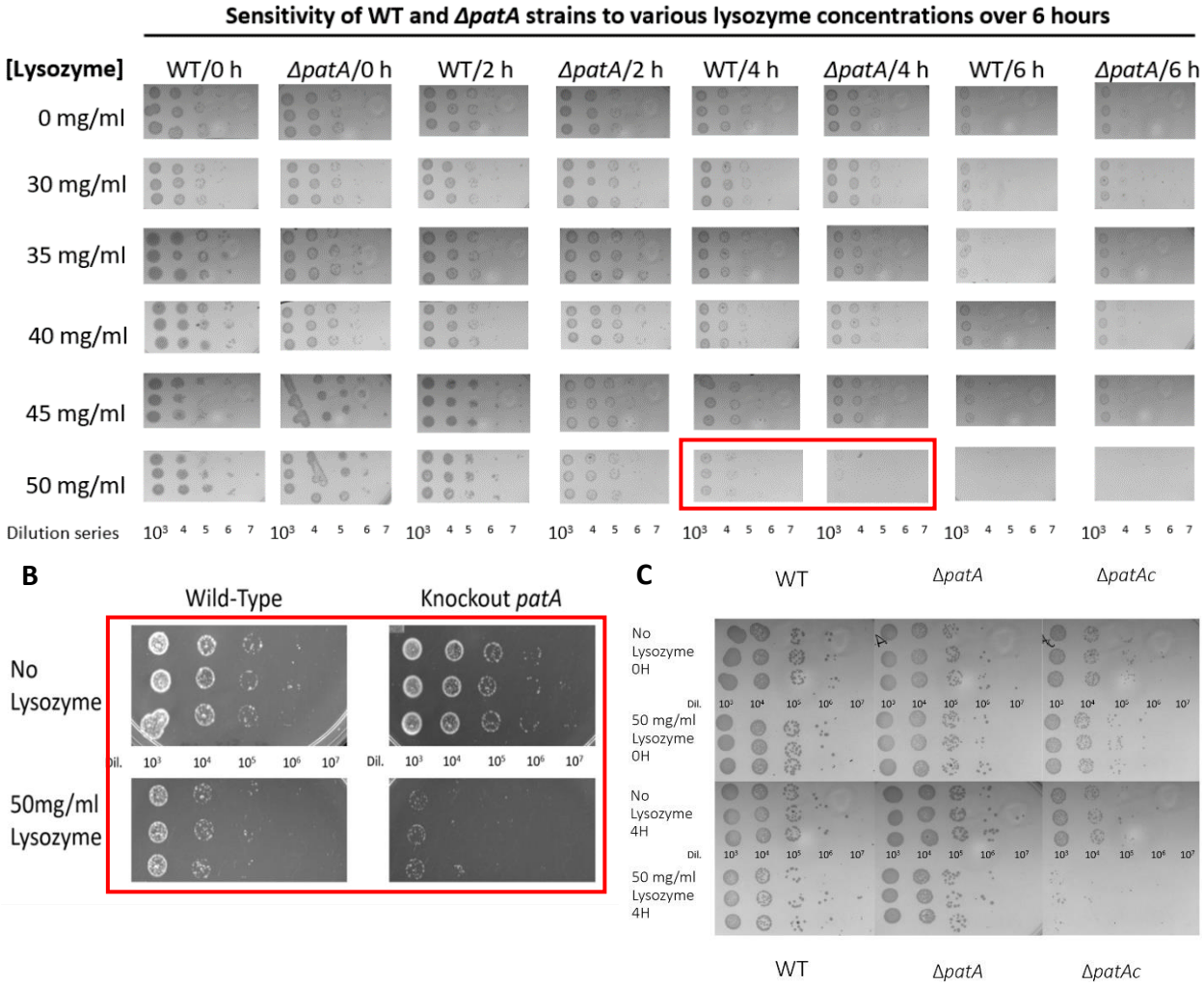

***Figure 3.7*. Lysozyme-sensitivity spot assay of WT and Δ*patA* and Δ*patA*c strains of *C. jejuni* 81-176.** Cells were subjected to treatment with various concentrations of lysozyme and times, and each spot was generated from 5 µL of culture taken from each dilution from 1000-fold dilution to 10^7-fold dilution and spotted onto MH agar plates, shown horizontally. Each dilution was spotted 3 times and incubated for 48 to 96 h at 37 °C in microaerophilic conditions. (A) Assay of WT and Δ*patA* over a 6-hour (h) period incubated in 50% MH broth and 50% 5.5 mM NaCl solution containing increasing concentrations of lysozyme from 30 – 50 mg/ml. A starting OD_{600} of approximately 0.5 was utilized. (B) Close up of the difference in survivability between WT and Δ*patA* of at 4 h and using 50 mg/ml lysozyme from (A). (C) Assay of WT, Δ*patA* and Δ*patA*c in the absence and presence of 50 mg/ml lysozyme and 5.5 mM NaCl for 4 h with a starting OD_{600} of approximately 0.4.

Attempts to reproduce this lysozyme-sensitivity test failed due to difficulties with getting the complemented Δ*patA* strain, Δ*patA*$_C$, to behave similarly to the WT strain as expected. Reproducing the larger difference in cell survivability between WT and Δ*patA* in subsequent trials

also mostly resulted in failure. For these reasons, a new approach was considered using other available engineered mutants of *C. jejuni.* The knockout *ape1* mutant of *C. jejuni* 81-176 (Δ*ape1*) has a PG O-acetylation level of 35.6 ± 2.25%[70], which is significantly higher than the WT strain (12.5 ± 0.71%) thereby potentially facilitating the detection of phenotypic changes with subsequent complements. Also, the Δ*oap* deletion mutant lacking the entire *oap* operon has a PG O-acetylation level of only 2.1%, thus providing the opportunity to monitor for a greater difference in complemented strains; complementation of this deletion mutant with both *CjpatA* and *CjpatB* was hypothesized to increase PG O-acetylation levels comparable to the Δ*ape1* mutant. Analyzing the strains' susceptibility to lysozyme with this greater difference in percent O-acetylation of PG might allow for a greater difference in lysozyme sensitivity, thereby allowing for more accurate observations on the importance of the specific functional residues that were chosen for analysis.

In these new lysozyme sensitivity assays, Δ*ape1* would replace WT, Δ*oap* would replace Δ*patA*, and the Δ*oap* mutant complemented with WT *CjpatA* and *CjpatB* (Δ$oap_{c\ (CjpatA\ +\ B)}$) would replace Δ$patA_C$. Since there appeared to be some limited success with the initial *C. jejuni* mutants in demonstrating a difference in sensitivity to 50mg/ml lysozyme for 4 h, another attempt was made to detect significant sensitivity differences between the new mutants when suspended in MH broth with lysozyme for 4 h (Figure 3.8A) or in PBS for 1 h (Figure 3.8B).

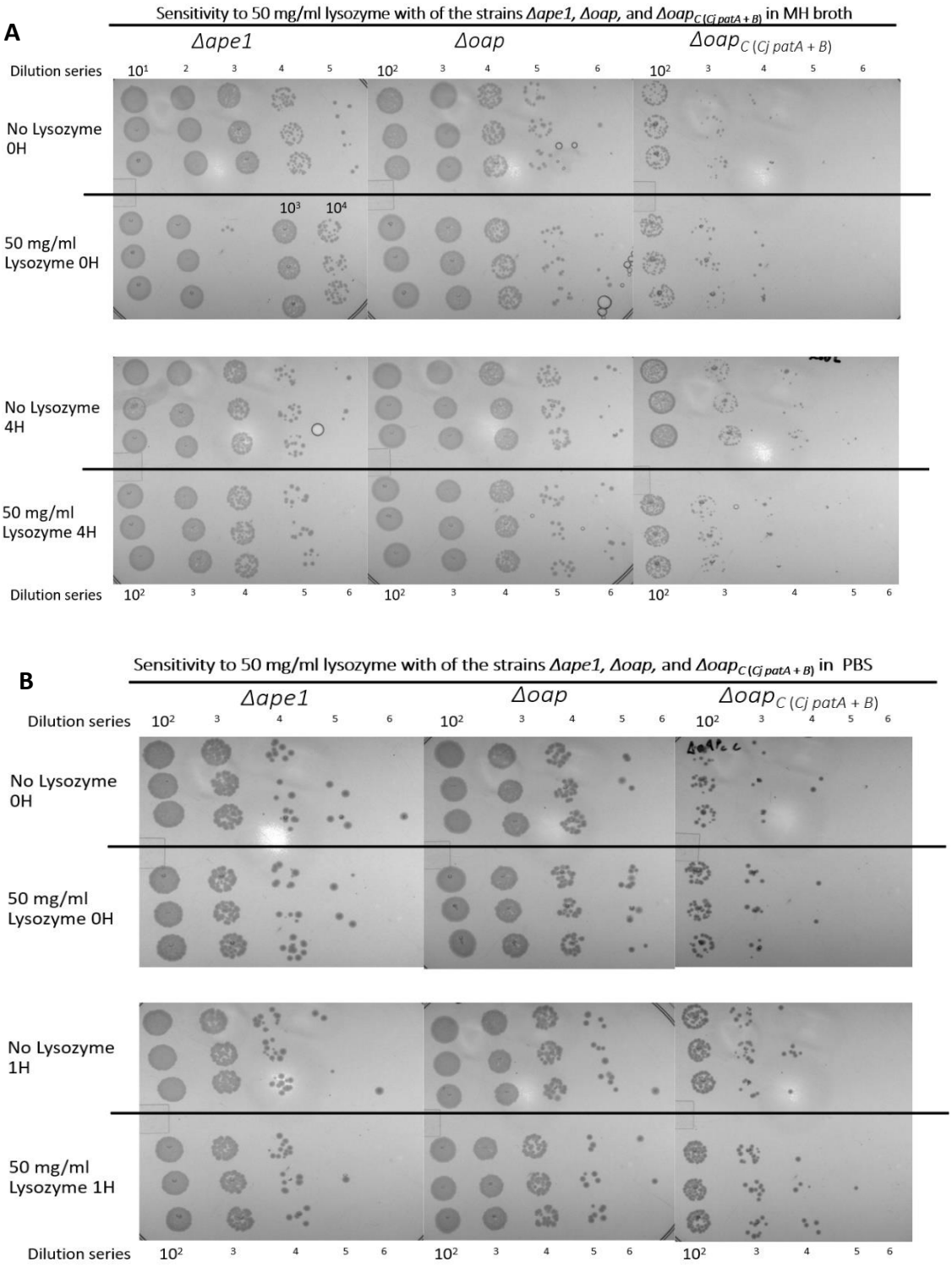

Figure 3.8. Sensitivity of strains Δ*ape1*, Δ*oap*, Δ*oap*$_{C(CjpatA+B)}$ to 50 mg/ml lysozyme. (A) *C. jejuni* 81-176 strains, Δ*ape1*, Δ*oap*, Δ*oap*$_{C(CjpatA+B)}$ adjusted to a starting OD_{600} value of 0.2 and incubated in MH broth with 50 mg/ml lysozyme for 4 h. Plates were incubated for 4 days at 37 ^{O}C in microaerophilic conditions. Each spot was generated from 5 µL of culture taken from each dilution from 100-fold dilution to 10^6-fold dilution shown horizontally. Each dilution was spotted 3 times. (B) Similar conditions were used compared to (A) but incubation for 1 h in PBS was used instead.

Even with the high concentrations of lysozyme that had been used previously, there was no sensitivity to lysozyme detected for these mutants in this way. In fact, it appeared that in the conditions of the assay, there was no noticeable sensitivity to lysozyme detected at all, relative to what was observed with WT and Δ*patA*. In a follow-up experiment, EDTA at a concentration of 100 µM was added in an attempt to sensitize the mutants to lysis. This was chosen in part due to the reported MIC_{50} values for EDTA when incubated with the Δ*ape1* mutant reported previously [70]. The concentration of lysozyme was also lowered with the intention to create a detectable difference in lysozyme between the mutants, Δ*ape1*, Δ*oap*, and Δ$oap_{c\ (CjpatA\ +\ B)}$, and the approximate starting OD_{600} was lowered from approximately 0.2 to 0.0002 (Figure 3.9). The control groups suspended in only PBS showed approximately a ten-fold decrease in population, while the experimental groups for Δ*ape1* and Δ$oap_{c\ (CjpatA\ +\ B)}$ appeared to be mildly affected by incubation with lysozyme and EDTA to different extents, where colonies of Δ$oap_{c\ (CjpatA\ +\ B)}$ could be identified in the 10^1 dilution range before and after incubation, while colonies of Δ*ape1* could no longer be identified in the 10^2 dilution range after incubation and instead could only be identified in the to 10^1 range. Although the Δ*oap* mutant was also greatly affected by the incubation period with lysozyme and EDTA, comparison of the magnitude of the effects between the mutants was difficult when observations of lysozyme sensitivity pertaining to Δ*ape1* and Δ$oap_{c\ (CjpatA\ +\ B)}$ mutants did not appear to be the same.

3.3.2 Lysozyme sensitivity: 96-well plates

To visualize if there was a significant difference in stressed growth when *C. jejuni* 81-176 mutants were incubated with various concentrations of lysozyme and EDTA, the new strains were

incubated in 96-well microplates which allowed for constant measurement of the OD_{600} value of cells over time. The *C. jejuni* mutants, Δ*ape1*, Δ*oap*, and Δ$oap_{C\ (CjpatA\ +\ B)}$ were grown from an

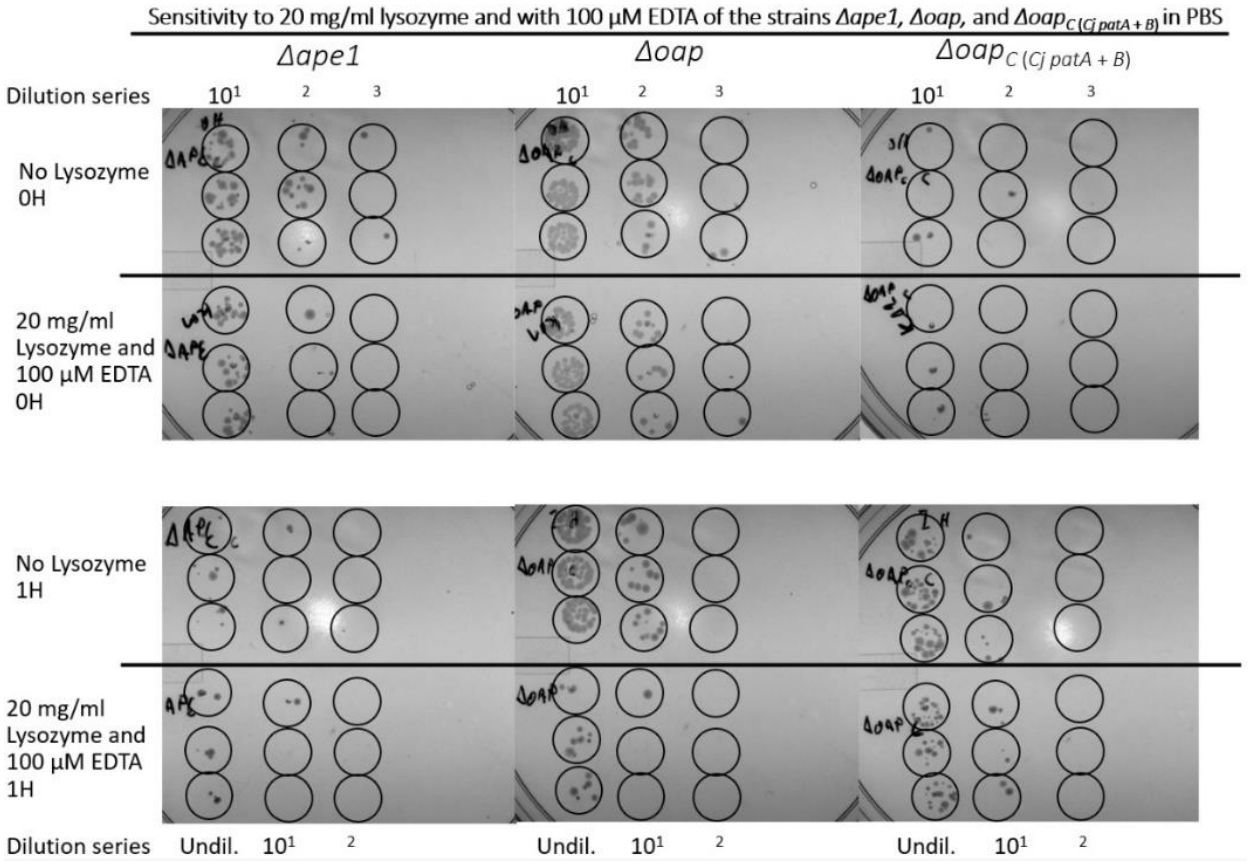

***Figure 3.9*. Lysozyme sensitivity assay in PBS using a starting OD_{600} value of approximately 0.0002 or 10^6 CFU/ml and utilizing EDTA as a membrane permeabilizer.** Cells were spotted onto MH agar plates, shown horizontally. Each dilution was spotted 3 times and incubated for 48 to 96 h at 37 °C in microaerophilic conditions. Experimental samples were incubated with both 20 mg/ml lysozyme and 100 µM EDTA to permeabilize the outer membrane. An alternative dilution series was utilized for the visualization of the cell populations after 1 h where undiluted samples, 10^1, and 10^2 times dilutions were plated instead of 10^{1-3} times dilutions. This was to better display the effects of lysozyme and EDTA on the cell populations. Black circles were added to help indicate where 5 µL of cell suspension was positioned on the agar surface.

approximate starting OD_{600} value of 0.05, initially measured with a path length of 1 cm, for 22 h (Figure 3.10). According to MIC_{50} assays with *C. jejuni* 81-176 [70], the MIC_{50} values for lysozyme were 5 mg/ml and for EDTA it was less than 150 µM which is why concentrations below or equal to these values were chosen first. Similar amounts of growth stress were observed for each

mutant (Figure 3.10A, B, and C), but the amount of growth stress caused by these concentrations of lysozyme and EDTA was negligible. The samples incubated with lysozyme and EDTA appeared

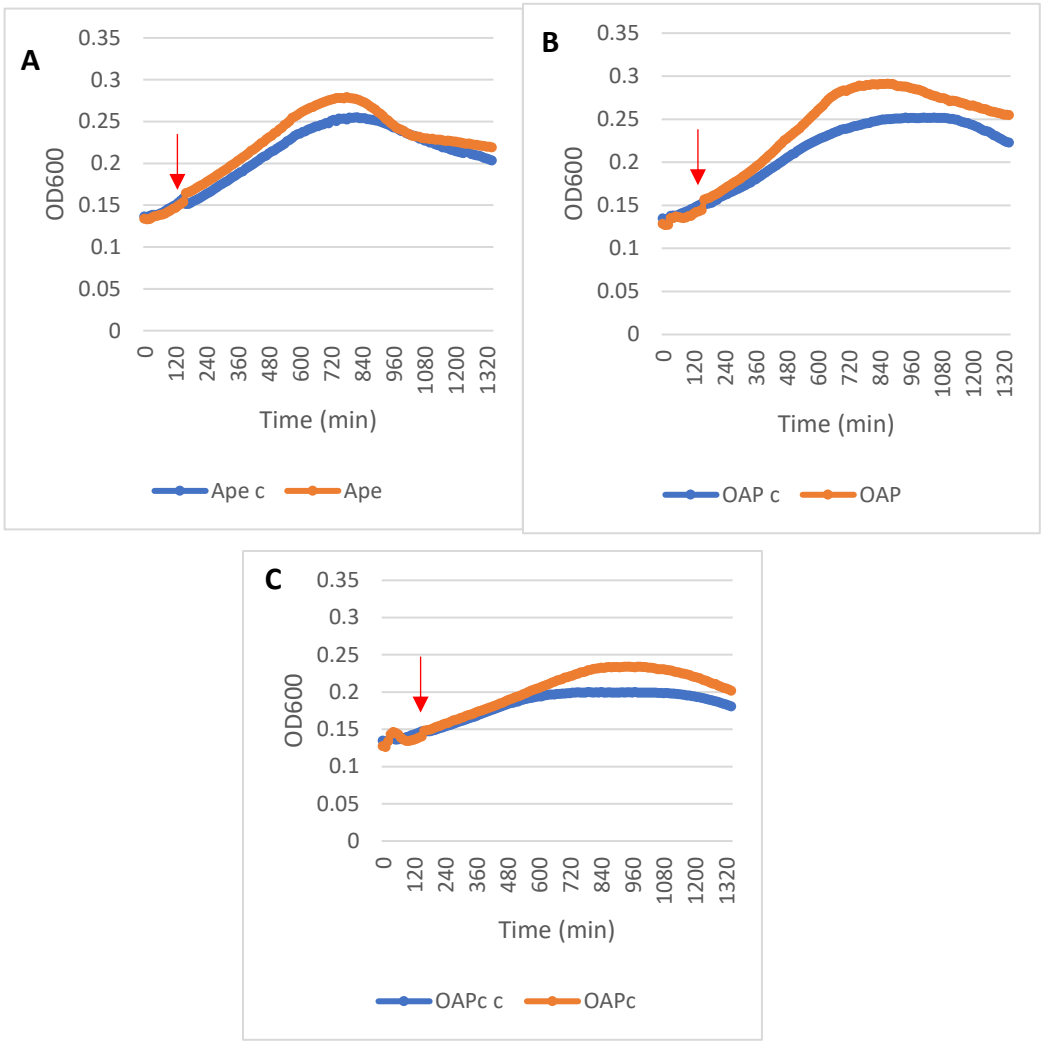

***Figure 3.10*. Effect of lysozyme and EDTA on the growth of *C. jejuni* mutants in a microplate.** Growth curves of *C. jejuni* mutants that were incubated for 22 h in a 96-well plate in MH broth alone (control samples) or with added lysozyme (5 mg/ml) and EDTA (100 µM) also suspended in MH for experimental samples. The *C. jejuni* 81-176 derivative strains, (A) Δ*ape1* (Ape c: Control, Ape: Experimental), (B) Δ*oap* (OAP c: Control, OAP: Experimental), and (C) Δ*oap*$_{c\ (CjpatA\ +\ B)}$ (OAPc c: Control, OAPc: Experimental) showed negligible difference in sensitivity to lysozyme and EDTA at the current concentrations. Eight replicates were used for each sample. Red arrows indicate where lysozyme and EDTA were added. Red arrows indicate where lysozyme and EDTA were added.

to outgrow the control samples that were solely incubated in MH broth. This indicated that the amount of sodium bicarbonate added to the cell suspension could have differed enough between control and experimental samples that growth was affected slightly. This also indicated that this concentration of lysozyme was not as effective at hydrolyzing the cell wall when paired with

100µM EDTA. Because the discrepancy between control and experimental samples was observed in this way, it was reasonable to assume that the concentrations of lysozyme and EDTA used were not significant enough to inhibit the growth of the experimental samples enough to account for any small discrepancy in the amount of sodium bicarbonate present in the experimental and control samples. To this end, increased concentrations of lysozyme were used to improve the difference in growth defects between the mutants.

Samples were grown from a starting OD_{600} value of 0.05 but were then incubated with 10 mg/ml lysozyme and 100 µM EDTA. What appeared to be a slightly greater difference in lysozyme sensitivity could be observed in this trial between samples Δ*ape* and Δ*oap*$_{c\ (CjpatA\ +\ B)}$ against Δ*oap* (Figure 3.11A, C, and B, respectively). Although it was unknown if this difference was significant, the discrepancy identified in the previous trial where experimental samples outperformed control samples was notably absent from this trial. While this had been the case, there had also not been a very large increase in OD_{600} readings from when the recordings first began in this trial. This indicated that *C. jejuni* cultures in 96-well microplates were not growing optimally and that growth of *C. jejuni* 81-176 in this way would add an extra layer of variance to an already complicated experiment that required partitioning of volume to be used for lysozyme and EDTA addition later instead of added initially for the growth of cells.

Given the change in growth between control and experimental Δ*oap* samples were minimal, and of course that the growth of the cells in the wells of the microplate seemed weaker than growth in a flask or tube, a new strategy was developed to assay for autolysis to detect changes in PG O-acetylation rather than relying on the hydrolysis caused by the addition of exogenous lysozyme. Significantly, this autolysis assay would not be impeded by the protective

effects of the outer membrane to an extent by relying on endogenous autolysins to lyse cells rather than relying on various concentrations of lysozyme. The working principle of the autolysis assay is that when cells are exposed to strenuous conditions over some time, such as incubation

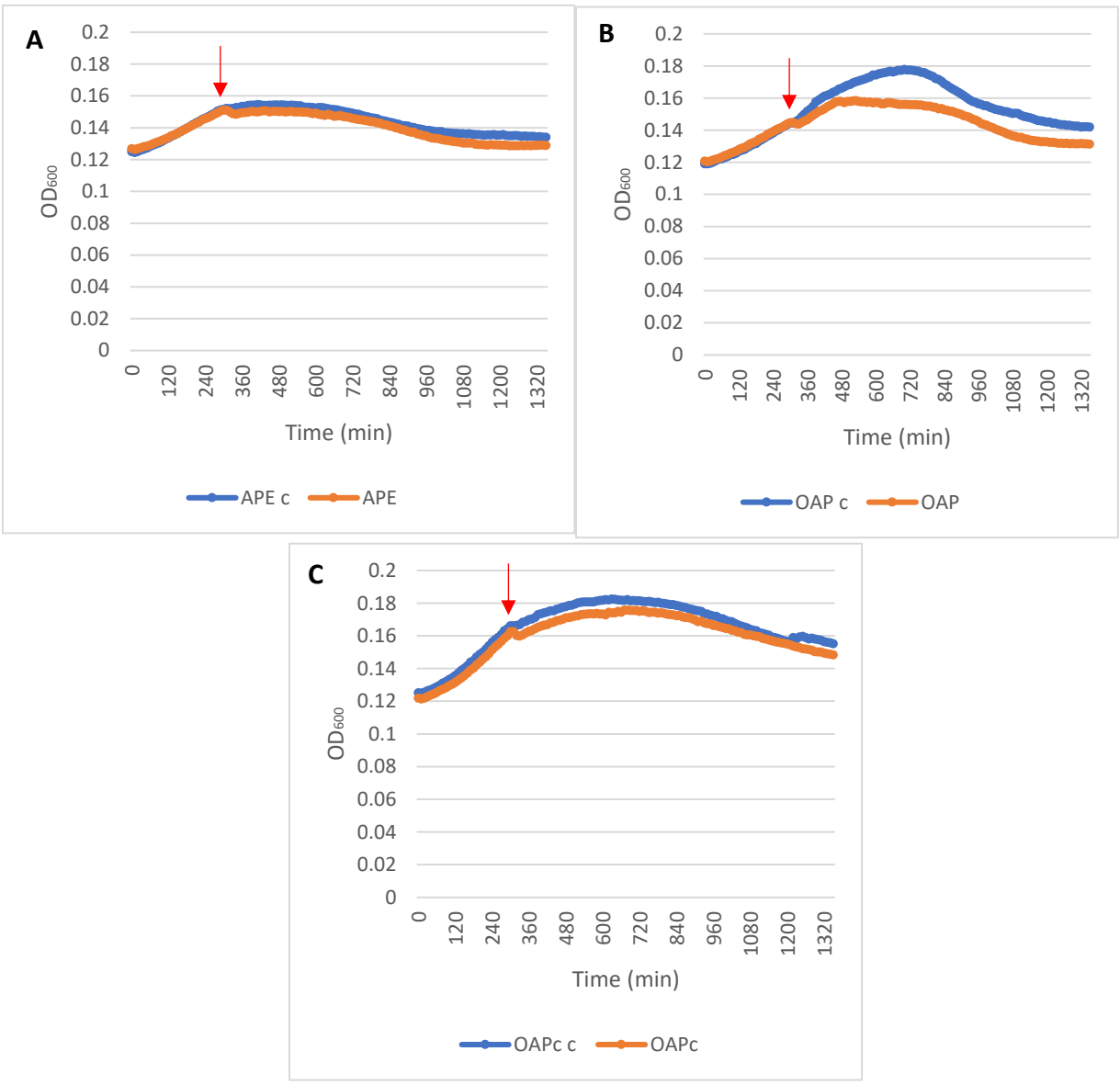

***Figure 3.11*. Effect of increased lysozyme and EDTA on the growth of *C. jejuni* mutants in a microplate.** Growth curves of *C. jejuni* mutants that were incubated for 22 h in a 96-well plate in MH broth alone (control samples) or with added lysozyme (10 mg/ml) and EDTA (100 µM) also suspended in MH for experimental samples. The *C. jejuni* 81-176 derivative strains, (A) Δ*ape1* (Ape c: Control, Ape: Experimental), (B) Δ*oap* (OAP c: Control, OAP: Experimental), (C) Δ$oap_{c\ (CjpatA\ +\ B)}$ (OAPc c: Control, OAPc: Experimental). The strains appear to show some sensitivity to lysozyme and EDTA at the current concentrations. Eight replicates were used for each sample. Red arrows indicate where lysozyme and EDTA were added.

in high or low pH buffer, or lack nutrients for sufficient growth, the cells will lyse through the mechanisms of their cellular machinery. In particular, the LTs that recycle the cell wall in *C. jejuni* 81-176 would participate as one of the primary instruments of this process. By subjecting the different strains of *C. jejuni* 81-176 used in this study to these conditions, different rates of autolysis would be expected to be observed based on the functionality of the strain's PatA enzyme. Strains of *C. jejuni* with reduced activity of PatA may possess a lower overall percent O-acetylation of PG, and as mentioned before (Section 1.4), since *O*-acetyl groups that are positioned on C-6 hydroxyl groups preclude the binding of LTs to PG, decreased O-acetylation of PG may increase the rate in which the LTs can disassemble PG. Based on this assumption, the functionality of *Cj*PatA can be indirectly inferred based on the rate of autolysis of the different *C. jejuni* 81-176 strains.

3.4 Autolysis of mutants in cuvettes and through 96-well microplate readings

With the failure to generate a useful lysozyme-based assay for monitoring the effects of PG O-acetylation, attention was turned to the applicability of an autolysis-based assay. The experimental design of the autolysis assay was based upon a previous autolysis assay used to study autolysis in *N*. *gonorrhoeae* [73], which involved resuspending a broth culture of *N*. *gonorrhoeae* in 50 mM HEPES buffer with or without 4 mM EDTA as a membrane permeabilizer to help induce autolysis. The addition of EDTA in this case was able to induce autolysis significantly more than just incubating in 50mM HEPES buffer. Since the autolysis assay was shown to successfully induce autolysis in *N. gonorrhoea,* the experimental design was adapted for *C. jejuni* 81-176 with the hope that the assay would produce the same general results for other Gram-negative pathogens. The new *C. jejuni* 81-176 mutants, Δ*ape1*, Δ*oap*, and Δ*oap*$_{c(patA}$

$_{+ B)}$ were first subjected to this autolysis assay to test if the increased PG O-acetylation in both Δ*ape1* and Δ*oap*$_{C(patA + B)}$ would cause slower rates of autolysis, presumably due to higher percent O-acetylation of their PG, which precludes LT activity. The first trial of the autolysis turbidity assay showed the experimental samples incubated with 10 mM EDTA survived at about the same rate as the control samples that were incubated in just 50 mM HEPES buffer. Although Δ*ape1* was shown to survive to the greatest degree (Figure 3.12A), this difference in the rate of autolysis was not significant. The final recorded OD_{600} value for Δ*oap*$_{C\ (CjpatA + B)}$ was the second highest in terms

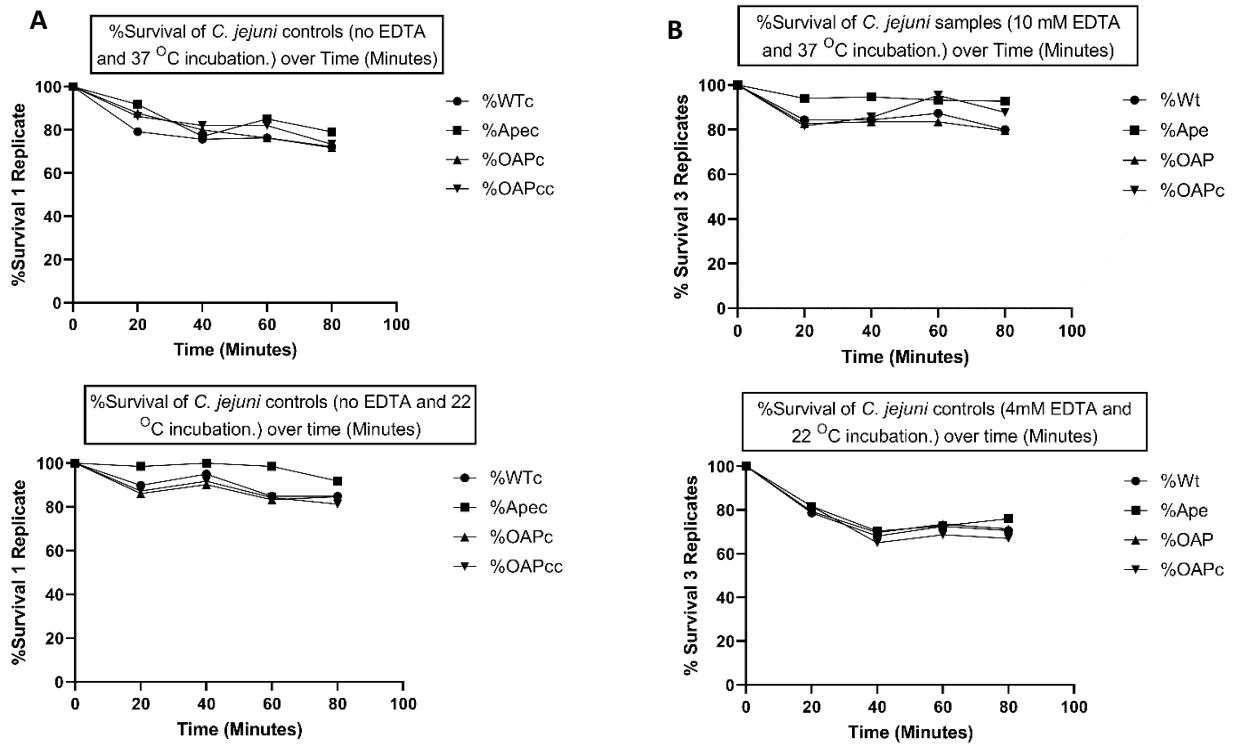

***Figure 3.12*. Autolytic rates of Wild-Type and mutants of *C. jejuni* 81-176.** Tested *C. jejuni* strains (WT: Wild-type, Ape: Δ*ape1*, OAP: Δ*oap*, OAP$_C$: Δ*oap*$_{C\ (CjpatA + B)}$) were suspended in 50 mM HEPES buffer alone (control: denoted "c") or in combination with 10 mM EDTA (experimental). Observations based on analysis of turbidity of each sample starting at approximately 0.130 showed neither a significant difference between the control and experimental samples and between the experimental samples themselves when incubated at 37 °C in microaerophilic conditions (A). Control and experimental samples showed a greater difference in autolytic when incubated at 22 °C but still no large difference between experimental samples was observed (B).

of total percentage from the initial (Figure 3.12A), which was not a significant difference from the other samples. The next trial utilized an incubation temperature of 22 °C, as this temperature

affects the stability of *C. jejuni* and could perhaps increase the rate of autolysis [68] (Figure 3.12B). The rate of autolysis was increased but again showed no significant difference in the rate of autolysis between tested samples.

Observations on the turbidity of the *C. jejuni* strains undergoing autolysis were revisited to take advantage of the constant monitoring of the microplate reader. Samples were incubated again in 50 mM HEPES buffer and left to incubate while at 37 ^{O}C overnight, but not in microaerophilic conditions. This was presumed to help promote autolytic conditions for *C. jejuni* because they would be nutrient deprived, in addition to exposure to atmospheric gas compositions containing high oxygen [68]. The *C. jejuni* strains Δ*oap*$_{c\ (CjpatA\ +\ B)}$, Δ*ape1, and* Δ*oap* together with the derivative mutants of Δ*oap*$_{c\ (CjpatA\ +\ B)}$, S122A, R164A, and H275A, were tested

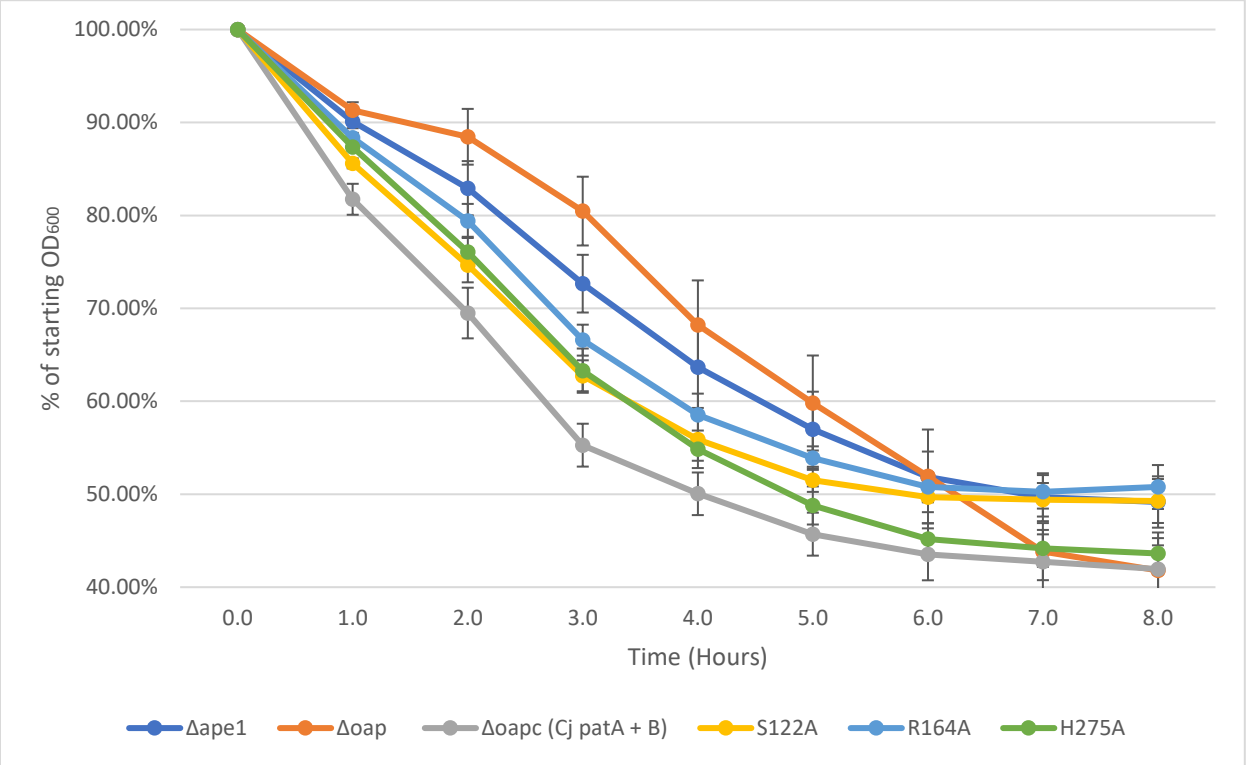

Figure 3.13. **Autolysis of mutant *C. jejuni* 81-176 mutant samples in a 96-well micro-plate at 37 ^{O}C.** Samples Δ*ape1*, Δ*oap*, Δ*oap*$_{c\ (CjpatA\ +\ B)}$, S122A, R164A, and H275A were incubated in 50 mM HEPES buffer for 8 h at 37 ^{O}C with the purpose of inducing autolysis of cells. The OD_{600} values of each sample were normalized to 100% and each data point changed from OD_{600} values to percent OD_{600} of its original value. Three replicates were used for each sample.

in another autolysis assay where samples were incubated for 8 h at 37 ^{O}C (Figure 3.13). Interestingly, while it was expected that Δ*oap*$_{c\ (CjpatA\ +\ B)}$ and Δ*ape1* would undergo autolysis at a slower rate than Δ*oap*, the opposite occurred as observations on the autolytic rate of these mutants revealed that Δ*oap*$_{c\ (CjpatA\ +\ B)}$ lysed at a much quicker rate than both Δ*oap* and Δ*ape1*. This appeared to be a replicable result and prompted testing of the Δ*oap*$_{c\ (CjpatA\ +\ B)}$ derivates. Even more interesting was that the mutants complemented with plasmids encoding (S122A)-, (R164A)-, and (H275A) PatA lysed at slower rates than the Δ*oap*$_{c\ (CjpatA\ +\ B)}$ mutant, but not faster than the Δ*ape1* mutant.

To determine if the rate and magnitude of autolysis could be accentuated in the Δ*oap*$_{C\ (CjpatA\ +\ B)}$ strain relative to its derivative mutants (S122A, R164A, H275A, R283A, H315A) and comparative controls (WT, Δ*patA*$_{C}$, Δ*oap*, and Δ*ape1*), the autolysis assay was performed again at a temperature of 27 ^{O}C (Figure 3.14). The OD_{600} measurements of cell populations for each strain indicated that Δ*oap*$_{C(patA\ +\ B)}$ continued to decrease at a rate and magnitude greater than the others using this new temperature. In contrast, the mutant strains initially appeared to decrease at a rate and magnitude similar to that of the control strains. While the discrepancy between the Δ*oap*$_{C\ (CjpatA\ +\ B)}$ strain and other strains in terms of survivability remained reproducible, the order in which the amino acid replacement strains would decrease appeared to randomize with each trial. Each strain appeared to lyse at slower rates than the Δ*oap*$_{C\ (CjpatA\ +\ B)}$ strain but did not adhere to a pattern with the other strains. Additionally, as shown in this trial (Figure 3.13), all of the strains besides the Δ*oap*$_{C(patA\ +\ B)}$ strain recorded OD_{600} measurements

greater than what it started with in the 27 ^{O}C autolysis trial, which should not be possible with populations of cells suspended in nutrient deprived media. For this reason, populations were visually assessed by spotting 5 µL of serially diluted cell suspension in PBS onto MH-TV agar (Table 3.1). These spots represented cell suspensions before and after 16 h of incubation in 50 mM

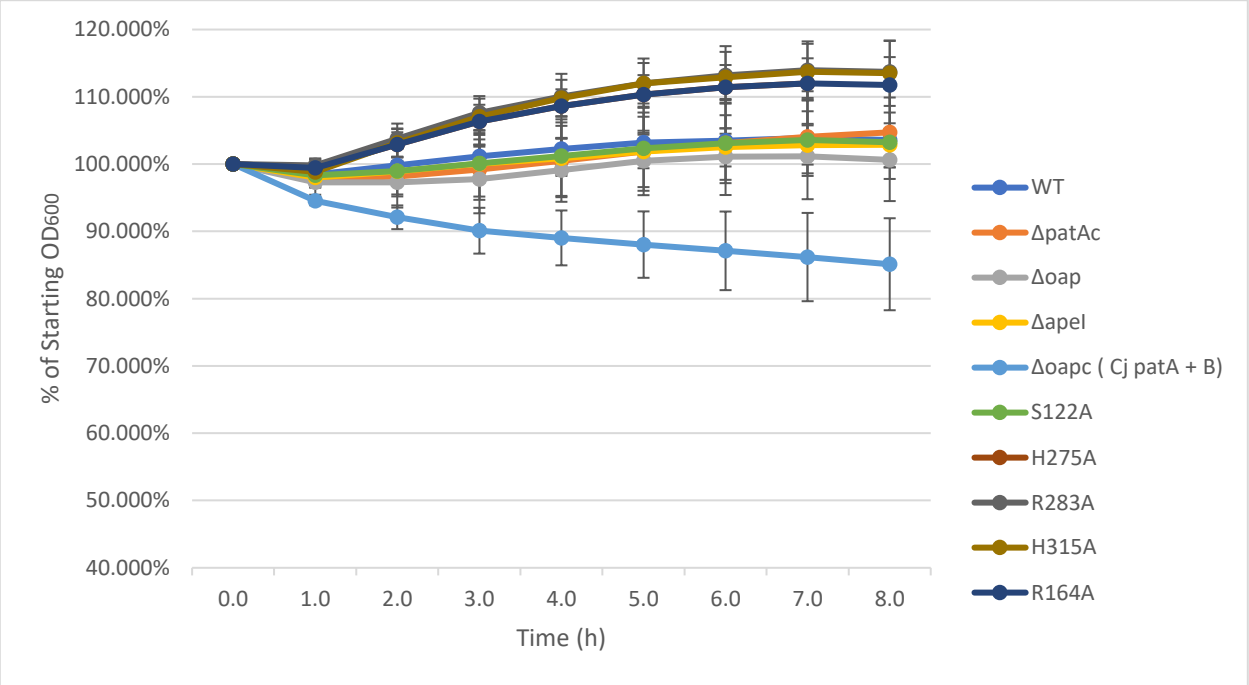

Figure 3.14 Autolysis of mutant C. jejuni 81-176 mutant samples in a 96-well micro-plate at 27 ^{O}C. Samples WT, Δ*patA*$_C$, Δ*ape1*, Δ*oap*, Δ*oap*$_{c\ (CjpatA+B)}$, S122A, R164A, and H275A, R283A, and H315A were incubated in 50 mM HEPES buffer for 8 h at 37 ^{O}C. The OD_{600} values of each sample were normalized to 100% and each data point changed from OD_{600} values to percent OD_{600} of its original value.

HEPES buffer. Notably, the decreases in population among the strains were not equal when controlling for the incubation environment. The control strains, WT, Δ*patA*$_C$, Δ*oap*, and Δ*ape1* lysed or became non-culturable in proportions that could be predicted based on their percent O-acetylation of MurNAc. The populations of the WT, Δ*patA*$_C$, and Δ*ape1* strains dropped roughly equally, while the population of the Δ*oap* strain decreased more than the other three control strains, which did not adhere to what was shown by the Δ*oap* autolysis curve. The Δ*oap*$_{C(patA+B)}$ control strain decreased in population more than WT, Δ*patA*$_C$, and Δ*ape1* but as much as what

was observed with the Δ*oap* strain. The site-directed mutant strains appeared to decrease in population at different rates, which could indicate a correlation between each residue to the function PatA. The amino acid replacements, S122A, H275A, and H315A appeared to cause the smallest drop in population when compared to the Δ$oap_{C(patA + B)}$ control. Alternatively, the two arginine replacements, R164A and R283A still cause the populations to persist in greater proportions than Δ$oap_{C(patA + B)}$ but are not as effective as the three previously mentioned replacements, especially for the R164A replacement.

Table 3.1: Proportion of cell population decrease during incubation in 50mM HEPES at 27^{O}C for 16 h

Strain	Before Incubation	After Incubation (16 h)	Difference
WT	10^6	10^5	10^1
Δ$patA_C$	10^7	10^6	10^1
Δ*oap*	10^7	10^4	10^3
Δ*ape1*	10^7	10^6	10^1
Δ$oap_{C(patA + B)}$	10^7	10^4	10^3
S122A	10^6	10^5	10^1
R164A	10^7	10^4	10^3
H275A	10^7	10^6	10^1
R283A	10^6	10^4	10^2
H315A	10^6	10^5	10^1

3.5 Analysis of PG O-acetylation

The PG from ten strains of *C. jejuni* corresponding to WT, Δ*patAc*, Δ*oap*, Δ*ape1*, Δ$oap_{C(CjpatA + B)}$, S122A, R164A, H275A, R283A, and H315A were harvested, quantified, and related to the amount of acetate that could be released from the purified PG. The percent O-acetylation of

Table 3.2: Percent O-Acetylation of MurNAc in C. jejuni 81-176 strains. Muramic acid was determined using HPAEC-PAD and acetate was quantified using an acetic acid analysis kit by Megazyme. Asterisks (*) represent the number of replicates for the determination of nmoles of both muramic acid and acetate in the PG samples.

Strains	Muramic Acid (nmol)	Acetate (nmol)	%O-acetylation
WT	42.31 ± 8.93**	6.58*	15.90 ± 3.36
Δ*patA*$_C$	6.44 ± 1.85**	0.83*	13.48 ± 3.87
Δ*oap*	54.99 ± 11.52**	0.55*	1.02 ± 0.21
Δ*ape1*	6.63 ± 1.39**	2.05*	31.58 ± 6.63
Δ*oap*$_{C(patA + B)}$	21.19 ± 2.72**	6.34*	30.19 ± 3.88
Δ*patA*$_C$ (Repeat)	51.78 ± 6.28**	6.33 ± 1.27***	12.32 ± 1.50
S122A	14.76 ± 1.85**	10.86 ± 0.60***	74.17 ± 9.33
R164A	22.69 ± 3.44**	14.49 ± 1.57***	64.59 ± 9.78
H275A	14.61 ± 4.63**	9.29 ± 5.34***	66.93 ± 21.22
R283A	6.21 ± 1.57**	5.31 ± 1.28***	88.24 ± 22.28
H315A	8.35 ± 2.29**	3.33 ± 1.62***	41.44 ± 11.38

PG in each strain during the logarithmic phase of growth of *C. jejuni* 81-176 was then determined (Table 3.2). The percent O-acetylation of the control strains, WT, Δ*patA*$_C$, Δ*oap*, and Δ*ape1* all conformed to expected levels that had been determined previously during the early to mid logarithmic phase of growth[70]. The resultant percent O-acetylation of the Δ*oap*$_{C(patA + B)}$ strain indicates that the expression of both *patA* and *patB* together will emulate the phenotype of the Δ*ape1* mutant, at least in the context of percent O-acetylation of MurNAc residues. The resulting

percent O-acetylation of the mutant strains, however, did not fall within the range provided by Δ*oap* and Δ*ape1*/Δ*oap*$_{C\ (CjpatA\ +\ B)}$ (approximately 0.8% – 39% O-acetylation of MurNAc residues). This indicates that more work is needed to determine why the levels of percent O-acetylation are elevated in the mutants.

In one investigation into why the percent O-acetylation was much higher than expected in the mutants, the chromosomal DNA of the mutant strain, H315A, was used in PCR in conjunction with site-specific primers for all three intergenic rRNA regions (Figure 3.15). Here, a band of approximately 5000 base pairs can be observed. This band includes the genes *CjpatA*,

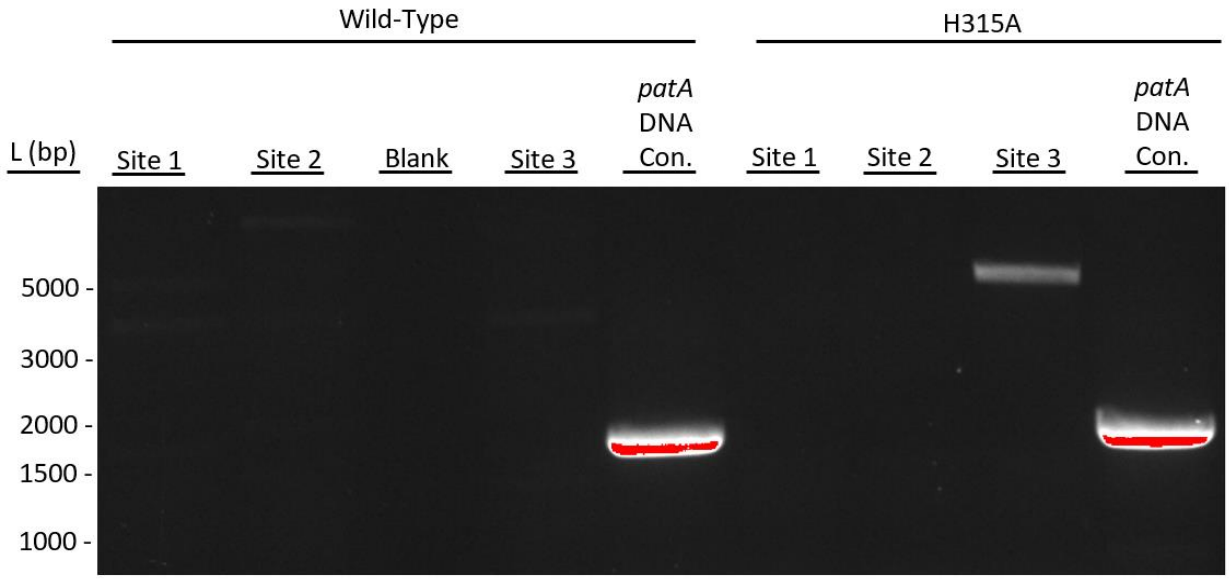

Figure 3.15 Investigation into the copy number of *CjpatA* within the chromosome of the site-directed mutant, H315A. Chromosomal DNA from both the WT strain and H315A were used as a template for PCR using the site-specific forward primers Ak233 (Site 1), Ak234 (Site 2), and Ak235 (Site 3), while using the reverse *CjpatA* complement primer. Both sets of chromosomal DNA were tested for quality using the forward and reverse complement *CjpatA* primers (*patA* DNA Con.).

cat, and *16s rRNA* region. As a negative control, chromosomal DNA from the WT strain was used to show that nothing should appear from the use of these site-specific primers since the reverse primer is simply the *CjpatA* reverse complement primer (Table 2.2). Only one copy of *CjpatA* was

detected in the third *rRNA* intergenic region in H315A, meaning that the reason for the inflated levels of percent O-acetylation could not be attributed to multiple copies of *CjpatA*.

Discussion

4.1 Expression of *patA* homologues

The expected size of recombinant *Pm*PatA produced by *E. coli* is 55 kDa. A previous master's student in the lab, Victoria Petruccelli [65], appeared to have had some success visualizing unique banding patterns on a western blot that was associated with *PmpatA* overexpression. However, a 37 kDa band was detected within the membrane fraction of transformed *E. coli* C43 harbouring PACVP3 and it was assumed to have been the consequence of a post-translational truncation of *Pm*PatA [65]. Denaturing purifications conditions were used to isolate putative *Pm*PatA from the membrane fraction to allow for the exposure of the His_6-tag to both primary mouse anti-His_6 antibody during western blot analysis or Ni^{2+} beads during IMAC purification if the fold of *Pm*PatA blocked the accessibility of the tag [65]. As a result of this work, the presence of the 37 kDa band was the expected result of repeated overexpression and purification trials. However, current attempts described herein to replicate the early overexpression trials of *PmpatA* resulted in no success; even promising results such as those presented in Figures 3.4 A and B could not be replicated. Despite the modification of conditions and expression systems used in subsequent trials, identical bands in both control and experimental samples were observed (Figure 3.4 C, D, E, and F). Thus, it would appear that the earlier results were misleading and that the observed bands were most likely *E. coli* proteins. However, analyzing the gathered recombinant protein using mass spectrometry could have helped to identify what exactly was happening with these

vectors. Switching to more controlled expression vectors, such as the pBAD18-Cm, and utilizing different *patA* homologues, such as *CjpatA,* did not alleviate the problem of *patA* expression. In all, the data suggest that the expression of *patA* leads to the accumulation of toxic recombinant protein in *E. coli*.

Experiments designed to monitor the growth of *E. coli* hosts transformed with vectors harbouring *patA* clearly revealed the toxicity resulting from expressions. This is especially true in the host cells expressing *NgpatA* and *CjpatA* as shown by the growth curves in Figures 3.3B and 3.5A, respectively. This toxicity was quite pronounced after inducing to obtain overexpression with IPTG in these trials. A potential contributor to the toxicity of overexpression of *patA* homologues was initially thought to be the large number of disulfide bonds present in PatA that may become misaligned; such erroneous structures would aggregate. However, the use of *E. coli* SHuffle T7 (NEB) to express *CjpatA* did not alleviate the situation. This *E. coli* strain constitutively expresses disulfide bond isomerase DsbC, which helps to properly form disulfide bonds for the appropriate folding of proteins in the cytoplasm. A current hypothesis now being tested is that, as an integral membrane protein with a solvent-accessible channel that runs through it, PatA produced alone results in the presence of an open pore, which would allow the uncontrolled dissipation of proton-motive force. It remains a mystery though why the expression and overproduction of a homologous MBOAT protein, DltB, is possible [76]. Presumably, the additional structural elements unique to DltB serve to control access to its membrane-spanning central pore.

A major reason for the misunderstanding that the production of recombinant PatA could be achieved alone was the observation that the growth of transformed cells recovered following prolonged incubations. However, such situations occurred with host cells harbouring constructs

containing ampicillin resistance genes as markers. It has been demonstrated by others that this phenomenon will occur as the β-lactamase resistance factor will have sufficiently reduced ampicillin levels below toxicity levels thereby allowing cells that have expelled the expression plasmids to now grow [81].

4.2 Lysozyme sensitivity: spot assay and growth curves

Lacking the availability of recombinant PatA for *in vitro* biochemical analysis, an attempt was made to develop and use a lysozyme sensitivity assay as the primary means to elucidate the functional residues of *Cj*PatA. To this end, residues that were invariantly conserved amongst *patA* homologues were replaced by alanine residues and would then be subjected to a suitable bioassay when one was available with enough sensitivity to distinguish between the importance of each residue. Many variations of the spot assay were tested to determine the best media, lysozyme concentration, and concentration of other additives needed to produce significant and measurable differences in lysozyme sensitivity relative to differences in PG O-acetylation levels. With the original mutants, this difference was between 2.45% and 12.5% for *ΔpatA* and WT/(and potentially Δ*patAc*), respectively. The larger range tested was between 2% and 36% for Δ*oap* and Δ*ape1*/(and potentially Δ$oap_{c\ (CjpatA\ +\ B)}$), respectively [69]. Before testing the spot assay on *C. jejuni* variants harbouring replacements of functional residues, the difference in tolerance to lysozyme of these control strains had to be confirmed.

The objective of the initial lysozyme sensitivity spot assay trials was to search for significant differences between WT and Δ*patA* strains. If a significant difference in tolerance to lysozyme was detected, then the complement (Δ$patA_C$) could be tested, which should

theoretically match the phenotype of the WT strain. Similar assays had been previously performed by others where a knockout *patA* strain of *H. pylori* was compared in its sensitivity to lysozyme to its respective wild-type strain. In this study lysozyme paired with lactoferrin and lysozyme alone at a high concentration (50 mg/ml) was utilized[59]. Further, lysozyme sensitivity of WT *C. jejuni* 81-176 was compared to individual knockouts of *patA* and *patB* strains, and then to their corresponding complement variants [82]. The latter assay also utilized a lysozyme (3 mg/ml) in combination with lactoferrin (1.5 mg/ml) to test the sensitivity of the *C. jejuni* mutants to lysozyme while suspended in PBS for 6 h. An approximate x10 difference in cell survival to these conditions was observed when *CjpatA* or *CjpatB* were knocked out [82].

The initial trials of the lysozyme sensitivity assay that were attempted but not included in this thesis were based on the replication of these reported findings. These trials were fraught with inconsistency in cell growth where the results of each assay would retain high levels of variance. A lot of the variability in these initial trials could have stemmed from the improper handling of the fastidious *C. jejuni* 81-176 in tandem to attempting to subject *C. jejuni* 81-176 to some of the initial variations of the lysozyme sensitivity assay that were mentioned in section 3.3.1. However, the results that were also presented herein, after utilizing greater skill in growing *C. jejuni* 81-176, did not conform well to those results. The large x100 difference in lysozyme sensitivity that was found between the WT and Δ*patA* could never be replicated, but occasionally an approximate x10 difference could be observed, similar to what was observed previously with *C. jejuni* 81-176[82]. However, this was not always apparent and replicable, and when the lysozyme sensitivity of the Δ*patA*c mutant was tested alongside the WT and Δ*patA* strains, the Δ*patA*c mutant appeared to have a higher sensitivity to lysozyme than the latter strains. The reason for

the discrepancy between WT and Δ*patAc* could be attributed to the difference in growth rates between the two strains, where the WT cells may have had the ability to recover their population somewhat during the hours that it was incubated with lysozyme, while Δ*patA*c may not have been able to do so as easily. Additionally, the minimal difference between WT and Δ*patA* strains in terms of cell survival when subjected to the conditions of the lysozyme sensitivity assay might also be attributed to the small difference in percent O-acetylation that was reported in the strains (12.5 ± 0.71 and 2.45 ± 0.14, respectively)[70].

In an attempt to circumvent these issues, the new mutant, Δ$oap_{c\ (CjpatA+B)}$ was generated to then replicate the phenotype of Δ*ape1* to thereby establish a control with a much higher level of PG O-acetylation compared to WT. With this strain, it was anticipated that changes in PatA activity resulting from the replacement of specific residues would be more evident. Unfortunately, with the spot assay conditions used, there was still no real significant difference between the sensitivity of Δ*oap* and Δ*ape1*/Δ$oap_{c\ (CjpatA+B)}$ (Figures 3.8 and 3.9). Despite the larger difference in the expected percent O-acetylation between Δ*oap* and Δ*ape1*/Δ$oap_{c\ (CjpatA+B)}$, the conditions used for the spot assay were still not able to generate a significant difference in lysozyme sensitivity. A possible reason for this could be that the spot assay does not apply constant pressure on the cell populations, and only during the incubation times is there any possible effect. Since the doubling time of *C. jejuni* 81-176 is around 2 h in optimal conditions [83], the samples of *C. jejuni* that were held in the detrimental growth conditions of the suspension may persist longer due to a slower metabolism. Once the cells were removed from the suspension, the pressure generated from lysozyme and other factors of the suspension would be removed. One solution to this would be to add lysozyme to MH agar plates, but this requires

considerable amounts of lysozyme to affect the cells, making it quite costly. Conditions should still be tested that can eliminate a large proportion of cells in the time it is incubated with lysozyme and other additional additives. This could be an accurate method of cell population enumeration otherwise.

The sensitivity to lysozyme of the different *C. jejuni* mutants were also tested with constant monitoring by utilizing growth in a 96-well microplate. The format for this assay utilized 50 mM sodium bicarbonate in the cell suspension to generate a high percent CO_2 atmosphere that was maintained by applying a Breath-Easy gas permeable sealing membrane to the 96-well microplate. The initial trials using the microplate reader resulted in data that were not replicable. This could have been caused by uneven amounts of sodium bicarbonate added to the cell suspensions, or leaks in the permeable membrane that allowed the CO_2 to escape if not properly applied to the 96-well plate. The best attempts at the lysozyme sensitivity assay were shown in Figures 3.10 and 3.11. Rather than incubating samples immediately with lysozyme and EDTA, they were added after 5 h of growth to help stop any selection of cells that had more resistance to lysozyme and therefore, generated more similar curves despite the alleged difference in percent O-acetylation. As mentioned in section 3.3.2, according to MIC_{50} assays with *C. jejuni* 81-176 showed that concentrations 5mg/ml lysozyme and 150 µM EDTA would halt growth by 50% [70] which is why they were chosen first. While the growth curves with and without lysozyme and EDTA did not verify this data, this could have been because they utilized a starting OD_{600} value of approximately 0.0002 while the starting OD_{600} values for experiments conducted here were 0.05. Perhaps a greater concentration of lysozyme/EDTA to cell ratio could have been used to fully replicate the conditions of their MIC_{50} assay. While some difference in sensitivity was observed

when increasing the concentration of lysozyme to 10 mg/ml, the addition of larger volumes of compounds after 5 h of growth began distorting the measured OD_{600} values of the cell suspensions. Finally, it should be noted that some of this variability in the lysozyme sensitivity assays could still be attributed to the growth of *C. jejuni* 81-176 in conditions that were suboptimal for its growth. Tri-gas incubators, for instance, are typically used to grow *C. jejuni* 81-176 in an atmosphere of 85% N2, 10% CO2, and 5% O2[68], where the addition of a candle to a jar or addition of sodium bicarbonate to media, would not fully replicate.

4.3 Autolysis assay: cuvettes and microplate

Given the lack of success with producing reliable data using the lysozyme-based assay, attention was turned to monitoring the autolytic rate of the *C. jejuni* mutants. Initial attempts to determine if the mutants had different rates of autolysis yielded no significant results. This was most likely due to the format of the assay where the incubation times were 20 min in length, but it also took roughly 10 min to complete the measurements for every sample including the replicates. In combination with only one replicate for the controls, the assay was used mostly to determine if a significant difference could be observed between the mutant samples and the WT strain of *C. jejuni* 81-176. The issue that arose first was that the control samples would lyse at very similar rates as those also incubated with 10 mM EDTA, the reagent used to induce autolysis (Figure 3.12). As a metal chelator, EDTA perturbs the outer membrane which consequently induces autolysis in many Gram-negative bacteria, including *C. jejuni* [72]. The concentration of EDTA and the incubation temperature were both lowered to match the conditions used in the autolysis of *N. gonorrhoeae* [73]. Since the difference between the samples was not significant despite the larger drop in OD_{600}, a change was made to use the micro-plate reader again to try

and observe more closely any larger discrepancies in the rate of autolysis. The mutant, Δ*oap*$_{C\ (CjpatA\ +\ B)}$, was found to lyse much more quickly than both Δ*ape1* and Δ*oap* despite having an expected equal percent O-acetylation to the Δ*ape1* mutant. When analyzing the insert containing *CjpatA* and *B* that was cloned out of the *C. jejuni* chromosome and then reintroduced back into the chromosome via allelic exchange, it was discovered that a second promoter was being used for the expression of *CjpatA* and *CjpatB*, in addition to the chloramphenicol resistance cassette (Cam^r) gene promoter. For example, the mutant, Δ*ape1*, expresses *CjpatA* and *CjpatB* using only the native *oap* operon promoter, whereas in Δ*oap*$_{C\ (CjpatA\ +\ B)}$ the expression of the complemented *CjpatA* and *B* was mediated by both the promoter for Cam^r and the native *oap* promoter. In this case, Cam^r was introduced into the *C. jejuni* chromosome upstream of the reintroduced *CjpatA* and *CjpatB* genes and the native *oap* promoter which was mistakenly cloned in just upstream of *CjpatA*. Primers used by Ha et al. (2016) to clone *CjpatA* also cloned the promoter for the *oap* operon, but it was not used as extensively in the study relative to the Δ*ape1* and Δ*ape1*$_C$ mutants. These specific mutants did not contain the extra promoter and so the extra promoter in the Δ*patA*$_C$ and Δ*oap*$_C$ strains were not removed. A possible downstream effect of the extra promoter was the possible uneven and potentially mildly upregulated expression of *CjpatA* and *B*. Within the amino acid replacement mutant strains, the inhibition of *CjpatA* through the replacement of critical residues, and therefore a decrease in the metabolization of critical resources in the cell such as acetyl-CoA, which is the presumed source of acetyl groups for PatA homologues, could potentially mitigate the toxic effect of overexpression of *patA* to an extent and could cause slower rates of lysis. However, experimental evidence is still required to verify that double promoters are a contributing factor to the greater decrease in the cell population of the Δ*oap*$_C$

(CjpatA + B) mutant. This assay appears to have an unintended and roundabout effect of being able to partially elucidate functional residues of *CjpatA*, but not necessarily through sensitivity to autolysis relative to levels of *O*-acetylation, but possibly through the relief of detrimental effects on the cell that would be caused by the extra allocation of resources to the cell wall in a nutrient-deprived environment. The longevity of the site-directed mutant cells may also increase possibly through a decrease in active PatA enzymes that may not be forming complexes with PatB and causing a detrimental effect on the cell.

The discrepancy in OD_{600} measurements at the temperatures of $27^{O}C$ and $37^{O}C$, pertaining to the population of *C. jejuni* 81-176 cells in the autolysis assay, could partially be explained by the usage of light scattering to quantify the population instead of directly measuring the population as accomplished in the $27^{O}C$ autolysis trial afterward. While measuring optical density for the $27^{O}C$ autolysis trial, it was noted that all of the strains, with the exception of Δ*oap*$_{C\ (CjpatA\ +\ B)}$, remained above 100% of their starting OD_{600} value. Most of the cells absolutely become non-viable as shown by spotting the population, but because the autolysis assay relies on the action of LTs, there is less complete lysis of cells than what would be observed if treated with lysozyme instead. The mechanism of autolysis with LTs would then produce whole cell debris that scatters light in the cultures and conserves the high OD_{600} values. As for why the OD_{600} measurements for the $37^{O}C$ trial were not showing the same level of sustainability as the $27^{O}C$ trial, this might be attributed to other mechanisms in *C. jejuni* 81-176 that were tailored for maximum function at $37 – 42^{O}C$, as opposed to $27^{O}C$. Some of these mechanisms might contribute to complete lysing of cells during periods of autolysis at optimal temperature, but not at $27^{O}C$.

More work needs to be done to make sure that replacing functional residues in this assay does relieve cellular stress. This can be done by testing residues that are not predicted to disturb the structural integrity of the protein or disrupt the catalytic function of the protein. If the autolytic curve that is generated from this hypothetical mutant follows the same path as Δ*oap*$_{C\ (CjpatA\ +\ B)}$, then it can be assumed that this is at least partially what is causing the increased autolytic rate. The OD_{600} measurements could be a good initial test as to whether the catalytic function of the enzyme is interrupted, but cell populations should also be verified in other ways such as colony-forming unit (CFU) counting. While spotting diluted cell populations that underwent autolysis was informative, it could be more precise by counting CFUs instead of observing whole cell spots representing serial dilutions. An interesting result from the spot assay of the autolysis curves was that the Δ*oap* strain and Δ*oap*$_{C(patA\ +\ B)}$ strains both had a x10^3 drop in viable cell populations, while the autolysis curves indicated that the Δ*oap* population would exhibit a x10 decrease like that of the WT, Δ*ape1*, and Δ*patA*$_C$ strains. This discrepancy between the spot assay and the autolysis curves denotes a need to quantify the incubated cell populations using continued spot assay or CFU counting assessment to appropriately determine the effects of the environment on the rate of autolysis in the *C. jejuni* 81-176 strains. The cell spotting assay performed alongside autolysis curve generation in this study should also be repeated to ensure replication of the results will occur.

4.4 Quantification of *O*-acetylation of PG

The quantification of PG O-acetylation in the initial control strains was successful despite rather large standard deviations in the muramic acid and free acetate samples. The values determined for the control samples, WT, Δ*oap*, and Δ*ape1* mostly were consistent with those

reported in Ha *et al.* (2016)[70]. The Δ*patA*$_C$ and Δ*oap*$_{C(patA + B)}$ strains had comparable levels of O-acetylation to those found in the WT and Δ*ape1* strains, which meant that the complementation of *patA* or *patA* and *patB* was successful. This indicated that the method used to analyze the PG was viable and could be applied to find the percent O-acetylation of the mutant strains as well. Unfortunately, however, an error may have occurred during the analysis of the amino acid replacement strains, which led to inflated levels of percent O-acetylation. The much higher levels of percent O-acetylation determined for these strains exceeded the range that these mutants were expected to fall within (approximately 0.8% – 39% O-acetylation of MurNAc residues based on the results from Δ*oap* and Δ*ape1*/Δ*oap*$_{C\ (CjpatA + B)}$). An issue with the PG purification was considered, but since Δ*patA*$_C$ was purified a second time together with the amino acid replacement mutants and mostly adhered to the results of the first attempt, a contaminant co-purifying with the PG samples of the amino acid replacement strains was also considered plausible. While O-acetylation of capsular polysaccharide (CPS) occurs in specific strains, *e.g., C. jejuni* 81116 with serotype HS:6, the CPS of strain 81-176 is not known to be O-acetylated [84]. There may also be extracellular polysaccharides from strain 81-176 that are O-acetylated, but these polysaccharides have not been detected previously if they do exist. Consequently, these analyses need to be repeated with care to avoid the isolation of any other extracellular material.

It was shown in section 3.5 that there is no extra copy of *CjpatA* in the chromosome of the H315A mutant strain, yet it still possesses higher than expected percent O-acetylation. If no contaminating polysaccharide is found, then the higher then expected O-acetylation might be a function, somehow, of the interruption of these catalytic residues of *Cj*PatA. In a similar way to validating the autolysis assay using perceived unimportant amino acid residues for function or

structural stability and testing to see if the population decreases by a significant amount, the same could be tested using PG quantification and determining if there is no great increase in percent O-acetylation. Also, the mutated (amino acid replacement) *patA* genes could be reintroduced into the Δ*patA* strain to check if the unexpected phenotype persists. This would be to check if somehow the double complementation of *CjpatA* and *CjpatB* contributes to the increased levels of O-acetylation, since the root cause has not been determined as of yet.

Concluding remarks

Despite a variety of strategies and approaches taken, attempts to express *PmpatA* and *CjpatA* and isolate their protein products were continually met with no success. In an attempt to nonetheless characterize PatA, while further attempts to express *patA* continued by others in the Clarke lab, experiments were conducted to identify functional residues of *Cj*PatA. PatA is a member of the MBOAT family of proteins, for which very little is known biochemically and mechanistically. So far, there is only one X-ray crystal structure of an MBOAT, DltB from *S. thermophilus* (PDB 6BUH) [76]. This structure was used to base an investigation of the catalytic mechanism and structure-function relationship of many residues of DltB through *in vitro* assays, but the characterization of the protein was also performed using *in situ* assays such as lysozyme sensitivity of whole cells to test functional residues of DltB. A structural model of PatA was generated using the crystal coordinates for DltB, and invariant residues of PatA homologs were chosen for testing, which included S122, R164, H275, R283, and H315. An attempt to use a lysozyme sensitivity spot assay was made to detect a discernible difference in survivability between the WT/Δ$patA_C$ and Δ*patA* strains of *C. jejuni* when incubated with lysozyme. Different conditions for the assay were tested, but due to issues replicating the lysozyme sensitivity of the

initial control strains, WT, Δ*patA*, and Δ*patA*$_C$, the site-directed mutants of singularly complemented Δ*patA* strains were never tested in this way. To increase the sensitivity of the lysozyme sensitivity assay, the construct, PACBL3, was generated and its derivative plasmids, PACBL4-8 were generated using site-directed mutagenesis. These were used to create the mutants, Δ*oap*$_{c\ (CjpatA\ +\ B)}$, S122A, R164A, H275A, R283A, and H315A using allelic exchange.

With these new mutants created, the lysozyme sensitivity spot assay was utilized again to try and discern a significant difference in survivability to incubation with lysozyme combined with different membrane permeabilizers and incubation mediums. The survivability of Δ*oap*$_{c\ (CjpatA\ +\ B)}$ in these suspensions was compared to that of Δ*ape1* and Δ*oap*, but again no significant difference could be observed, while using the spot assay.

Attention was turned to an autolysis-based assay with the understanding that PG O-acetylation controls autolysin activity in Gram-negative bacteria. This was met with initial success in measuring the rate of autolysis with the site-directed mutant strains of *C. jejuni* 81-176 and hence remaining efforts focused on optimizing the autolysis assay and quantifying O-acetylation of PG in these strains. The O-acetylation values of the mutants should not have exceeded the O-acetylation values of Δ*oap*$_{C(patA\ +\ B)}$/Δ*ape1*, and yet all of the mutants exceeded the threshold of what was expected. While the results for the levels of O-acetylation of the site-directed mutants remain inconclusive for now, the control strains adhered to what was previously reported in Ha *et al.* (2016)[70]. For this reason, it should still be possible to discern the levels of O-acetylation of the site-directed mutants once the reason for the elevated levels is discovered.

Going forward, higher concentrations of lysozyme and/or EDTA could be used in the turbidity assay with the microplate reader to see if a significant difference in lysozyme sensitivity can be observed. Although proper growth conditions for *C. jejuni* 81-176 should also be investigated that will allow it to grow in more optimal conditions within the plate reader to limit the amount of extra stress placed on the cells. This could require higher growth temperatures or an increased amount of sodium bicarbonate. Residues suspected of minimally contributing to catalysis or structural integrity should also be replaced. This way, if the reason for the difference in the rate of autolysis between Δ*ape1* and Δ$oap_{c\ (CjpatA\ +\ B)}$ is that more PatA and PatB are being produced in the Δ$oap_{c\ (CjpatA\ +\ B)}$ mutant, then the autolysis curve of this new mutant might adhere to the curve of Δ$oap_{c\ (CjpatA\ +\ B)}$ in contrast to how replacing functionally important residues appears to decrease the rate of autolysis. This same strategy would also apply to PG isolation and *O*-acetate quantification, where an unimportant residue might not increase to the levels of percent O-acetylation beyond the expected range set by the Δ*ape1*/Δ$oap_{c\ (CjpatA\ +\ B)}$ strains and the Δ*oap* strain.

The native *oap* promoter should also be removed from the *patA* and *patA* + *patB* complement strains to ascertain the promoter's contribution to toxic effects in the cell, if any, during periods of incubation within environments with low concentrations of metabolic resources. The chloramphenicol promoter should not be removed because it is upstream of all inserted genes and removing it would increase the complemented strain's ability to be selected using chloramphenicol. Counting CFUs of the different *C. jejuni* 81-176 strains incubated in conditions that would induce autolysis should also be performed to precisely delineate the effects of the autolytic conditions on each strain. These more precise measurements can be

related to the percent O-acetylation of the amino acid replacement mutants to determine if a correlation between the two measurements exists. To complete this goal, the PG O-acetylation analysis of the amino acid replacement strains should be repeated to determine if the high percent O-acetylation could be replicated or if the inflated percent O-acetylation values of these strains was an anomalous effect of the purification process or muramic acid and acetate analysis methods. General growth curves of all *C. jejuni* 81-176 mutants with the WT strain should be generated to measure the maximum population and growth speed between all the mutants. In this way, another measurement of the functional importance of residues might be discovered if growth curves are affected by the amount and functionality of *CjpatA*.

The accumulation of antibiotic resistance in pathogenic bacteria is a global health threat that could result in much higher rates of morbidity in the future spurred for example by liberal usage of antibiotics in agriculture and incorrect usage by individuals [85]. One solution to the problem is to try and circumvent the acquired resistance to antibiotics by finding new targets for antibiotic therapy and finding antimicrobials that efficiently disrupt the growth of pathogenic populations while restricting harm to the host they are administered to. With this, the study of PatA is important because it is involved in the mechanism of O-acetylation of the C-6 hydroxyl group of MurNAc in PG. This is used as a defensive mechanism against lysozyme attack from the host and to regulate the recycling of the cell wall for healthy growth and division of the pathogenic bacterial cell [11]. More information on the mechanism and structure of PatA is needed to be considered a suitable target for antibiotic therapy, but by characterizing this protein, an important step will be taken in understanding an important mechanism within pathogenic Gram-negative bacteria, which is the O-acetylation of PG.

References:

(1) Martinez, J. L. General Principles of Antibiotic Resistance in Bacteria. *Drug Discov. Today Technol.* **2014**, *11* (1), 33–39. https://doi.org/10.1016/j.ddtec.2014.02.001.

(2) Andersson, D. I.; Hughes, D. Persistence of Antibiotic Resistance in Bacterial Populations. *FEMS Microbiol. Rev.* **2011**, *35* (5), 901–911. https://doi.org/10.1111/j.1574-6976.2011.00289.x.

(3) Brown, E. D.; Wright, G. D. Antibacterial Drug Discovery in the Resistance Era. *Nature* **2016**, *529* (7586), 336–343. https://doi.org/10.1038/nature17042.

(4) Chambers, H. F. Penicillin-Binding Protein-Mediated Resistance in Pneumococci and Staphylococci. *J. Infect. Dis.* **1999**, *179* (s2), S353–S359. https://doi.org/10.1086/513854.

(5) Christaki, E.; Marcou, M.; Tofarides, A. Antimicrobial Resistance in Bacteria: Mechanisms, Evolution, and Persistence. *J. Mol. Evol.* **2020**, *88* (1), 26–40. https://doi.org/10.1007/s00239-019-09914-3.

(6) Limbago, B. M.; Kallen, A. J.; Zhu, W.; Eggers, P.; Mcdougal, L. K.; Albrecht, S. Report of the 13th Vancomycin-Resistant Staphylococcus Aureus Isolate from the United States. *J Clin Microbiol.* **2014**, *52* (3), 998–1002. https://doi.org/10.1128/JCM.02187-13.

(7) Marston, H. D.; Dixon, D. M.; Knisely, J. M.; Palmore, T. N.; Fauci, A. S. Antimicrobial Resistance. *JAMA - J. Am. Med. Assoc.* **2016**, *316* (11), 1193–1204. https://doi.org/10.1001/jama.2016.11764.

(8) Clarke, A. J.; Dupont, C. O-Acetylated Peptidoglycan: Its Occurrence, Pathobiological

Significance, and Biosynthesis. *Can. J. Microbiol.* **1992**, *38* (2), 85–91. https://doi.org/10.1139/m92-014.

(9) Schleifer, K. H.; Kandler, O. Peptidoglycan Types of Bacterial Cell Walls and Their Taxonomic Implications. *Bacteriol. Rev.* **1972**, *36* (4), 407–477. https://doi.org/10.1128/mmbr.36.4.407-477.1972.

(10) Vollmer, W.; Blanot, D.; De Pedro, M. A. Peptidoglycan Structure and Architecture. *FEMS Microbiol. Rev.* **2008**, *32* (2), 149–167. https://doi.org/10.1111/j.1574-6976.2007.00094.x.

(11) Sychantha, D.; Brott, A. S.; Jones, C. S.; Clarke, A. J. Mechanistic Pathways for Peptidoglycan O-Acetylation and De-O-Acetylation. *Front. Microbiol.* **2018**, *9*, 1–17. https://doi.org/10.3389/fmicb.2018.02332.

(12) Silhavy, T. J.; Kahne, D.; Walker, S. The Bacterial Cell Envelope. *Cold Spring Harb Perspect Biol* **2010**, *2*, 1–16. https://doi.org/10.1101/cshperspect.a000414.

(13) Vaara, M. Agents That Increase the Permeability of the Outer Membrane. *Microbiol. Rev.* **1992**, *56* (3), 395–411. https://doi.org/10.1128/mr.56.3.395-411.1992.

(14) Masschalck, B.; Michiels, C. W.; Masschalck, B.; Michiels, C. W. Antimicrobial Properties of Lysozyme in Relation to Foodborne Vegetative Bacteria Antimicrobial Properties of Lysozyme in Relation to Foodborne Vegetative Bacteria. *Crit. Rev. Microbiol.* **2008**, *23* (3), 191–214. https://doi.org/10.1080/713610448.

(15) Melo, A. M. S. C. D.; Cassar, C. A.; Miles, R. J. Trisodium Phosphate Increases Sensitivity of

Gram-Negative Bacteria to Lysozyme and Nisin. *J. Food Prot.* **1998**, *61* (7), 839–843. https://doi.org/10.4315/0362-028x-61.7.839.

(16) Brown, S.; Santa Maria, J. P.; Walker, S. Wall Teichoic Acids of Gram-Positive Bacteria. *Annu. Rev. Microbiol.* **2013**, *67* (6), 313–336. https://doi.org/10.1146/annurev-micro-092412-155620.

(17) Elè Ne Barreteau, H. ´; Kovač, A.; Boniface, A.; Sova, M.; Gobec, S.; Blanot, D. Cytoplasmic Steps of Peptidoglycan Biosynthesis. *FEMS Microbiol. Rev.* **2008**, *32*, 168–207. https://doi.org/10.1111/j.1574-6976.2008.00104.x.

(18) Egan, A. J. F.; Vollmer, W. The Physiology of Bacterial Cell Division. *Ann. N. Y. Acad. Sci.* **2013**, *1277* (1), 8–28. https://doi.org/10.1111/j.1749-6632.2012.06818.x.

(19) Taguchi, A.; Welsh, M. A.; Marmont, L. S.; Lee, W.; Sjodt, M.; Kruse, A. C.; Kahne, D.; Bernhardt, T. G.; Walker, S. FtsW Is a Peptidoglycan Polymerase That Is Functional Only in Complex with Its Cognate Penicillin-Binding Protein. *Nat Microbiol* **2019**, *4* (4), 587–594. https://doi.org/10.1038/s41564-018-0345-x.FtsW.

(20) Sauvage, E.; Kerff, F.; Terrak, M.; Ayala, J. A.; Charlier, P. The Penicillin-Binding Proteins: Structure and Role in Peptidoglycan Biosynthesis. *FEMS Microbiol. Rev.* **2008**, *32* (2), 234–258. https://doi.org/10.1111/j.1574-6976.2008.00105.x.

(21) Dik, D. A.; Fisher, J. F.; Mobashery, S. Cell-Wall Recycling of the Gram-Negative Bacteria and the Nexus to Antibiotic Resistance. *Chem. Rev.* **2018**, *118* (12), 5952–5984. https://doi.org/10.1021/acs.chemrev.8b00277.

(22) Johnson, J. W.; Fisher, J. F.; Mobashery, S. Bacterial Cell-Wall Recycling. *Ann. N. Y. Acad. Sci.* **2013**, *1277* (1), 54–75. https://doi.org/10.1111/j.1749-6632.2012.06813.x.

(23) Henrissat, B.; Daviest, G. Structural and Sequence-Based Classification of Glycoside Hydrolases. *Curr. Opin. Struct. Biol.* **1997**, *7*, 637–644. https://doi.org/10.1016/S0959-440X(97)80072-3.

(24) Davies, G.; Henrissat, B. Structures and Mechanisms of Glycosyl Hydrolases. *Structure* **1995**, *3* (9), 853–859. https://doi.org/10.1016/S0969-2126(01)00220-9.

(25) Henrissat, B.; Bairoch, A. Updating the Sequence-Based Calssification of Glycosyl Gydrolases. *Biochem. J.* **1996**, *316*, 695–696. https://doi.org/10.1042/bj3160695.

(26) Henrissat, B.; Bairoch, A. New Families in the Classification of Glycosyl Hydrolases Based Amino Acid Sequence Similarities. *Biochem. J.* **1993**, *293*, 781–788. https://doi.org/10.1042/bj2930781.

(27) Henrissat, B. A Classification of Glycosyl Hydrolases Based on Amino Acid Sequence Similarities. *Biochem. J.* **1991**, *280*, 309–316. https://doi.org/10.1042/bj2800309.

(28) Drula, E.; Garron, M.; Dogan, S.; Lombard, V.; Henrissat, B.; Terrapon, N. The Carbohydrate-Active Enzyme Database : Functions and Literature. *Nucleic Acids Res.* **2022**, *50* (November 2021), 571–577. https://doi.org/10.1093/nar/gkab1045.

(29) Brott, A. S.; Clarke, A. J. Peptidoglycan O-Acetylation as a Virulence Factor: Its Effect on Lysozyme in the Innate Immune System. *Antibiotics* **2019**, *8* (94), 1–15. https://doi.org/10.3390/antibiotics8030094.

(30) Ohno, N.; Yadomae, T.; Miyazaki, T. Identification of 2-Amino-2-Deoxyglucose Residues in the Peptidoglucan of Streptococcus Pneumoniae. *Carbohydr. Res.* **1982**, *107* (1), 152–155. https://doi.org/10.1016/S0008-6215(00)80785-5.

(31) Araki, Y.; Nakatani, T.; Hayashi, H.; Ito, E. Occurrence of Non-N-Substituted Glucosamine Residues in Lysozyme-Resistant Peptidoglycan from Bacillus Cereus Cell Walls. *Biochem. Biophys. Res. Commun.* **1971**, *42* (4), 691–697. https://doi.org/10.1016/0006-291X(71)90543-2.

(32) Zipperle, G. F.; Ezzell, J. W.; Doyle, R. J. Glucosamine Substitution and Muramidase Susceptibility in Bacillus Anthracis. *Can. J. Microbiol.* **1984**, *30* (5), 553–559. https://doi.org/10.1139/m84-083.

(33) Davis, K. M.; Weiser, J. N. Modifications to the Peptidoglycan Backbone Help Bacteria to Establish Infection. *Infect. Immun.* **2011**, *79* (2), 562–570. https://doi.org/10.1128/IAI.00651-10.

(34) Hébert, L.; Courtin, P.; Torelli, R.; Sanguinetti, M.; Chapot-Chartier, M. P.; Auffray, Y.; Benachour, A. Enterococcus Faecalis Constitutes an Unusual Bacterial Model in Lysozyme Resistance. *Infect. Immun.* **2007**, *75* (11), 5390–5398. https://doi.org/10.1128/IAI.00571-07.

(35) Fittipaldi, N.; Sekizaki, T.; Takamatsu, D.; De La Cruz Domínguez-Punaro, M.; Harel, J.; Bui, N. K.; Vollmer, W.; Gottschalk, M. Significant Contribution of the PgdA Gene to the Virulence of Streptococcus Suis. *Mol. Microbiol.* **2008**, *70* (5), 1120–1135. https://doi.org/10.1111/j.1365-2958.2008.06463.x.

(36) Abrams, A. O-Acetyl Groups in the Cell Wall of Streptococcus Faecalis. *J. Biol. Chem.* **1957**, *230* (2), 949–959. https://doi.org/10.1016/S0021-9258(18)70518-8.

(37) Brumfitt, W.; Wardlaw, A. C.; Park, J. T. Development of Lysozyme-Resistance in Micrococcus Lysodiekticus and Its Association with an Increased O-Acetyl Content of the Cell Wall. *Nature* **1958**, *181* (4626), 1783–1784. https://doi.org/10.1038/1811783a0.

(38) Brumfitt, W. The Mechanism of Development of Resistance to Lysozyme by Some Gram-Positive Bacteria and Its Results. *Br. J. Exp. Pathol.* **1959**, *40*, 441–451.

(39) Pushkaran, A. C.; Nataraj, N.; Nair, N.; Götz, F.; Biswas, R.; Mohan, C. G. Understanding the Structure-Function Relationship of Lysozyme Resistance in Staphylococcus Aureus by Peptidoglycan o-Acetylation Using Molecular Docking, Dynamics, and Lysis Assay. *J. Chem. Inf. Model.* **2015**, *55* (4), 760–770. https://doi.org/10.1021/ci500734k.

(40) Bera, A.; Biswas, R.; Herbert, S.; Götz, F. The Presence of Peptidoglycan O-Acetyltransferase in Various Staphylococcal Species Correlates with Lysozyme Resistance and Pathogenicity. *Infect. Immun.* **2006**, *74* (8), 4598–4604. https://doi.org/10.1128/IAI.00301-06.

(41) Dupont, C.; Clarke, A. J. In Vitro Synthesis and O Acetylation of Peptidoglycan by Permeabilized Cells of Proteus Mirabilis. *J. Bacteriol.* **1991**, *173* (15), 4618–4624. https://doi.org/10.1128/jb.173.15.4618-4624.1991.

(42) Gmeiner, J.; Sarnow, E. Murein Biosynthesis in Synchronized Cells of Proteus Mirabilis Quantitative Analysis of O-Acetylated Murein Subunits and of Chain Terminators

Incorporated into the Sacculus during the Cell Cycle. *FEBS* **1987**, *163* (2), 389–395. https://doi.org/10.1111/j.1432-1033.1987.tb10811.x.

(43) Snowden, M. A.; Perkins, H. R.; Wyke, A. W.; Hayes, M. V.; Ward, J. B. Cross-Linking and O-Acetylation of Newly Synthesized Peptidoglycan in Staphylococcus Aureus H. *J. Gen. Microbiol.* **1989**, *135* (11), 3015–3022. https://doi.org/10.1099/00221287-135-11-3015.

(44) Bera, A.; Herbert, S.; Jakob, A.; Vollmer, W.; Götz, F. Why Are Pathogenic Staphylococci so Lysozyme Resistant? The Peptidoglycan O-Acetyltransferase OatA Is the Major Determinant for Lysozyme Resistance of Staphylococcus Aureus. *Mol. Microbiol.* **2005**, *55* (3), 778–787. https://doi.org/10.1111/j.1365-2958.2004.04446.x.

(45) Bernard, E.; Rolain, T.; Courtin, P.; Guillot, A.; Langella, P.; Hols, P.; Chapot-Chartier, M. P. Characterization of O-Acetylation of N-Acetylglucosamine: A Novel Structural Variation of Bacterial Peptidoglycan. *J. Biol. Chem.* **2011**, *286* (27), 23950–23958. https://doi.org/10.1074/jbc.M111.241414.

(46) Jones, C. S.; Sychantha, D.; Lynne Howell, P.; Clarke, A. J. Structural Basis for the O-Acetyltransferase Function of the Extracytoplasmic Domain of OatA from Staphylococcus Aureus. *J. Biol. Chem.* **2020**, *295* (24), 8204–8213. https://doi.org/10.1074/JBC.RA120.013108.

(47) Sychantha, D.; Jones, C. S.; Little, D. J.; Moynihan, P. J.; Robinson, H.; Galley, N. F.; Roper, D. I.; Dowson, C. G.; Howell, P. L.; Clarke, A. J. In Vitro Characterization of the Antivirulence Target of Gram-Positive Pathogens, Peptidoglycan O-Acetyltransferase A (OatA). *PLoS Pathog.* **2017**, *13* (10), 1–26. https://doi.org/10.1371/journal.ppat.1006667.

(48) Sychantha, D.; Clarke, A. J. Peptidoglycan Modification by the Catalytic Domain of Streptococcus Pneumoniae OatA Follows a Ping-Pong Bi-Bi Mechanism of Action. *Biochemistry* **2018**, *57* (16), 2394–2401. https://doi.org/10.1021/acs.biochem.8b00301.

(49) Jones, C. S.; Anderson, A. C.; Clarke, A. J. Mechanism of Staphylococcus Aureus Peptidoglycan O-Acetyltransferase A as an O-Acyltransferase. *Proc. Natl. Acad. Sci. USA* **2021**, *118* (36). https://doi.org/10.1073/pnas.2103602118.

(50) Davis, E. O.; Evans, I. J.; Johnston, A. W. B. Identification of NodX, a Gene That Allows Rhizobium Leguminosarum Biovar Viciae Strain TOM to Nodulate Afghanistan Peas. *MGG Mol. Gen. Genet.* **1988**, *212* (3), 531–535. https://doi.org/10.1007/BF00330860.

(51) Firmin, J. L.; Wilson, K. E.; Carlson, R. W.; Davies, A. E.; Downie, J. A. Resistance to Nodulation of Cv. Afghanistan Peas Is Overcome by NodX, Which Mediates an O-acetylation of the Rhizobium Leguminosarum Lipo-oligosaccharide Nodulation Factor. *Mol. Microbiol.* **1993**, *10* (2), 351–360. https://doi.org/10.1111/j.1365-2958.1993.tb01961.x.

(52) Pearson, C. R.; Tindall, S. N.; Herman, R.; Jenkins, H. T.; Bateman, A.; Thomas, G. H.; Potts, J. R.; Van der Woude, M. W. Acetylation of Surface Carbohydrates in Bacterial Pathogens Requires Coordinated Action of a Two-Domain Membrane-Bound Acyltransferase. *MBio* **2020**, *11* (4), 1–19. https://doi.org/10.1128/mBio.01364-20.

(53) Dillard, J. P.; Hackett, K. T. Mutations Affecting Peptidoglycan Acetylation in Neisseria Gonorrhoeae and Neisseria Meningitidis. *Infect. Immun.* **2005**, *73* (9), 5697–5705. https://doi.org/10.1128/IAI.73.9.5697-5705.2005.

(54) Weadge, J. T.; Pfeffer, J. M.; Clarke, A. J. Identification of a New Family of Enzymes with Potential O-Acetylpeptidoglycan Esterase Activity in Both Gram-Positive and Gram-Negative Bacteria. *BMC Microbiol.* **2005**, *5*, 1–15. https://doi.org/10.1186/1471-2180-5-49.

(55) Weadge, J. T.; Clarke, A. J. Neisseria Gonorrheae O-Acetylpeptidoglycan Esterase, a Serine Esterase with a Ser-His-Asp Catalytic Triad. *Biochemistry* **2007**, *46* (16), 4932–4941. https://doi.org/10.1021/bi700254m.

(56) Franklin, M. J.; Ohman, D. E. Mutant Analysis and Cellular Localization of the AlgI, AlgJ, and AlgF Proteins Required for O Acetylation of Alginate in Pseudomonas Aeruginosa. *J. Bacteriol.* **2002**, *184* (11), 3000–3007. https://doi.org/10.1128/JB.184.11.3000-3007.2002.

(57) Moynihan, P. J.; Clarke, A. J. O-Acetylation of Peptidoglycan in Gram-Negative Bacteria: Identification and Characterization of Peptidoglycan O-Acetyltransferase in Neisseria Gonorrhoeae. *J. Biol. Chem.* **2010**, *285* (17), 13264–13273. https://doi.org/10.1074/jbc.M110.107086.

(58) Veyrier, F. J.; Williams, A. H.; Mesnage, S.; Schmitt, C.; Taha, M. K.; Boneca, I. G. De-O-Acetylation of Peptidoglycan Regulates Glycan Chain Extension and Affects in Vivo Survival of Neisseria Meningitidis. *Mol. Microbiol.* **2013**, *87* (5), 1100–1112. https://doi.org/10.1111/mmi.12153.

(59) Wang, G.; Lo, L. F.; Forsberg, L. S.; Maier, R. J. Helicobacter Pylori Peptidoglycan Modifications Confer Lysozyme Resistance and Contribute to Survival in the Host. *MBio*

2012, *3* (6), 1–9. https://doi.org/10.1128/mBio.00409-12.

(60) Moynihan, P. J.; Clarke, A. J. Assay for Peptidoglycan O-Acetyltransferase: A Potential New Antibacterial Target. *Anal. Biochem.* **2013**, *439* (2), 73–79. https://doi.org/10.1016/j.ab.2013.04.022.

(61) Moynihan, P. J.; Clarke, A. J. Substrate Specificity and Kinetic Characterization of Peptidoglycan O-Acetyltransferase B from Neisseria Gonorrhoeae. *J. Biol. Chem.* **2014**, *289* (24), 16748–16760. https://doi.org/10.1074/jbc.M114.567388.

(62) Moynihan, P. J.; Clarke, A. J. Mechanism of Action of Peptidoglycan O-Acetyltransferase B Involves a Ser-His-Asp Catalytic Triad. *Biochemistry* **2014**, *53* (49), 6243–6251.

(63) Brott, A. S.; Jones, C. S.; Clarke, A. J. Development of a High Throughput Screen for the Identification of Inhibitors of Peptidoglycan O-Acetyltransferases, New Potential Antibacterial Targets. *Antibiotics* **2019**, *8* (2). https://doi.org/10.3390/antibiotics8020065.

(64) Kelley, L. A.; Mezulis, S.; Yates, C. M.; Wass, M. N.; Sternberg, M. J. The Phyre2 Web Portal for Protein Modeling, Prediction and Analysis. *Nat. Protoc.* **2015**, *10* (6), 845–858. https://doi.org/10.1038/nprot.2015-053.

(65) Petruccelli, V. Expression of Peptidoglycan O -Acetyltransferase A from Neisseria Gonorrhoeae By. **2021**, *MSc thesis*.

(66) Jones, C. S. Structure, Function, and Inhibition of Peptidoglycan O-Acetyltransferase A from Staphylococcus Aureus. **2020**, *PhD thesis*.

(67) Tsirigos, K. D.; Peters, C.; Shu, N.; Käll, L.; Elofsson, A. The TOPCONS Web Server for Consensus Prediction of Membrane Protein Topology and Signal Peptides. *Nucleic Acids Res.* **2015**, *43* (W1), W401–W407. https://doi.org/10.1093/nar/gkv485.

(68) Davis, L.; Dirita, V. Growth and Laboratory Maintenance of Campylobacter Jejuni. *Curr. Protoc. Microbiol.* **2008**, *10*, 1–7. https://doi.org/10.1002/9780471729259.mc08a01s10.

(69) Miroux, B.; Walker, J. E. Over-Production of Proteins in Escherichia Coli : Mutant Hosts That Allow Synthesis of Some Membrane Proteins and Globular Proteins at High Levels. *J. Mol. Biol.* **1996**, *260*, 289–298.

(70) Ha, R.; Frirdich, E.; Sychantha, D.; Biboy, J.; Taveirne, M. E.; Johnson, J. G.; Di Rita, V. J.; Vollmer, W.; Clarke, A. J.; Gaynor, E. C. Accumulation of Peptidoglycan O-Acetylation Leads to Altered Cell Wall Biochemistry and Negatively Impacts Pathogenesis Factors of Campylobacter Jejuni. *J. Biol. Chem.* **2016**, *291* (43), 22686–22702. https://doi.org/10.1074/jbc.M116.746404.

(71) Karlyshev, A. V.; Wren, B. W. Development and Application of an Insertional System for Gene Delivery and Expression in Campylobacter Jejuni. *Appl. Environ. Microbiol.* **2005**, *71* (7), 4004–4013. https://doi.org/10.1128/AEM.71.7.4004-4013.2005.

(72) Beauchamp, J. M.; Leveque, R. M.; Dawid, S.; DiRita, V. J. Methylation-Dependent DNA Discrimination in Natural Transformation of Campylobacter Jejuni. *Proc. Natl. Acad. Sci. U. S. A.* **2017**, *114* (38), E8053–E8061. https://doi.org/10.1073/pnas.1703331114.

(73) Elmros, T.; Bruman, L. G.; Bloom, G. D. Autolysis of Neisseria Gonorrhoeae. *J. Bacteriol.*

1976, *126* (2), 969–976.

(74) Brott, A. S.; Clarke, A. J. Assays for the Enzymes Catalyzing the O-Acetylation of Bacterial Cell Wall Polysaccharides. In *Bacterial Polysaccharides; Methods and Protocols*; Brockhausen, I., Ed.; Methods in Molecular Biology; Springer New York: New York, NY, 2019; Vol. 1954, pp 115–135. https://doi.org/10.1007/978-1-4939-9154-9.

(75) Guzman, L.-M.; Belin, D.; Carson, M. J.; Beckwith, J. Tight Regulation, Modulation, and High-Level Expression by Vectors Containing the Arabinose P BAD Promoter. *J Bacteriol.* **1995**, *177* (14), 4121–4130.

(76) Ma, D.; Wang, Z.; Merrikh, C. N.; Lang, K. S.; Lu, P.; Li, X.; Merrikh, H.; Rao, Z.; Xu, W. Crystal Structure of a Membrane-Bound O-Acyltransferase. *Nature* **2018**, *562* (7726), 286–290. https://doi.org/10.1038/s41586-018-0568-2.

(77) Coupland, C. E.; Andrei, S. A.; Ansell, T. B.; Carrique, L.; Kumar, P.; Sefer, L.; Schwab, R. A.; Byrne, E. F. X.; Pardon, E.; Steyaert, J.; Magee, A. I.; Lanyon-Hogg, T.; Sansom, M. S. P.; Tate, E. W.; Siebold, C. Structure, Mechanism, and Inhibition of Hedgehog Acyltransferase. *Mol. Cell* **2021**, *81* (24), 5025-5038.e10. https://doi.org/10.1016/j.molcel.2021.11.018.

(78) Sui, X.; Wang, K.; Gluchowski, N. L.; Elliott, S. D.; Liao, M.; Walther, T. C.; Farese, R. V. Structure and Catalytic Mechanism of a Human Triglyceride Synthesis Enzyme. *Nature* **2020**, *581* (7808), 323–328. https://doi.org/10.1038/s41586-020-2289-6.Structure.

(79) Wang, L.; Qian, H.; Nian, Y.; Han, Y.; Ren, Z.; Zhang, H.; Hu, L.; Prasad, B. V. V.;

Laganowsky, A.; Yan, N.; Zhou, M. Structure and Mechanism of Human Diacylglycerol O-Acyltransferase 1. *Nature* **2020**, *581* (7808), 329–332. https://doi.org/10.1038/s41586-020-2280-2.

(80) Ménard, R.; Sansonetti, P. J.; Parsot, C. Nonpolar Mutagenesis of the Ipa Genes Defines IpaB, IpaC, and IpaD as Effectors of Shigella Flexneri Entry into Epithelial Cells. *J. Bacteriol.* **1993**, *175* (18), 5899–5906. https://doi.org/10.1128/jb.175.18.5899-5906.1993.

(81) James, J.; Yarnall, B.; Koranteng, A.; Gibson, J.; Rahman, T.; Doyle, D. A. Protein Over-Expression in Escherichia Coli Triggers Adaptation Analogous to Antimicrobial Resistance. *Microb. Cell Fact.* **2021**, *20* (1), 1–11. https://doi.org/10.1186/s12934-020-01462-6.

(82) Iwata, T.; Watanabe, A.; Kusumoto, M.; Akiba, M. Peptidoglycan Acetylation of Campylobacter Jejuni Is Essential for Maintaining Cell Wall Integrity and Colonization in Chicken. *Appl. Environ. Microbiol.* **2016**, *82* (20), 6284–6290. https://doi.org/10.1128/AEM.02068-16.Editor.

(83) Han, F.; Pu, S.; Wang, F.; Meng, J.; Ge, B. International Journal of Antimicrobial Agents Fitness Cost of Macrolide Resistance in Campylobacter Jejuni. *Int. J. Antimicrob. Agents* **2009**, *34* (5), 462–466. https://doi.org/10.1016/j.ijantimicag.2009.06.019.

(84) Karlyshev, A. V.; Wren, B. W.; Moran, A. P. Campylobacter Jejuni Capsular Polysaccharide. In *Campylobacter*; Nachamkin, I., Szymanski, C. M., Blaser, M. J., Eds.; ASM Press: Washington, DC, 2008; pp 505–521. https://doi.org/10.1128/9781555815554.ch28.

(85) Christaki, E.; Marcou, M.; Tofarides, A. Antimicrobial Resistance in Bacteria: Mechanisms, Evolution, and Persistence. *J. Mol. Evol.* **2020**, *88* (1), 26–40. https://doi.org/10.1007/s00239-019-09914-3.

Appendix A: Multiple Sequence Alignment


Helicobacter.pylori_PDX10677.1 181
Proteus.mirabilis_KGA89191.1 157
Cosenzaea.myxofaciens_WP_0667488 157
Proteus.penneri_EEG87530.1 24
Proteus.sp_WP_099660474.1 157
Proteus.vulgaris_CRL61754.1 157
Proteus.hauseri_WP_023582996.1 157
Photorhabdus.asymbiotica_CAQ8595 157
Photorhabdus.temperate_WP_036841 157
Photorhabdus.luminescens_PQQ2461 157
Photorhabdus_WP_011144887.1 157
Xenorhabdus.poinarii_CDG20190.1 157
Xenorhabdus.bovienii_CBJ82832.1 157
Xenorhabdus.nematophila_CBJ91005 77
Morganella.morganii_AGG32564.1 157
Providencia.alcalifaciens_EEB465 157
Providencia.rustigianii_ZP_03315 157
Providencia.sneebia_WP_008916930 157
Providencia.burhodogranariea_WP_ 157
Providencia.stuartii_EDU58007.1 157
Providencia.heimbachae_WP_068437 157
Providencia.rettgeri_WP_00426119 157
Dickeya.dadantii_ADN00692.1 157
Dickeya.chrysanthemi_ACT04909.1 161
Citrobacter.youngae_ZP_03836337. 158
Cronobacter.sakazakii_ABU75603.1 158
Chromobacterium.sphagni_WP_07111 157
Chromobacterium.violaceum_WP_099 157
Moraxella.cuniculi_WP_076554312. 161
Moraxella.pluranimalium_WP_07825 162
Moraxella.canis_WP_078255751.1 150
Moraxella.catarrhalis_AIT43734.1 161
Moraxella.oblonga_WP_066805368.1 166
Moraxella.nonliquefaciens_WP_082 174
Moraxella.lacunata_WP_083108172. 165
Moraxella.caprae_WP_036387207.1 183
Moraxella.bovis_WP_078273490.1 183
Moraxella.equi_WP_079323840.1 183
Neisseria.shayeganii_EGY51425.1 153
Eikenella.corrodens_ZP_03713079. 153
Kingella.oralis_WP_003793826.1 154
Kingella.kingae_CRZ20803.1 152
Neisseria.cinerea_EEG62385.1 154
Neisseria.meningitides_AGX85509. 154
Neisseria.polysaccharea_WP_02545 154
Neisseria.gonorrhoeae_AKP14258.1 154
Neisseria.lactamica_WP_118779166 154
Neisseria.flavescens_EEG32499.1 154
Neisseria.subflava_ZP_03750679.1 89
Neisseria.mucosa_EFC89004.1 154
Neisseria.macacae_EGQ77128.1 154
Neisseria.sicca 154
Campylobacter.gracilis_EEV17612. 208
Helicobacter.mustelae_CBG39657.1 160
Helicobacter.cinaedi_BAM31349.1 170
Campylobacter.upsaliensis_WP_004 153
Campylobacter.cuniculorum_ARJ567 153
Campylobacter.coli_AGZ21047.1 153
Campylobacter.jejuni_AFU42713.1 153


Helicobacter.pylori_PDX10677.1 283
Proteus.mirabilis_KGA89191.1 257
Cosenzaea.myxofaciens_WP_0667488 257
Proteus.penneri_EEG87530.1 124
Proteus.sp_WP_099660474.1 257
Proteus.vulgaris_CRL61754.1 257
Proteus.hauseri_WP_023582996.1 257
Photorhabdus.asymbiotica_CAQ8595 257
Photorhabdus.temperate_WP_036841 257
Photorhabdus.luminescens_PQQ2461 257
Photorhabdus_WP_011144887.1 257
Xenorhabdus.poinarii_CDG20190.1 257
Xenorhabdus.bovienii_CBJ82832.1 257
Xenorhabdus.nematophila_CBJ91005 177
Morganella.morganii_AGG32564.1 257
Providencia.alcalifaciens_EEB465 257
Providencia.rustigianii_ZP_03315 257
Providencia.sneebia_WP_008916930 257
Providencia.burhodogranariea_WP_ 257
Providencia.stuartii_EDU58007.1 257
Providencia.heimbachae_WP_068437 257
Providencia.rettgeri_WP_00426119 257
Dickeya.dadantii_ADN00692.1 258
Dickeya.chrysanthemi_ACT04909.1 262
Citrobacter.youngae_ZP_03836337. 258
Cronobacter.sakazakii_ABU75603.1 258
Chromobacterium.sphagni_WP_07111 258
Chromobacterium.violaceum_WP_099 258
Moraxella.cuniculi_WP_076554312. 275
Moraxella.pluranimalium_WP_07825 276
Moraxella.canis_WP_078255751.1 264
Moraxella.catarrhalis_AIT43734.1 275
Moraxella.oblonga_WP_066805368.1 280
Moraxella.nonliquefaciens_WP_082 288
Moraxella.lacunata_WP_083108172. 279
Moraxella.caprae_WP_036387207.1 297
Moraxella.bovis_WP_078273490.1 297
Moraxella.equi_WP_079323840.1 297
Neisseria.shayeganii_EGY51425.1 264
Eikenella.corrodens_ZP_03713079. 264
Kingella.oralis_WP_003793826.1 266
Kingella.kingae_CRZ20803.1 263
Neisseria.cinerea_EEG62385.1 265
Neisseria.meningitides_AGX85509. 265
Neisseria.polysaccharea_WP_02545 265
Neisseria.gonorrhoeae_AKP14258.1 265
Neisseria.lactamica_WP_118779166 265
Neisseria.flavescens_EEG32499.1 265
Neisseria.subflava_ZP_03750679.1 200
Neisseria.mucosa_EFC89004.1 265
Neisseria.macacae_EGQ77128.1 265
Neisseria.sicca 265
Campylobacter.gracilis_EEV17612. 316
Helicobacter.mustelae_CBG39657.1 260
Helicobacter.cinaedi_BAM31349.1 268
Campylobacter.upsaliensis_WP_004 251
Campylobacter.cuniculorum_ARJ567 251
Campylobacter.coli_AGZ21047.1 251
Campylobacter.jejuni_AFU42713.1 251

Multiple sequence alignment of PatA homologues. A multiple sequence alignment of the sections of interest of *patA* homologues with residues that were chosen for experimentation. Black bars represent the residues that were chosen for further experimentation. Sequences were downloaded from NCBI database and contains the following species and sequences: *Neisseria gonorrhoeae* (AKP14258.1), *Neisseria cinerea* (EEG62385.1), *Neisseria flavescens* (EEG32499.1), *Neisseria lactamica* (WP_118779166.1), *Neisseria macacae* (EGQ77128.1), *Neisseria meningitides* (AGX85509.1), *Neisseria mucosa* (EFC89004.1), *Neisseria polysaccharea* (WP_025457096.1), *Neisseria shayeganii* (EGY51425.1), *Neisseria sicca* (EET44324.1), *Neisseria subflava* (ZP_03750679.1), *Chromobacterium sphagni* (WP_071114372.1), *Chromobacterium violaceum* (WP_099427642.1), *Eikenella corrodens* (ZP_03713079.1), *Kingella kingae* (CRZ20803.1), *Kingella oralis* (WP_003793826.1), *Citrobacter youngae* (ZP_03836337.1), *Cronobacter sakazakii* (ABU75603.1), *Dickeya dadantii* (AND00692.1), *Dickeya chrysanthemi* (ACT04909.1), *Morganella morganii* (AGG32564.1), *Proteus hauseri (*WP_023582996.1), *Proteus mirabilis* (KGA89191.1), *Proteus penneri* (EEG87530.1), *Proteus vulgaris* (CRL61754.1), *Proteus* sp (WP_099660474.1), *Providencia alcalifaciens* (EEB46553.1), *Providencia burhodogranariea*

(WP_008913753.1), *Providencia heimbachae* (WP_068437385.1), *Cosenzaea myxofaciens* (WP_066748883.1), *Providencia rettgeri* (WP_004261191.1), *Providencia rustigianii* (ZP_03315887.1), *Providencia sneebia* (WP_008916930.1), *Providencia stuartii* (EDU58007.1), *Photorhabdus asymbiotica* (CAQ85951.1), *Photorhabdus luminescens* (PQQ24615.1), *Photorhabdus* (WP_011144887.1), *Photorhabdus temperate* (WP_036841133.1), *Xenorhabdus bovienii* (CBJ82832.1), *Xenorhabdus nematophila* (CBJ91005.1), *Xenorhabdus poinarii* (CDG20190.1), *Moraxella bovis* (WP_078273490.1), *Moraxella canis* (WP_078255751.1), *Moraxella caprae* (WP_036387207.1), *Moraxella catarrhalis* (AIT43734.1), *Moraxella cuniculi* (WP_076554312.1), *Moraxella equi* (WP_079323840.1), *Moraxella lacunata* (WP_083108172.1), *Moraxella nonliquefaciens* (WP_082995533.1), *Moraxella oblonga* (WP_066805368.1), *Moraxella pluranimalium* (WP_078254947.1), *Campylobacter coli* (AGZ21047.1), *Campylobacter cuniculorum* (ARJ56739.1), *Campylobacter gracilis* (EEV17612.1), *Campylobacter jejuni* (AFU42713.1), *Campylobacter upsaliensis* (WP_004274816.1), *Helicobacter cinaedi* (BAM31349.1), *Helicobacter mustelae* (CBG39657.1), *Helicobacter pylori* (PDX10677.1)

Appendix B: Recipes

Terrific Broth

12g tryptone, 24 g yeast extract, and 4 mL glycerol into 1 L of water then autoclave

- Add before use
    - 2.31g KH_2PO_4 (Potassium phosphate monobasic – 0.17*M*)
    - 12.54g K_2HPO_4 (Potassium phosphate dibasic – 0.72*M*)

Super Broth

32 g tryptone, 20 g yeast extract, and 10 g NaCl dissolved into 1 L of water then autoclave

1M Tris-buffered solution

60.55g of Tris base dissolved into 400 mL of water, pH to 8.0 with concentrated HCL

Phosphate Buffered Saline Solution

4g NaCl, 0.1g KCl, 0.72g Na_2HPO_4, 0.1225g KH_2PO_4 dissolved into 500 mL and adjusted to pH 7.4

Lysis Buffer

50 mM Na_2HPO_4, 150 mM NaCl, 7M Urea, 1 µM RNase, 1µM DNase, approximately 0.5 mg/ml lysozyme, and one EDTA-free protease inhibitor cocktail tablet. Adjust to pH 7.0

Wash Buffer

50mM $Na2HPO_4$, 150 mM NaCl, 6M urea, and 20mM imidazole. Adjust to pH 7.8

Elution Buffer

50mM Na_2HPO_4, 150 mM NaCl, 6M urea, and 400mM imidazole. Adjust to pH 7.8

Eluents for Muramic Acid Analysis

Eluent A: 100 mM NaOH

Eluent B: 100 mM NaOH, 150 mM NaCHOOH

Eluent C: H_2O